MID-AMERICA TRANSPORTATION CENTER

Report # MATC-KU: 246

Final Report
WBS: 25-1121-0003-246

Repair of Skewed Steel Bridges Damaged by Distortion-Induced Fatigue

Caroline Bennett, Ph.D., P.E.
Associate Professor
CEAE Department
University of Kansas

Danquing Yu
Graduate Research Assistant

Yaqin Chen, Ph.D.
Visiting Scholar

Adolfo Matamoros, Ph.D., P.E.
Professor
CEE Department
Universtiy of Texas San Antonio

Stan Rolfe, Ph.D., P.E.
Distinguished Professor
CEAE Department
Universtiy of Kansas

2014

A Cooperative Research Project sponsored by
U.S. Department of Transportation- Office of the Assistant Secretary for Research and Technology

Final Report: Repair of Skewed Steel Bridges Damaged by Distortion-Induced Fatigue

PI: Caroline Bennett, Ph.D., P.E.
Associate Professor
CEAE Department
University of Kansas

Danqing Yu
Graduate Research Assistant
CEAE Department
University of Kansas

Co-PI: Adolfo Matamoros, Ph.D., P.E.
Professor
CEE Department
University of Texas San Antonio

Yaqin Chen, Ph.D.
Visiting Scholar
CEAE Department
University of Kansas

Co-PI: Stan Rolfe, Ph.D., P.E.
Distinguished Professor
CEAE Department
University of Kansas

A Report on Research Sponsored by

Mid-America Transportation Center

University of Nebraska–Lincoln

Dec 2014

Technical Report Documentation Page

1. Report No. 25-1121-0003-246	2. Government Accession No.	3. Recipient's Catalog No.
4. Title and Subtitle Repair of Skewed Steel Bridges Damaged by Distortion-Induced Fatigue		5. Report Date Dec 2014
		6. Performing Organization Code
7. Author(s) Caroline Bennett, Adolfo Matamoros, Stan Rolfe, Danqing Yu, and Yaqin Chen		8. Performing Organization Report No. 25-1121-0003-246
9. Performing Organization Name and Address Mid-America Transportation Center 2200 Vine St. PO Box 830851 Lincoln, NE 68583-0851		10. Work Unit No. (TRAIS)
		11. Contract or Grant No.
12. Sponsoring Agency Name and Address Research and Innovative Technology Administration 1200 New Jersey Ave., SE Washington, D.C. 20590		13. Type of Report and Period Covered June 2013-December 2014
		14. Sponsoring Agency Code RiP: 34772
15. Supplementary Notes		

16. Abstract

This study was aimed at assessing the performance of the newly-developed angles-with-plate retrofit for repairing distortion-induced fatigue in skewed girder-to-crossframe connections. Two physical tests were performed on skewed girder-crossframe assemblies, in which distortion-induced fatigue cracks were generated. One specimen was skewed 20-deg., and the other was skewed 40-deg. The angles-with-plate retrofit was applied in both set-ups, and the crack propagation rates were compared before and after retrofitting. It was found that the angles-with-plate retrofit was very effective in significantly reducing crack propagation in both of the skewed specimens. A series of computer simulations were performed in which the specimens were modeled in the uncracked, cracked, and retrofitted configurations. The computer simulation results agreed well with the experimental findings, showing that the retrofit successfully reduced stress demands in the connection details.

17. Key Words Skewed bridges; Steel bridges; retrofit; cracking; Distortion-induced fatigue	18. Distribution Statement		
19. Security Classif. (of this report) Unclassified	20. Security Classif. (of this page) Unclassified	21. No. of Pages 93	22. Price

Table of Contents

List of Figures

List of Tables

Acknowledgments (optional)

The research team would like to thank the MATC for supporting this research. Additionally, thanks are offered to the Kansas Department of Transportation who helped to provide information regarding skewed bridge details used in practice. Finally, we are thankful to the support provided by the laboratory staff at the University of Kansas.

Disclaimer

The contents of this report reflect the views of the authors, who are responsible for the facts and the accuracy of the information presented herein. This document is disseminated under the sponsorship of the U.S. Department of Transportation's University Transportation Centers Program, in the interest of information exchange. The U.S. Government assumes no liability for the contents or use thereof.

Abstract

This study was aimed at assessing the performance of the newly-developed angles-with-plate retrofit for repairing distortion-induced fatigue in skewed girder-to-crossframe connections. Two physical tests were performed on skewed girder-crossframe assemblies, in which distortion-induced fatigue cracks were generated. One specimen was skewed 20-deg., and the other was skewed 40-deg. The angles-with-plate retrofit was applied in both set-ups, and the crack propagation rates were compared before and after retrofitting. It was found that the angles-with-plate retrofit was very effective in significantly reducing crack propagation in both of the skewed specimens. A series of computer simulations were performed in which the specimens were modeled in the uncracked, cracked, and retrofitted configurations. The computer simulation results agreed well with the experimental findings, showing that the retrofit successfully reduced stress demands in the connection details.

Chapter 1 Introduction

1.1 Background

Distortion-induced fatigue is a serious problem faced by many aging bridges, caused by secondary stresses not accounted for in the original design. Secondary stresses are thought to cause approximately 90% of fatigue damage in steel bridges (Connor and Fisher 2005). For example, bolted or riveted girder-to-crossframe connections were only designed to transfer shear force. However, although the connections allow generally large rotations, they are not 100% free to rotate. As shown in Figure 1-1, when live loads produce relative displacement between adjacent girders, secondary fatigue stresses at the connections. Usually, the stresses are not large-magnitude, but for fatigue-sensitive details even small stress ranges may lead to cracking.

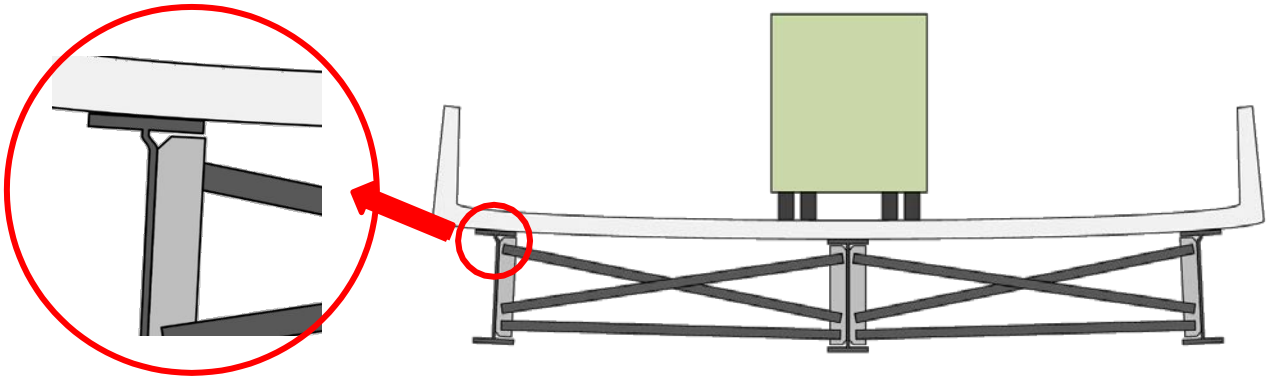

Figure 1-1: Out-of-plane deformation induced by relative displacement between adjacent members caused by living load (Hartman and Hassel, 2010)

The web-gap region is a detail that is highly sensitive to distortion-induced fatigue. Figure 1-2 depicts a web-gap region formed by a girder web, a flange and a cropped stiffener functioning as a connection plate. The cropped ends of the stiffeners were designed to avoid the intersection of two welds. In 1985, the AASHTO bridge design specification instituted the requirement that a connection plate must be connected to both of the flanges. However, in numerous bridges built prior to 1985, connection was not provided between stiffeners and

flanges, because engineers believed that doing so was a good practice to prevent cracking in flanges. This practice produced a very flexible web-gap region in which highly localized bending was able to occur under the rotation imposed by the crossframe.

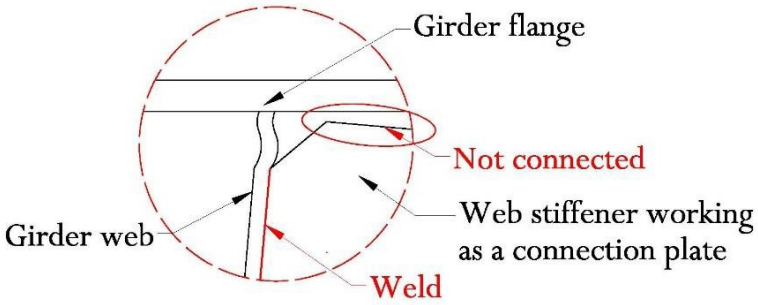

Figure 1-2: Distortion in a web-gap region

Many retrofit methods have been developed to repair distortion-induced fatigue damage. They can be generally be divided into two categories: softening methods and stiffening methods. Softening methods include diaphragm or crossframe removal, bolt/rivet removal, bolt loosening, connection plate shortening, and drilling a large hole (>3 in.) in the web gap region (Dexter and Ocel 2013). These methods are aimed at reducing the connection stiffness such that less moment is generated in the web gap. Stiffening methods, however, increase connection stiffness by providing positive attachments, such that alternative load paths are provided and stresses at damaged details are reduced.

Many studies have been aimed at developing new stiffening techniques, but methods that rely on bolting are generally accepted to be the best option to guarantee the efficacy of the attachments. Traditionally, attachments are provided between the flange and the stiffener, but to do so, the concrete deck must be removed to drill bolt holes through the steel flanges when cracking is in the top web-gap. The difficulty involved with removing the concrete deck gives rise to the need to develop an alternative method (Bennett et al. 2014). The angles-with-plate retrofit is a stiffening method that does not require removing the concrete deck.

Developed at the University of Kansas, the angles-with-plates retrofit has shown its potential in repairing straight girder-to-crossframe connections (Alemdar et al. 2014a, 2014b; Hartman et al. 2013; Bennett et al. 2014). As shown in Figure 1-3, the angles-with-plate retrofit provides connection between the stiffener and the girder web, instead of connecting the flange and the stiffener. The retrofit consists two steel angles and a backing plate for an exterior connection, and four angles for an interior connection. The angles connect the stiffener to the girder web, while the backing plate distributes the load across a broad area of the web, such that stresses are no longer concentrated in a small region. The good performance of the angles-with-plate retrofit on straight girder-to-crossframe connections established in prior testing is one of the motivations for investigating its performance in skewed connections.

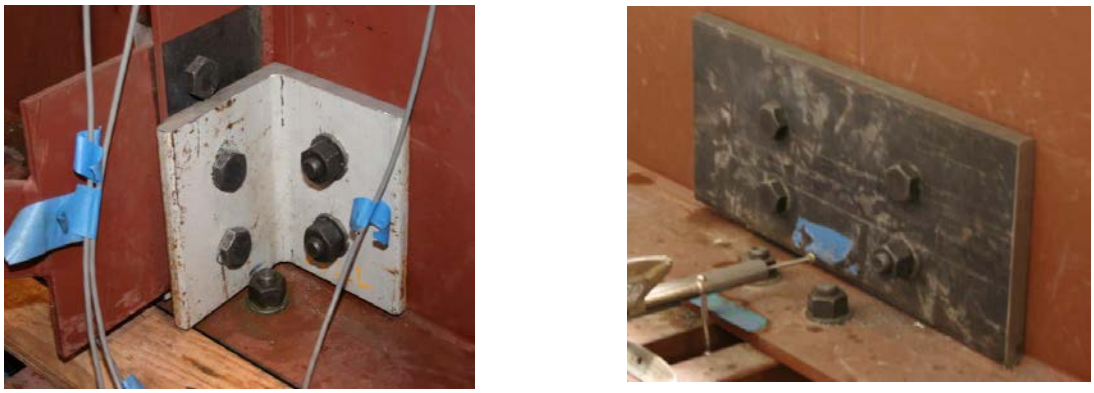

(a) Angle (b) Backing plate

Figure 1-3: Angles-with-plate retrofit (Alemdar et al. 2014a; 2014b)

Connections in skewed bridges have been shown to be more sensitive to distortion-induced fatigue than non-skewed bridges (Fisher and Mertz 1984). In a skewed bridge, with a layout such that crossframes are placed perpendicular to the girder web, each crossframe is connecting two different positions along the span. Therefore, the relative displacement between the two positions that the crossframe is connecting is usually larger than in a non-skewed bridge. When a layout is used such that bracing is placed parallel to the skew angle (a skewed

connection), distortion-induced fatigue is thought to be less of a concern (Hassel et al. 2013), since in this layout the crossframe is connecting the same span points. The AASHTO Bridge Design Specification [2013] requires that for a bridge with a skew angle larger than 20 deg.s, crossframes must be provided perpendicular to the girder web (AASHTO 2013), due to concerns regarding crossframe flexibility and the effectiveness of live load distribution. However, some states still allow the use of skewed connections beyond this limit (Hassel et al. 2013).

1.2 Objectives and Scope

This report presents the results of an experimental investigation, including physical tests conducted on 20-deg. and 40-deg. skewed girder-to-crossframe connection subassemblies. Additionally, a series of computer simulations were performed to complement the physical tests. A comparison of the physical test results and the computer simulation results is presented, along with a discussion of the influence of the angles-with-plate retrofit on stresses on the crossframe gusset plate.

The objective of this study to evaluate the efficacy of the angles-with-plate retrofit for repairing fatigue damage in web-gap regions of skewed girder-to-crossframe connections, as well as to generate a better understanding of the distortion-induced fatigue performance of skewed girder-to-crossframe connections.

Chapter 2 Physical Test of the 20-Deg. Skewed Girder-to-Crossframe Connection – Test Introduction

2.1 Description of the 20-Deg. Skewed Girder-to-Crossframe Specimen

The 20 deg. test specimen consisted of a built-up steel girder and a crossframe skewed 20 deg. from the girder. The specimen layout is shown in Figure 2-1. The built-up girder was 9 ft long, 36 in. tall, with a 34-1/2in. x 3/8 in. web, a 11 in. x 1 in. top flange and a 11 in.x 5/8 in. bottom flange. The specimen included a 34-3/8 in. x 5 in. x 3/8 in. transverse stiffener functioning as a connection plate with 1-1/4in. cropped ends. The stiffener was welded to the centerline of the girder web, but no connection was provided between the connection plate and the girder flanges, such that web gaps were created near the top and bottom flanges.

Four stiffeners were welded to both flanges and the web at the ends of the girder. Both ends of the top flange of the girder were restrained from lateral movement by two angles. The bottom flange of the girder was fixed to the laboratory strong floor by bolting to a tie-down system of post-tensioned C5x9 and C10x30 channels. Therefore, the specimen was tested upside-down, with the flange attached to the laboratory floor simulating a top flange connected to a laterally-stiff bridge deck.

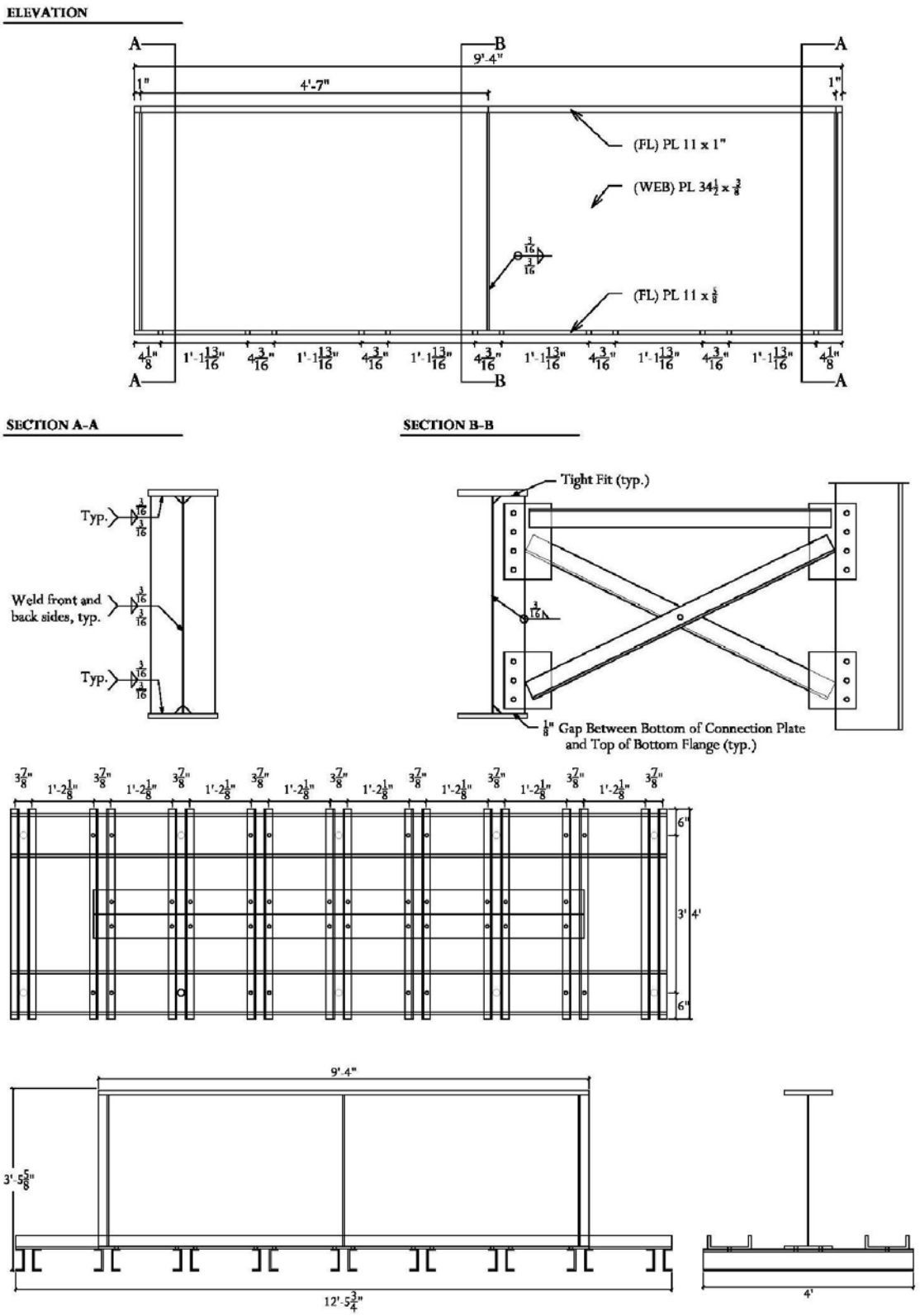

Figure 2-1: Specimen layout

In a real bridge system, the top flange of a girder is restrained by a bridge deck, but this situation is difficult to establish in a component test. By fixing the bottom flange to the laboratory floor, the displacement of the bottom flange was fully restrained, and the influence of in-plane bending was eliminated. Although this kind of component test is different from the in-plane and out-of-plane deformation that occurs in a real bridge, computer simulations performed for the previous girder-to-crossframe tests at the University of Kansas showed that the stress distribution in the component test was similar to that of a real bridge (Alemdar et al. 2014a; 2014b).

A 20-deg. skewed crossframe was bolted to the connection plate at the mid-length point of the girder. The details of the crossframe are presented in Figure 2-2. The far end of the crossframe was bolted to a WT section, which was then connected to a servo-hydraulic actuator. In the test, the actuator applied upwards cyclic loading to simulate the effect of passing traffic. Lateral movement of the actuator was restrained by two pairs of rollers.

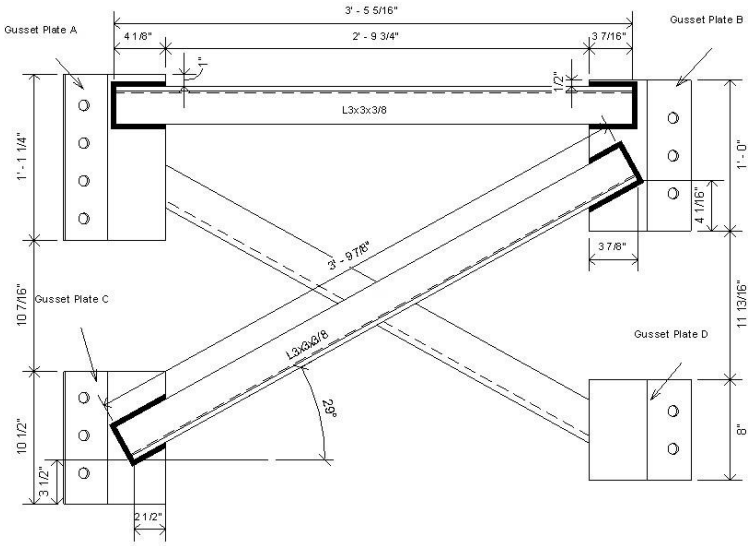

Figure 2-2: Dimensions of the 20-deg. skewed crossframe

The stiffened angles-with-plate retrofit was used in the test; it consisted of two stiffened angles and one backing plate, as presented in Figure 2-3. Photographs of the specimen and retrofit are shown in Figure 2-4.

The bolted connections were made using 3/4 in. A325-SC bolts. All welds in the tests were 3/16 in. fillet welds.

(a) South angle (b) North angle

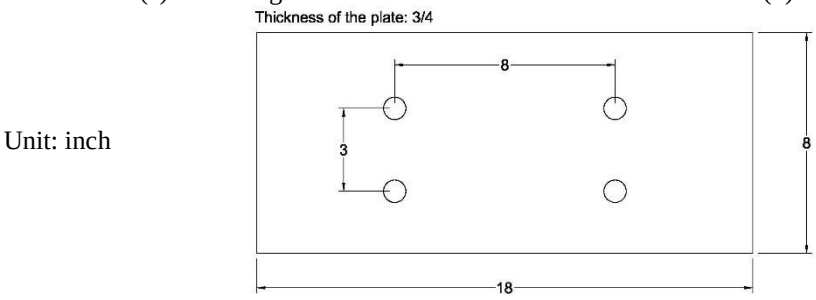

(c) Backing plate

Figure 2-3: Angles-with-plate retrofit dimensions

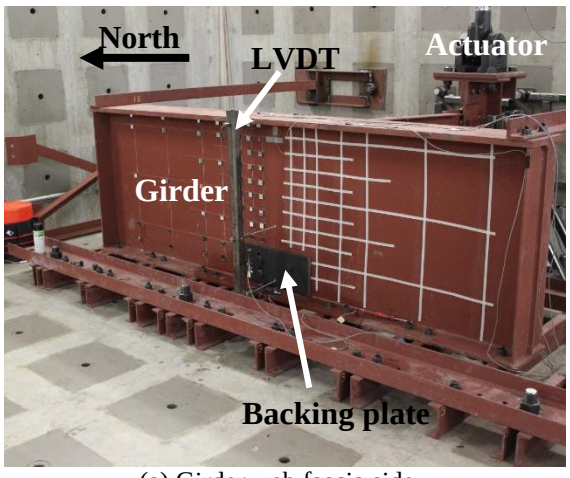

(a) Girder web fascia side

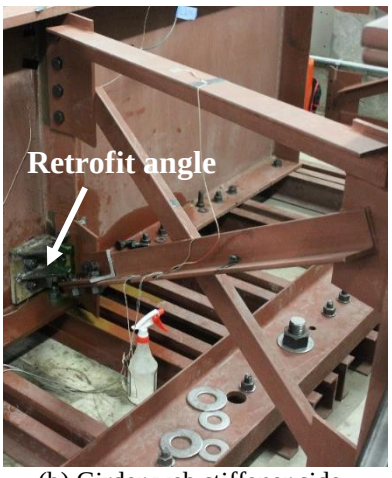

(b) Girder web stiffener side

(c) Restraining rollers

Figure 2-4: Photographs of 20-deg. skewed specimen and retrofit

2.2 Instrumentation

Actuator displacements were measured using the integrated LVDT and actuator force data was recorded simultaneously via a load cell. Strain gages were attached to the specimen at regions susceptible to fatigue as detected through finite element analysis and existing literature. In this test, the primary susceptible region was the bottom web-gap. Three LVDTs (Linear Variable Differential Transformers) were attached at different depths on the girder web at mid-span to measure out-of-plane deformations. Strain gage readings, LVDT readings, actuator displacement and actuator force were recorded while performing monotonic tests. Schematic drawings showing the LVDT and strain gage placements are presented in Figure 2-5.

Rotations of the girder web were measured using an array of mirrors attached to the girder web and a laser pointer. Figure 2-6 shows the placement of the mirrors. During the test, the mirrors reflected the laser on a wall opposite to the girder web, such that the movement of the web was magnified and could be recorded. The rotation of the web at the location of each mirror was calculated from the displacement of the reflected light, as shown in Figure 2-7.

When θ is small, $\tan\theta=\theta$

$$\tan\theta_1 = \theta_1 = \frac{\Delta_1}{L}, \quad \tan\theta_2 = \theta_2 = \frac{\Delta_2}{L}$$

$$\theta = \theta_1 - \theta_2 = \frac{\Delta_1 - \Delta_2}{L} = \frac{\Delta}{L}$$

$$\text{Mirror Rotation } \alpha = \frac{\theta}{2} = \frac{\Delta}{2L} \quad \text{(Equation 2-1)}$$

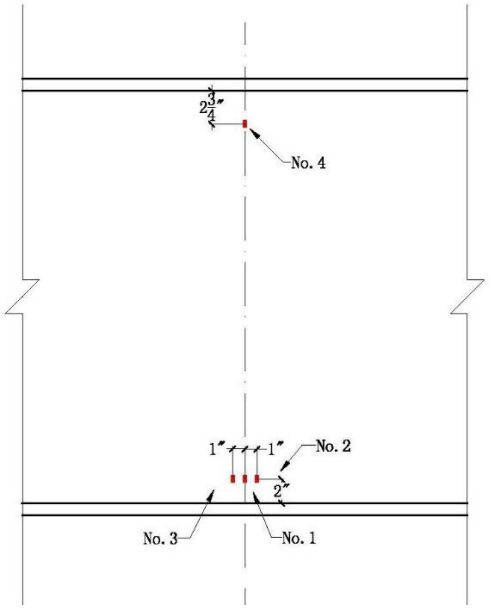

(a) Strain gages on girder web fascia side

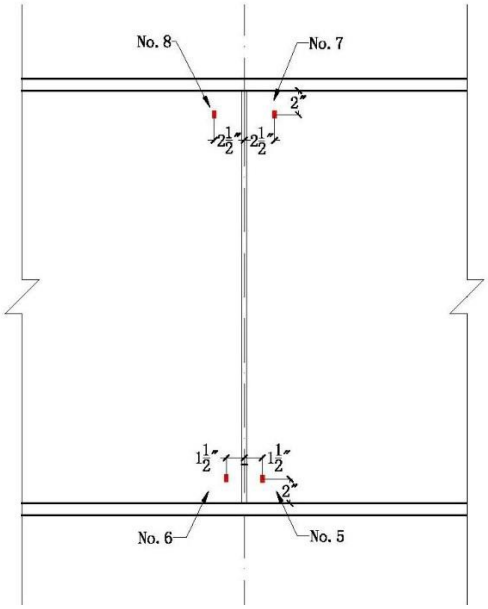

(b) Strain gages on girder web stiffener side

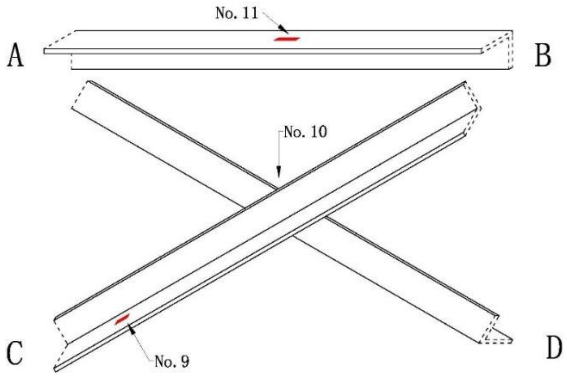

(c) Strain gages on crossframe

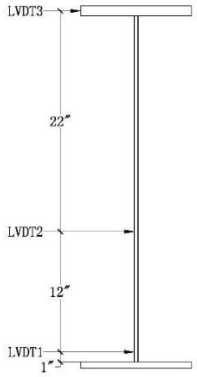

(d) LVDTs

Figure 2-5: Strain gage and LVDT placements for 20-deg. skewed specimen

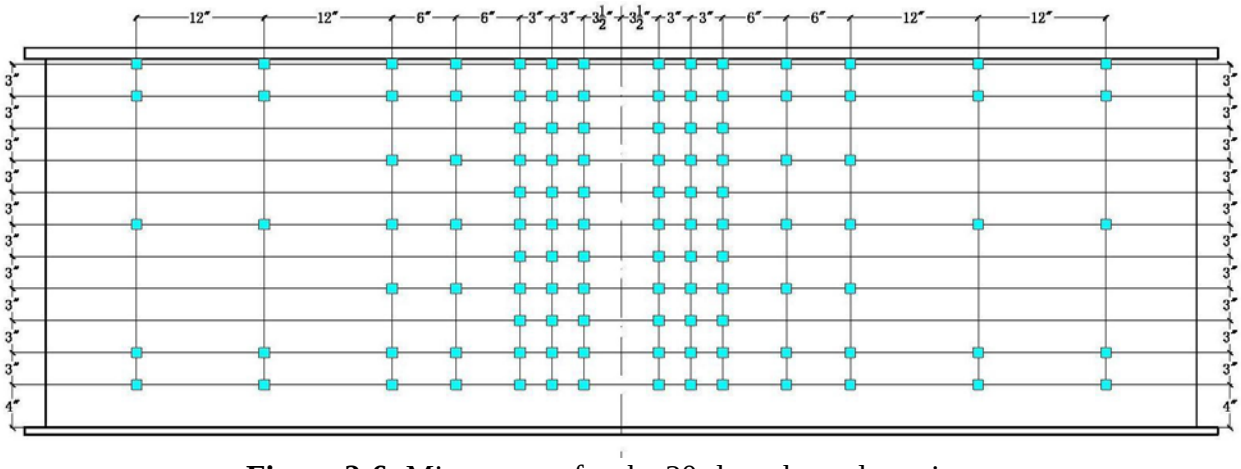

Figure 2-6: Mirror array for the 20-deg. skewed specimen

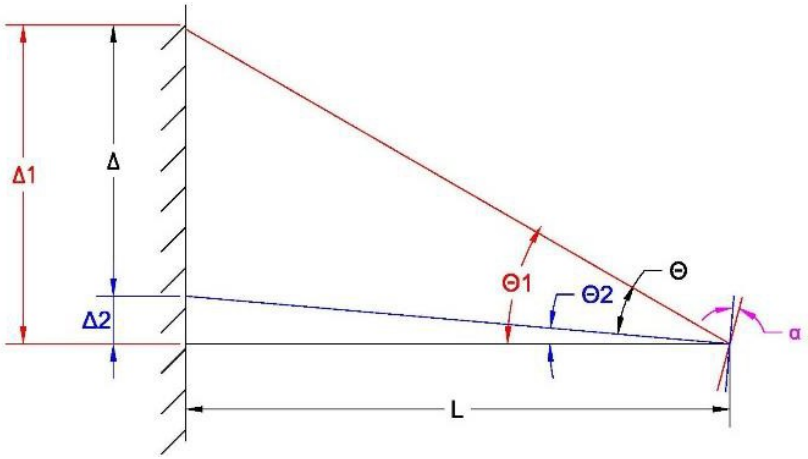

Figure 2-7: Girder web rotation computations, using measured displacement of reflected laser light

2.3 Test Procedure

A summary of the test trials performed on the 20-deg. skewed girder-to-crossframe specimen is presented in Table 2-1.

Table 2-1: Test summary of 20-deg. skewed specimen

Trial	Retrofit status	Number of cycles	Total cycles
Trial 20-1	Unretrofitted	16,504	16,504
Trial 20-2	Retrofitted	1,200,000	1,216,504
Trial 20-3	Unretrofitted	20,000	1,236,504

Load range: 0.5-6.2 kip
Load frequency: 2 Hz

In the test, the actuator provided a cyclic load range of 0.5 - 6.2 kip, applied upward, with a sinusoidal wave shape. The specimen was examined at regular intervals for cracking using dye penetrant.

The test consisted of three trials. In Trial 20-1, the specimen was cycled without retrofit to initiate cracks. Trial 20-2 was aimed at testing the efficacy of the angles-with-plate retrofit. In this trial, the retrofit was installed at the bottom web-gap when crack length reached 1-1/4 in. on the north side of the stiffener and 1/4 in. on the south side of the stiffener. The girder was loaded

monotonically every 25,000 cycles by slowly increasing the actuator force from 0 - 6 kip while recording actuator force, actuator displacement, LVDT data, and strain gage data (these loadings are referred to as “monotonic tests”). The retrofit was removed every 100,000 cycles to measure crack lengths at the web-gap, and then reinstalled. 1,200,000 cycles were applied in Trial 20-2. In Trial 20-3, the retrofit was removed and the cracks were allowed to grow freely. Measurements were taken using the mirror array in both the retrofitted and unretrofitted conditions to evaluate the efficacy of the retrofit.

Chapter 3 Physical Test of 20-Deg. Skewed Girder-to-Crossframe Connection – Test Results

3.1 Crack Initiation and Propagation

3.1.1 Cracks at Girder Bottom Web-Gap

Cracks were observed in the bottom web-gap region of the 20-deg. specimen 16,504 cycles into Trial 20-1. They grew vertically along the girder web-stiffener weld. When the cracks were detected, they were 1-1/4 in.-long on the north side of the stiffener and 1/4-in. long on the south side of the stiffener. The north side was the side that the skewed crossframe formed an obtuse angle with the girder web.

The angles-with-plate retrofit was installed immediately after cracks were observed. In Trial 20-2, the retrofit was removed to examine the cracks every 100,000 cycles. The crack propagation rate was slowed dramatically with the retrofit in place. After 1,200,000 cycles had been applied in Trial 20-2, the cracks had grown to approximately 1.6 in. on the north side of the stiffener and 1 in. on the south side of the stiffener, as shown in Figure 3-1.

In Trial 20-3, the retrofit was removed, and the cracks were allowed to grow freely. The crack propagation rate increased again, and the crack lengths reached 4-1/4 in. on the north side and 2.8 in. on the south side over just 20,000 cycles.

Throughout the test, cracks propagated vertically along both weld lines connecting the girder web and the stiffener, but never propagated into the girder web.

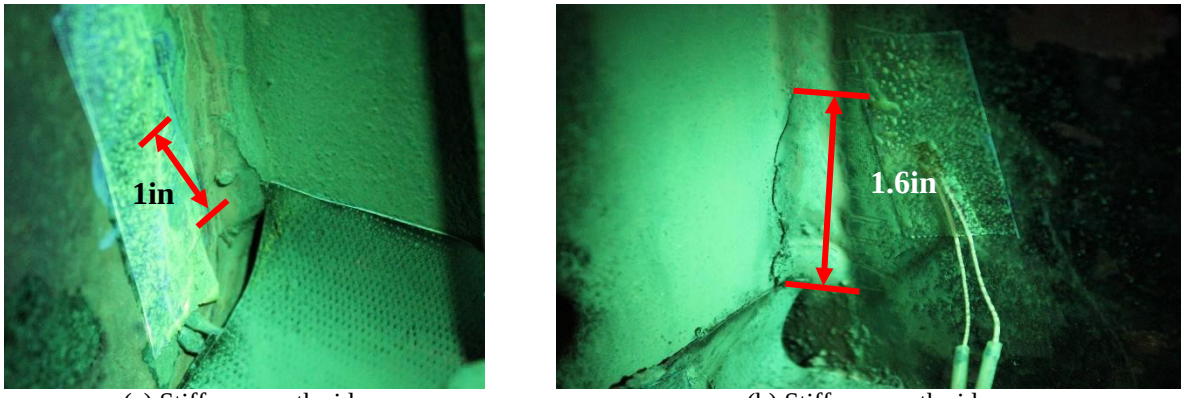

(a) Stiffener south side (b) Stiffener north side

Figure 3-1: Cracks at bottom web-gap for 20-deg. skewed specimen 1,200,000 cycles into Trial 20-2

3.1.2 Cracks on Crossframe

The crossframe was not considered to be sensitive to fatigue since crossframe cracking has rarely been reported. However, unexpectedly, the crossframe failed four times in Trial 20-2. 697,000 cycles into Trial 20-2, the actuator displacement interlock was triggered. After inspecting, a crack was observed at the junction of the crossframe angle and the bottom gusset plate. As presented in Figure 3-2, when it was observed, the crack had already cut through the vertical leg of the angle. The exact time of the crack initiation was unknown. However, initiation occurred near this cycle count since the girder had been inspected just 22,000 cycles earlier and the crack was not observed. After the crack was detected, a steel angle was bolted as a retrofit on the damaged crossframe, as shown in Figure 3-2. However, it was not able to provide enough stiffness and was unable to stop the crack growth. The crack propagated through the remainder of the crossframe member in less than 100,000 cycles.

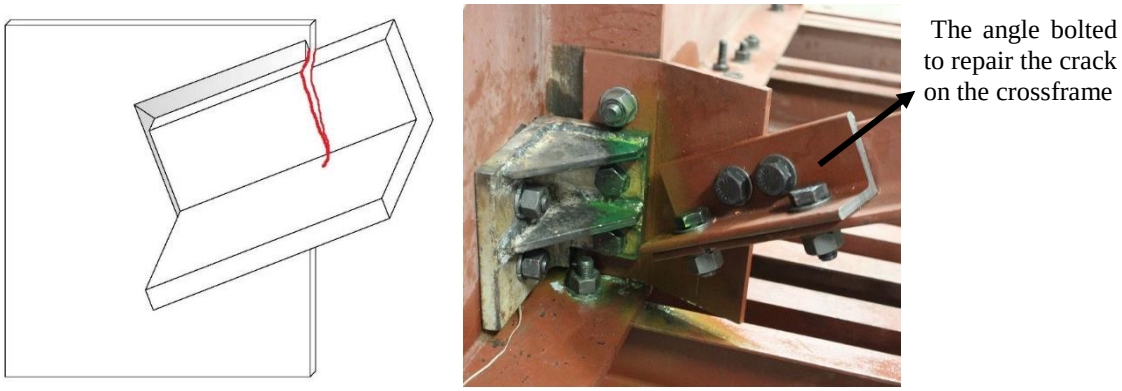

Figure 3-2: Crack on 20-deg. skewed crossframe 697,000 cycles into Trial 20-2, and the bolted steel angle used to repair it

775,000 cycles into Trial 20-2, a large crack was observed on the bottom gusset plate of the crossframe (Figure 3-3). The crack propagated along the crossframe angle-to-gusset plate weld.

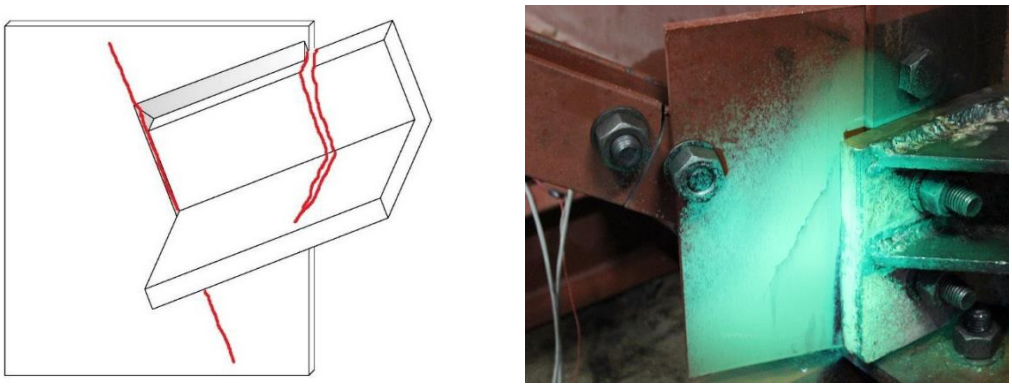

Figure 3-3: Cracks on 20-deg. skewed crossframe 775,000 cycles into Trial 2

A plate was then attached to the cracked gusset plate so that test could continue. 875,000 cycles into Trial 20-2, a bolt on the steel angle used to repair the crack on the crossframe failed in shear, as shown in Figure 3-4. When it was noticed, the bolt had already failed entirely. The crack on the gusset plate continued growing and extended beyond the attached plate. The test continued after replacing the bolt and plate. However, after 22,000 cycles (897,000 cycles into Trial 2), the bolt failed again at the same location.

Figure 3-4: Shear failure of the bolt connecting the steel angle and crossframe

As presented in Figure 3-5, a decision was made to grind/weld the cracks on the crossframe, as well as to bolt the angle and the plate, and more bolts were added on the crossframe retrofit angle. The test continued, and no more problems occurred in the crossframe for the remainder of the test.

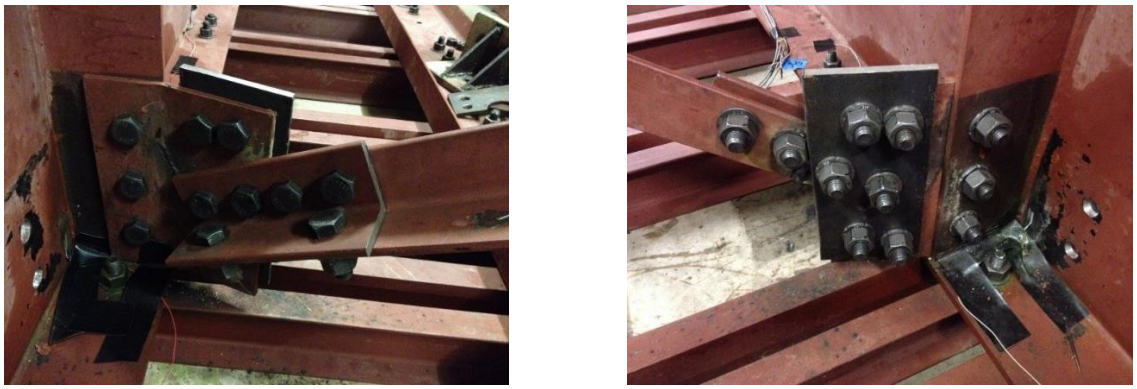

Figure 3-5: Crossframe after re-welding and repair

3.1.3 Bottom Web-Gap Crack Growth

Figure 3-6 depicts the propagation of the bottom web-gap crack versus the number of applied cycles. In the retrofitted trial, the growth rates were extremly small compared with the rates in the unretrofitted trials. In the unretrofitted trials, the crack growth rates in the south bottom and north bottom web-gap regions were 58.2 and 106.2 in. per million cycles, respectively, while in the retrofitted trials, the crack growth rates were only 0.6 and 0.3 in. per one million cycles.

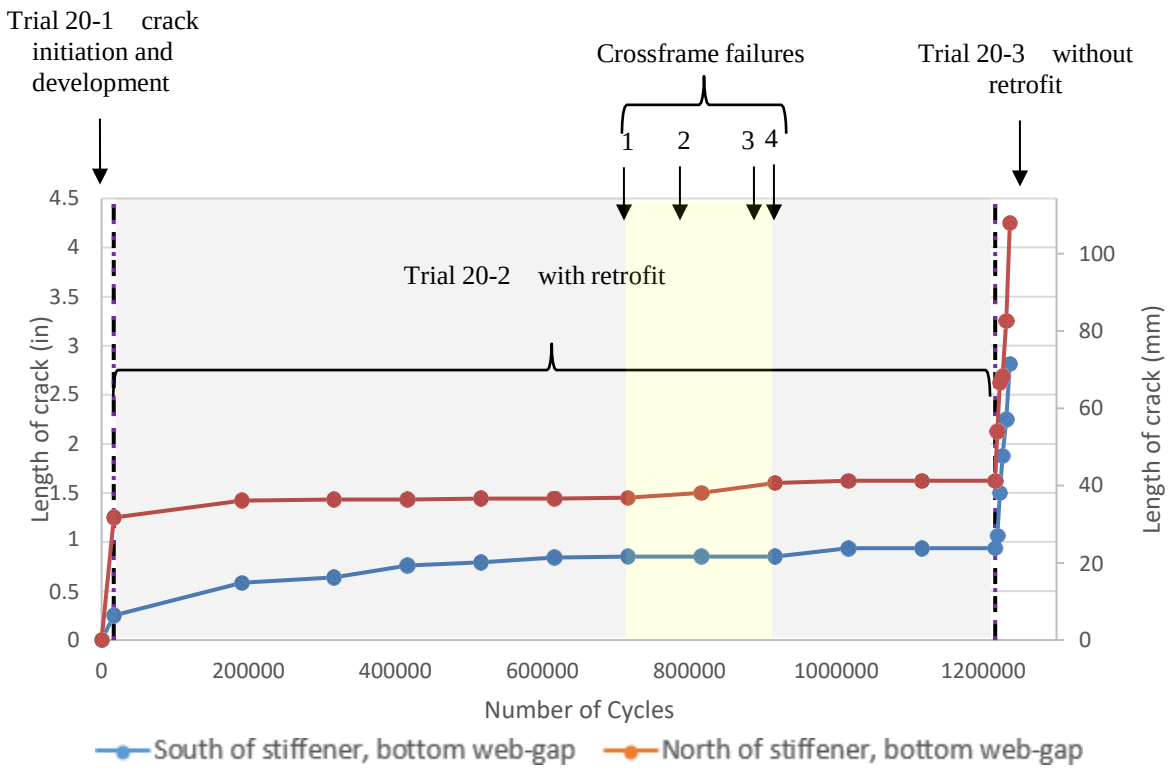

Figure 3-6: Crack propagation vs. number of applied cycles for 20-deg. skewed specimen

Explained below, the notations 1, 2, 3, and 4 in Figure 3-6 corresponded to the four failures of the crossframe.

1. A crack was observed at the junction of the crossframe angle and the bottom gusset plate. A steel angle was bolted on the crossframe to repair the damage.
2. A large crack was observed on the gusset plate of the crossframe along the weld connecting the crossframe angle to the gusset plate. A plate was then bolted to the gusset plate to strengthen it.
3. The bolt used to repair the damaged crossframe angle cracked in shear. The broken bolt was replaced with a new one.

4. The bolt used to repair the damaged crossframe failed. A decision was made to grind/weld the cracks on the crossframe as well as to bolt the angle and the plate. More bolts were added to strengthen the connection.

3.2 Actuator Displacement

Actuator displacement was examined because of possible insights into the relative flexibility of the specimen with and without the angles-with-plate retrofit installed, including potential indication of softening of the connection as cracks initiated and propagated. Figure 3-7 presents the measured actuator displacement versus the number of cycles for the test of the 20-deg. skewed specimen.

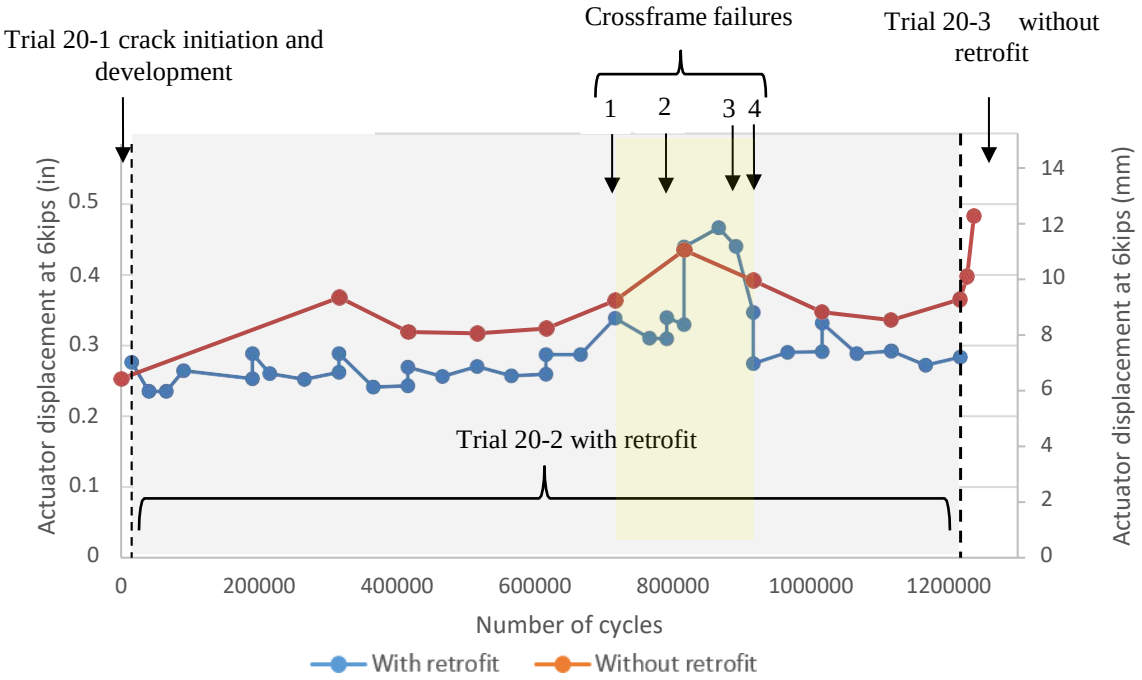

Figure 3-7: Actuator displacement at 6 kip of actuator force for the 20-deg. skewed specimen

Ignoring the period in which the crossframe was broken, the retrofit increased the connection stiffness approximately 26%, on average.

The actuator displacement increased and become abnormal during the period in which the crossframe was broken. The angle and the plate bolted on the crossframe were not able to provide enough stiffness, thus the behavior of the damaged crossframe governed the actuator displacement. This phenomenon ended after the cracks on the crossframe were welded.

In Trial 20-3, the growth of cracks in the web-gap region led to an increase in the actuator displacement. The connection stiffness decreased 25% over 20,000 cycles. Compared to the beginning of the test, the connection stiffness decreased approximately 47.6%.

3.3 Stress

Figure 3-8 and Figure 3-9 present the strain gage readings at 6 kip of actuator force. The strain gage data were recorded during the intermittent monotonic tests. In Trial 20-2, the retrofit was removed every 100,000 cycles to examine the crack length. At that time, the readings made without the retrofit in place were recorded. The strain gages were fragile, especially those underneath the retrofit. That is why only a few of the gages on the lower part of the girder web were available for measurement after retrofitting.

Stresses on the upper part of the girder web (strain gages 4, 7, 8) were insensitive to the retrofit status and crack growth. However, stresses on the lower part of the specimen (strain gages 1, 2, 3, 5, 6) were very sensitive to the retrofit. When the retrofit was not attached, the length of cracks significantly influenced the stresses in the lower region. They changed dramatically with respect to the number of cycles. In Trial 20-3, while the specimen was cycled without the retrofit installed, the stresses in the lower region changed significantly. Even the stresses obtained from strain gages 9 and 10, which were located on the crossframe, were clearly affected by the growth of cracks.

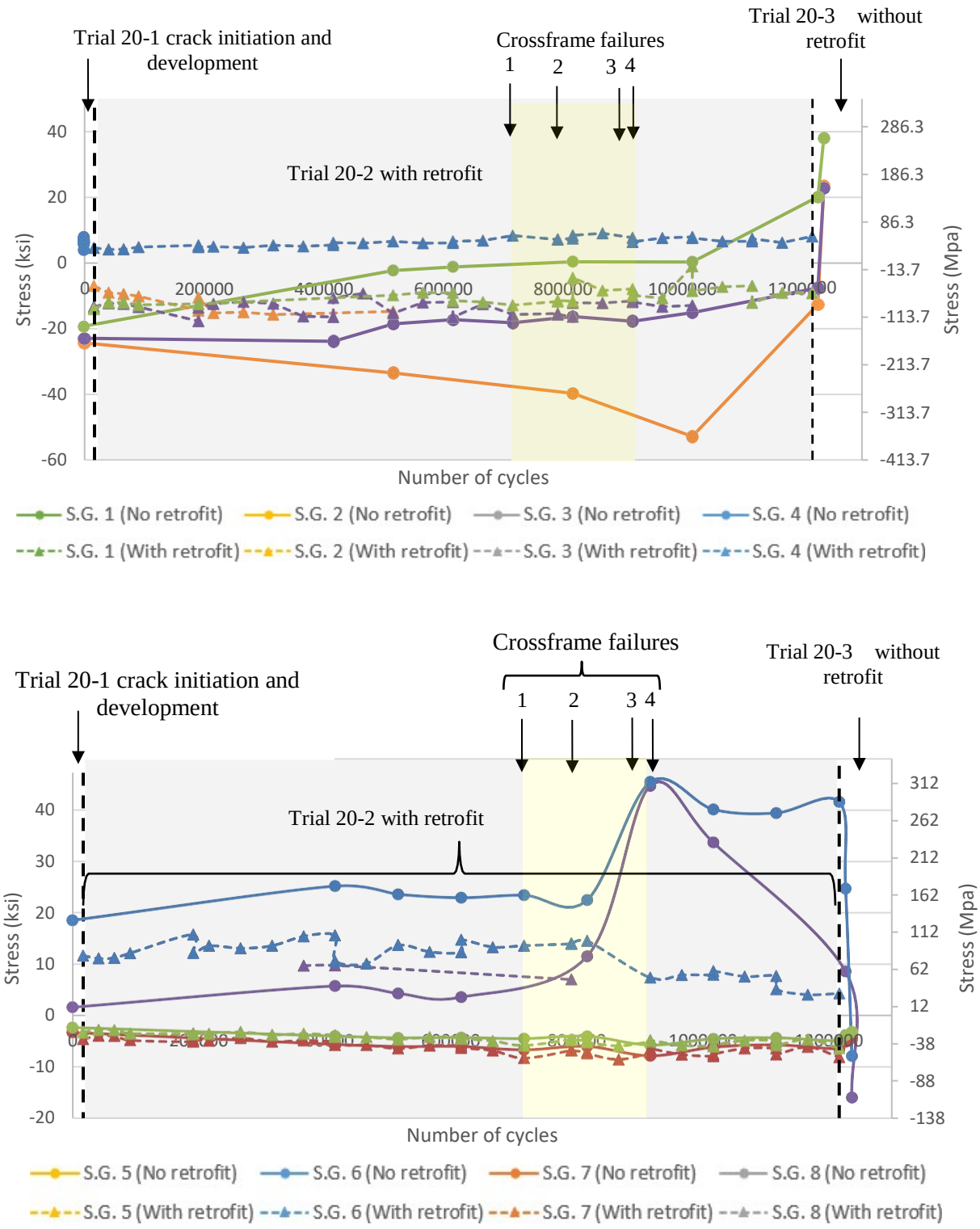

Figure 3-8: Stresses computed from strain gages placed on girder web at 6 kip actuator force for 20-deg. skewed specimen

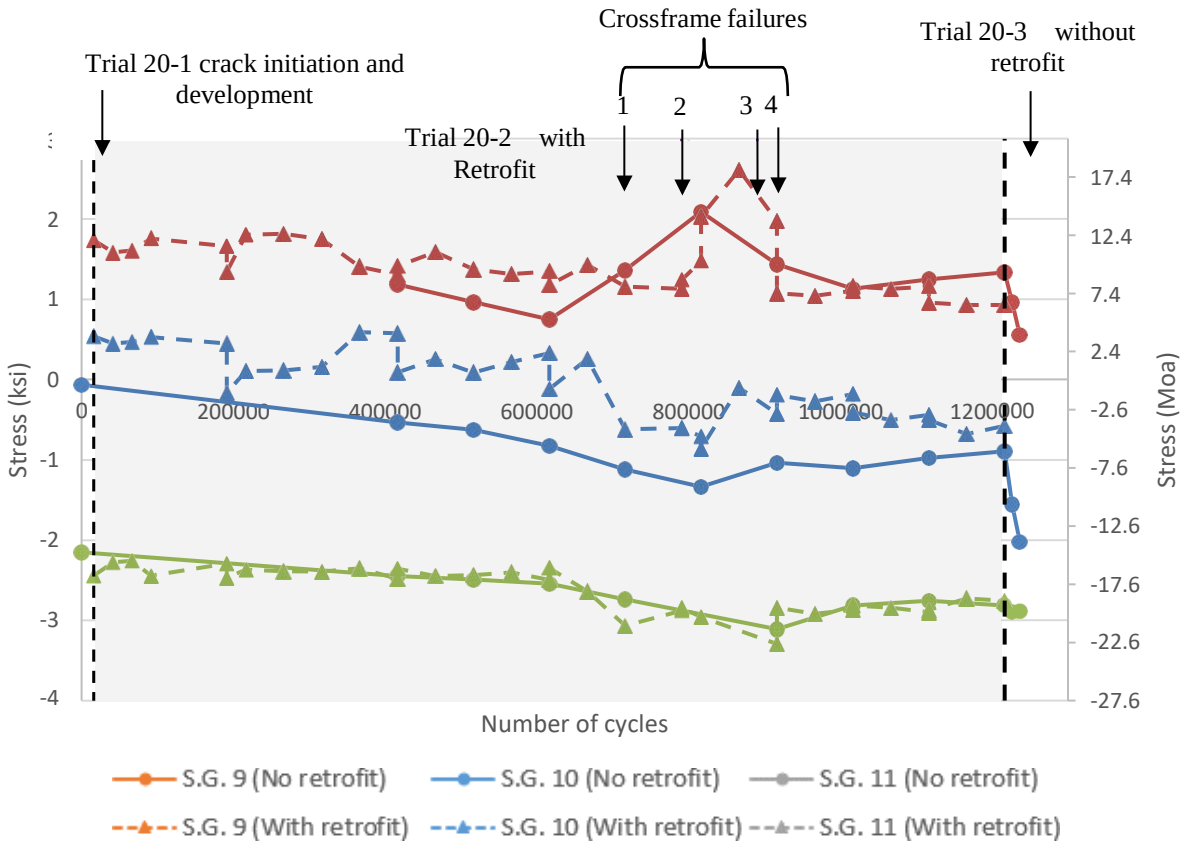

Figure 3-9: Stresses measured by strain gages placed on crossframe at 6 kip actuator force for 20-deg. skewed specimen

3.4 LVDT

The LVDT placements are shown in Figure 2-5. Figure 3-10 shows that the retrofit significantly reduced local deformations in the web-gap region. LVDT 1, located 1 in. above the bottom flange, showed a 94% decrease in out-of-plane deformations after retrofitting.

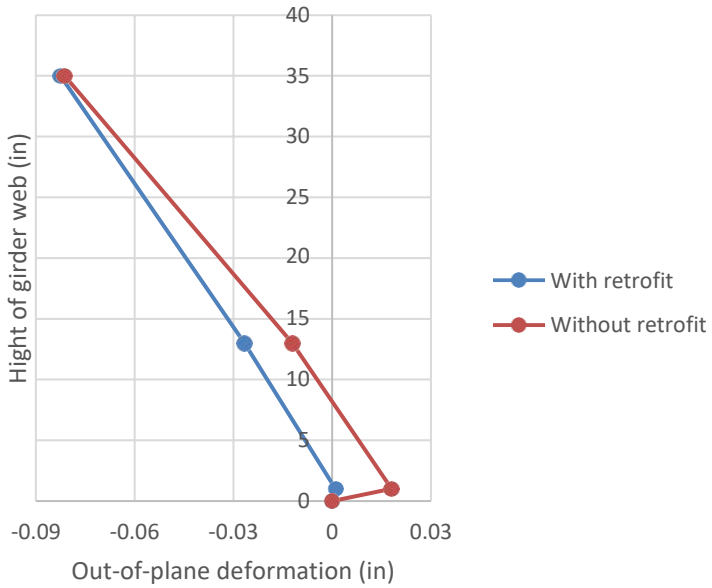

Figure 3-10: LVDT readings for 6 kip of actuator force for 20-deg. skewed specimen

3.5 Mirror Array Measurements

The results presented in this section were calculated from the data gathered at the end of Trial 20-2 (with retrofit) and the beginning of Trial 20-3 (without retrofit).

3.5.1 Girder Web Rotation

As discussed in Section 2.2, the girder web rotation can be calculated using Equation 2-1:

$$\alpha = \frac{\Delta}{2L} \qquad \text{(Equation 2-1)}$$

where:

α = Girder web rotation angle

Δ = Distance of laser point movement on the measurement wall

L = Distance from the mirror to the measurement wall

Created using Matlab 2014a, the contour plots of the rotations about Y-axis and X-axis are presented in Figure 3-11 and Figure 3-12, respectively. In these figures, the rectangular borders correspond to the edges of the girder web. Data were not recorded in the blank areas of

the figures. Data were not recorded near the girder ends since it was not a region of high interest. Data in the regions near the bottom of the girder web could not be measured, as the steel channels connecting the specimen to the floor interfered with the laser sight-line.

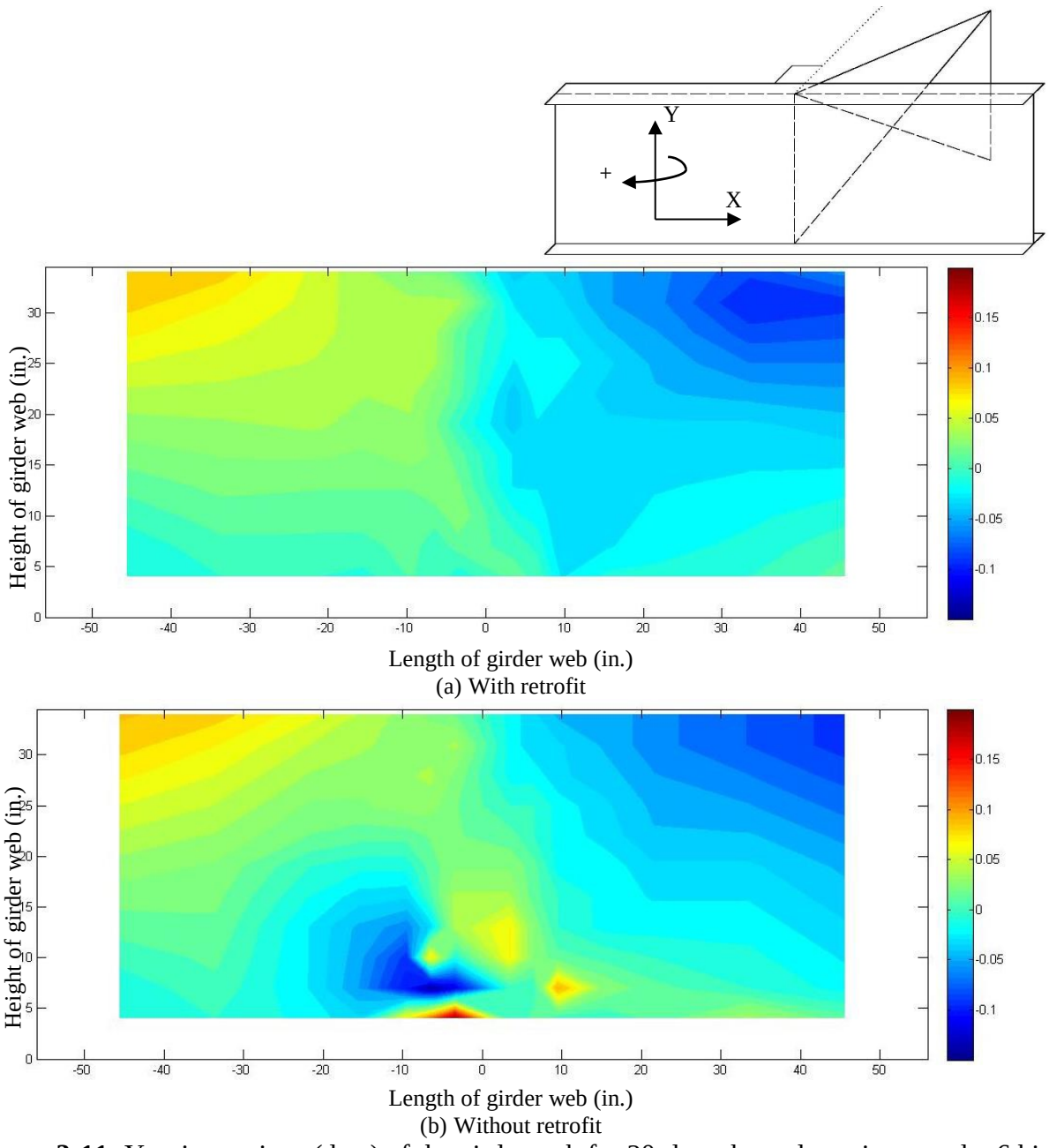

Figure 3-11: Y-axis rotations (deg.) of the girder web for 20-deg. skewed specimen under 6 kip of actuator force, computed from the mirror array measurements

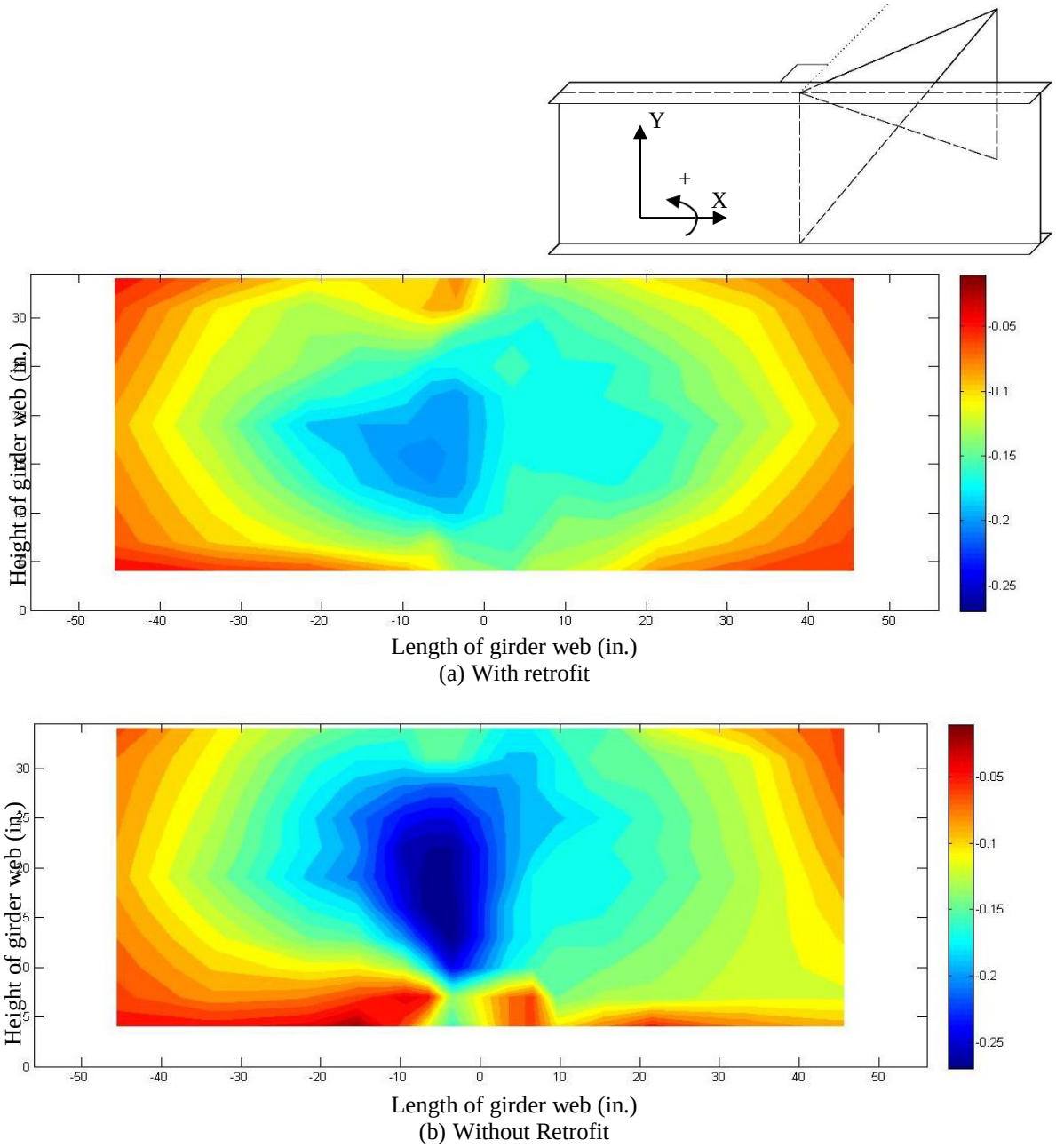

Figure 3-12: X-axis rotations (deg.) of the girder web for 20-deg. skewed specimen under 6 kip of actuator force, computed from the mirror array measurements

3.5.2 Approximated Stress Calculated from Girder Web Rotation

A method for calculating girder web stresses from girder web rotations was described by Bonet (2014). As depicted in Figure 3-13, assuming that stress and deformation are zero at the

center layer of the girder web thickness, then stress at the surface of the girder web can be derived as the following:

$$\sigma = \varepsilon \cdot E = \frac{\Delta d}{d} \cdot E = \frac{R \cdot \Delta\alpha - r \cdot \Delta\alpha}{d} \cdot E = \frac{\Delta\alpha}{d} \cdot (R - r) \cdot E = \frac{\Delta\alpha}{d} \cdot \frac{t}{2} \cdot E \qquad \text{(Equation 3-1)}$$

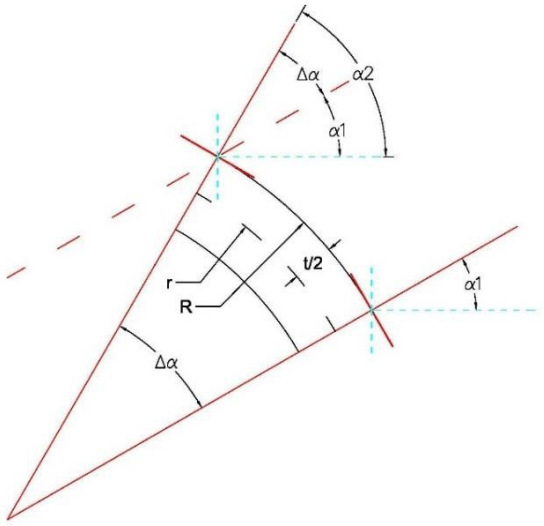

Figure 3-13: Calculating approximate girder web stress from web rotation

Then approximated stresses can be expressed as:

$$\sigma = \frac{\Delta\alpha}{d} \cdot \frac{t}{2} \cdot E \qquad \text{(Equation 3-2)}$$

σ = Stress

t = Thickness of girder web

$\Delta\alpha$ = Rotation angle difference between two mirrors

E = Elastic modulus of steel

d = Distance between two mirrors

For calculating stresses in the X and Y directions, Equation 3-3 and Equation 3-4 were used:

$$\sigma_x = \frac{\Delta\alpha_y}{d_x} \cdot \frac{t}{2} \cdot E \qquad \text{(Equation 3-3)}$$

$$\sigma_y = \frac{\Delta\alpha_x}{d_y} \cdot \frac{t}{2} \cdot E \qquad \text{(Equation 3-4)}$$

Equation 3-2 was derived by assuming the center layer of the web thickness was the neutral layer where deformations and stresses were zero (pure bending). Any stresses caused by axial elongations in the X and Y directions and rotations about the Z-axis (in-plane bending) were neglected (Figure 3-14). In this test, the bottom flange of the girder was restrained by the lab floor so that rotations about the Z-axis were largely eliminated, and since loads were only applied on the far end of the crossframe, elongations in the X and Y directions of the girder web were negligible. The method described is reasonable for estimating the stress distribution for this specific test setup. However, it may not be applicable in some other cases.

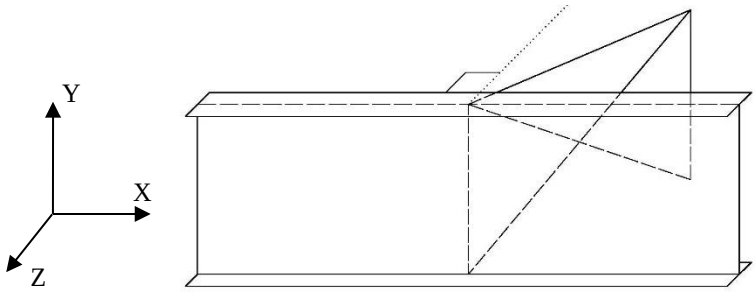

Figure 3-14: Specimen coordinate system

The approximated stresses in X and Y direction are presented in Figure 3-15 and Figure 3-16. The coordinate origin of the calculated stress was set as the center of the two mirrors. The contour plots were created using Matlab 2014a.

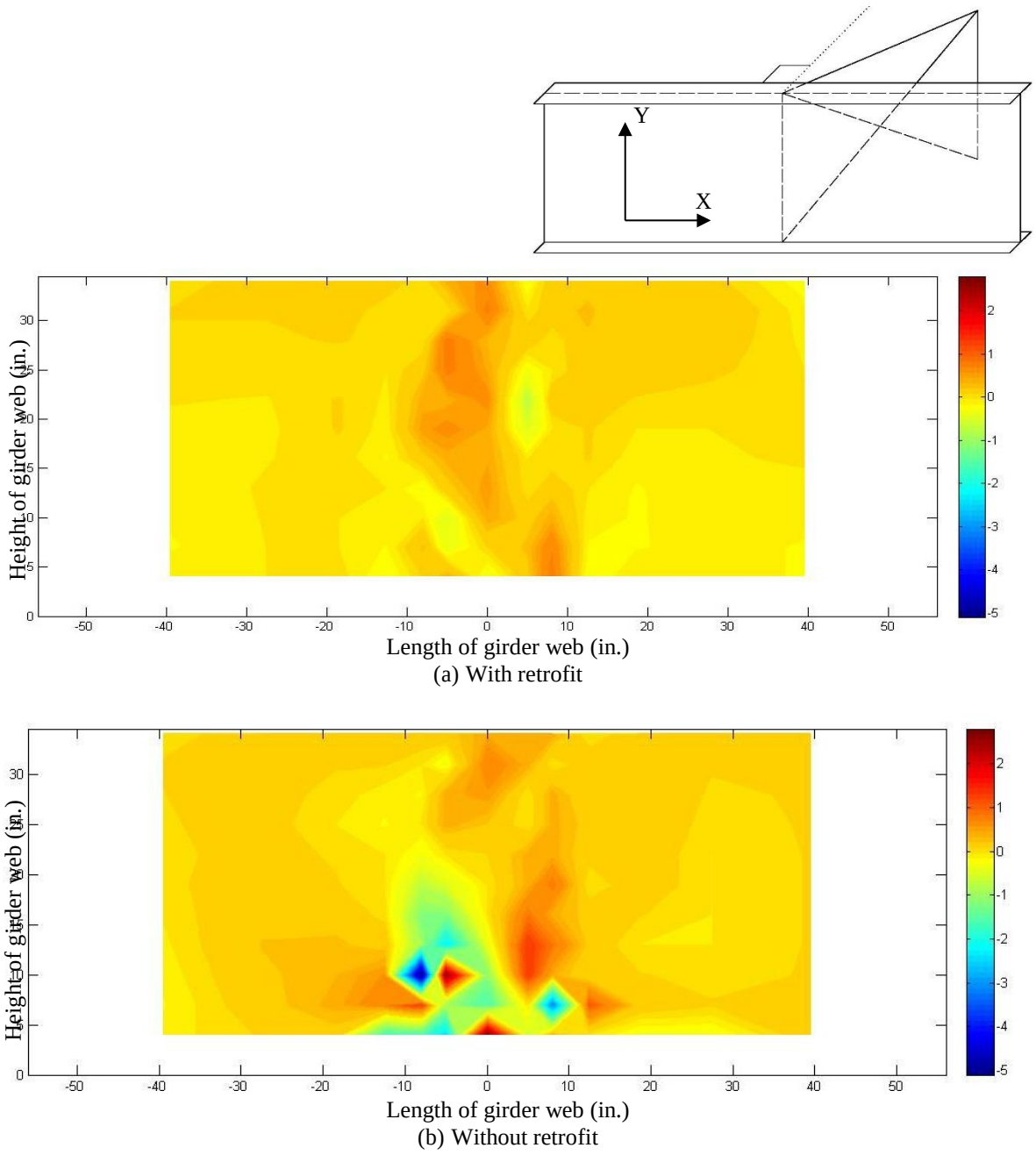

Figure 3-15: Approximated stress (ksi) in the girder web in X direction for 20-deg. skewed specimen under 6 kip of actuator force, computed from the mirror array measurements

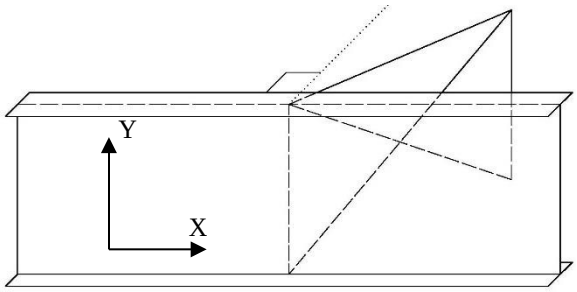

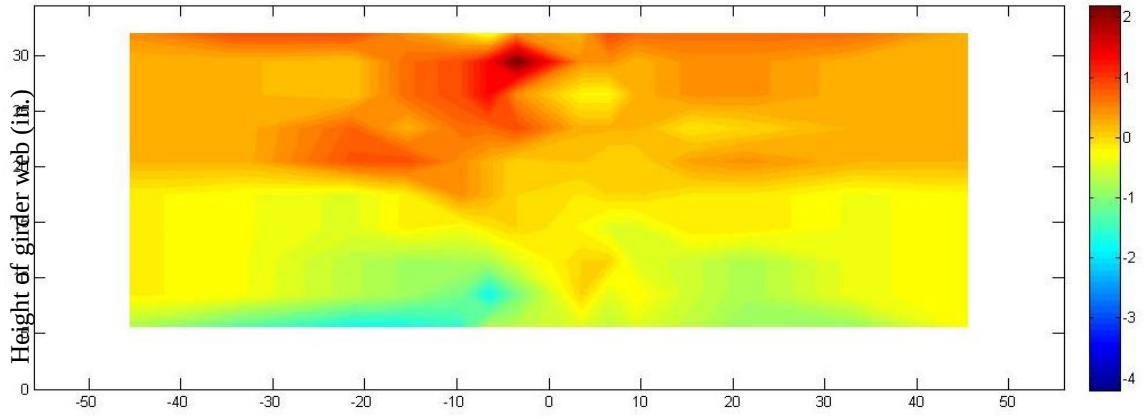

(a) With retrofit

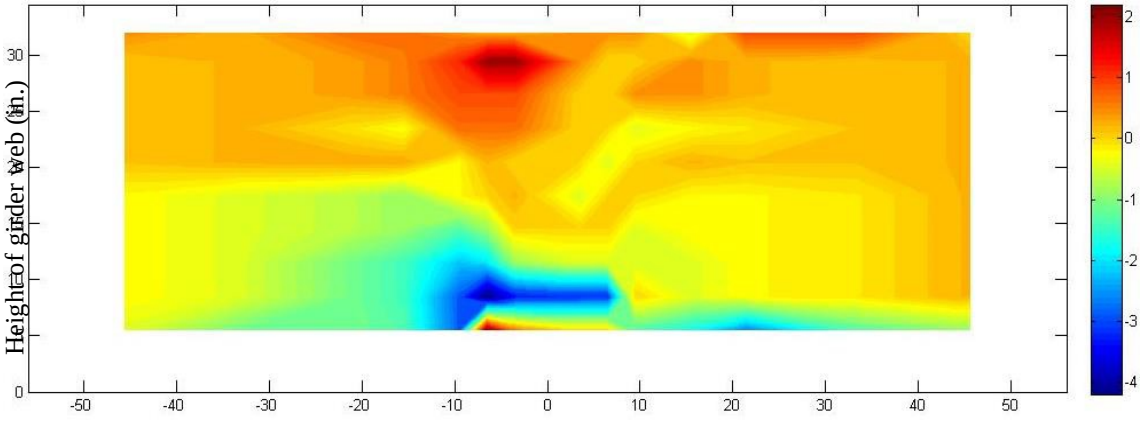

(b) Without retrofit

Figure 3-16: Approximated stress (ksi) in Y direction of the girder web for 20-deg. skewed specimen under 6 kip of actuator force, computed from the mirror array measurements

After retrofitting, the maximum tension stress in the X direction decreased 68%, and the maximum compression stress in the X direction was reduced 87%, based on computations from the mirror array measurements.

In the Y direction, the maximum compression stress was reduced 58%, but the maximum tension stress remaind nearly the same. The larger-magnitude stresses in Y direction were distributed at the top part of the girder web, therefore were not affected by the retrofit which was installed at the bottom web-gap. This finding is consistent with the strain gages measurement discussed in Section 3.3.

Since the retrofit was aimed at repairing the bottom web-gap, it might not be reasonable to analyze the results of the whole girder web. If only considering the results for the region underneath the retrofit, in the X direction, the maximum tension stress and maximum compression stress were reduced 68% and 89% respectively. In the Y direction, the maximum tension stress was reduced 99% and the maximum compression stress decreased 58%.

The results indicated that the retrofit was very effective in reducing local stresses in the damaged web-gap region.

Chapter 4 Physical Test of the 40-Deg. Skewed Girder-to-Crossframe Connection – Introduction

4.1 Description of the 40-Deg. Skewed Girder-to-Crossframe Specimen

The crossframe attached to the girder specimen described in this section was skewed 40-deg. from the position perpendicular to the girder web. This was the only difference between the 40-deg. skewed specimen and the 20-deg. skewed specimen. Other specimen details have already been introduced in Section 2.1, thus are not presented in this section.

The dimensions of the 40-deg. skewed crossframe are presented in Figure 4-1.

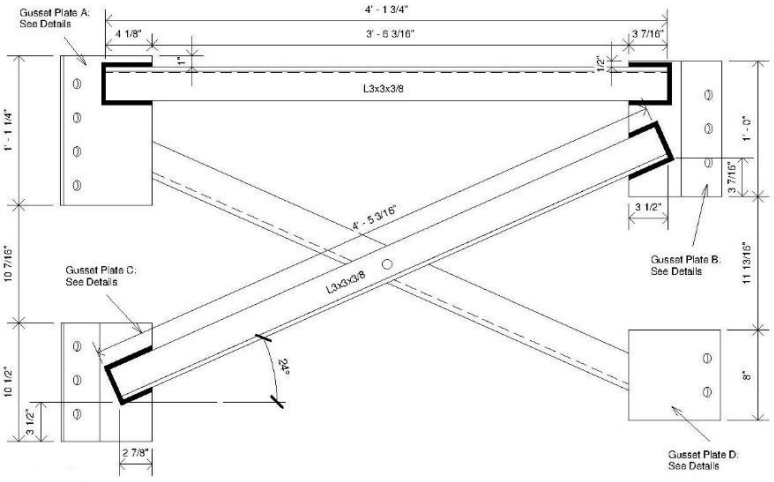

Figure 4-1: Dimensions of 40-deg. skewed crossframe

In this test, the angles-with-plate retrofits were installed in both the top and the bottom web-gap, since cracks were found in both of the two regions. The angles-with-plate retrofit used in this test had the same dimensions as the retrofit used in the 20-deg. skewed test. Figure 4-2 presents the photographs of the 40-deg. skewed specimen and test set-up.

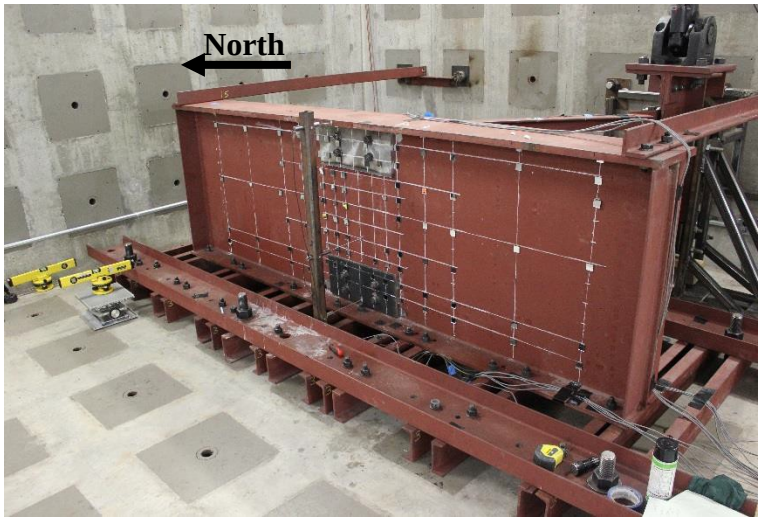

(a) Girder web fascia side

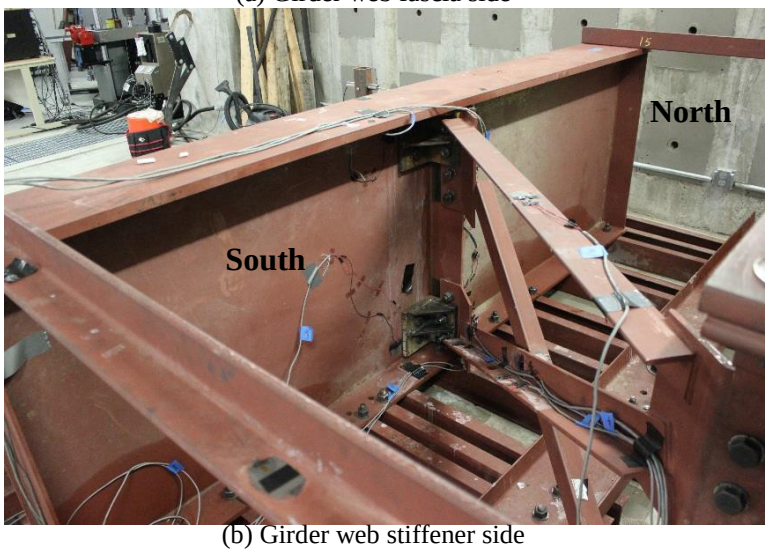

(b) Girder web stiffener side

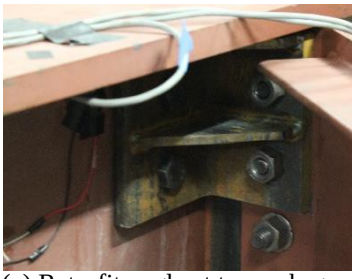

(c) Retrofit angle at top web-gap

(d) Retrofit angle at bottom web-gap

(e) WT section and restraining rollers

Figure 4-2: Photographs of 40-deg. skewed specimen with angles-with-plate retrofit installed

4.2 Instrumentation

Actuator displacement and load cell readings were collected in the test of the 40-deg. skewed system, as for the 20-deg. skewed system.

Strain gages were attached to the specimen at regions known to be susceptible to fatigue problems (bottom web-gap), to indicate the influence of the crack propagation on the stresses, and to verify the reliability of the finite element models by comparing with the stresses extracted from the models. Unlike the 20-deg. skewed test, in this test, the strain gages behind the retrofit

angles and the plates were abandoned after installing retrofit, as the strain gages were so delicate that most were broken after application of the retrofit.

Four LVDTs (Linear Variable Differential Transformers) were attached to the centerline of the girder web to measure out-of-plane deformations. Strain gage readings, LVDT readings, actuator displacement, and actuator force were recorded while performing monotonic tests. The LVDT and strain gage placements are presented in Figure 4-3.

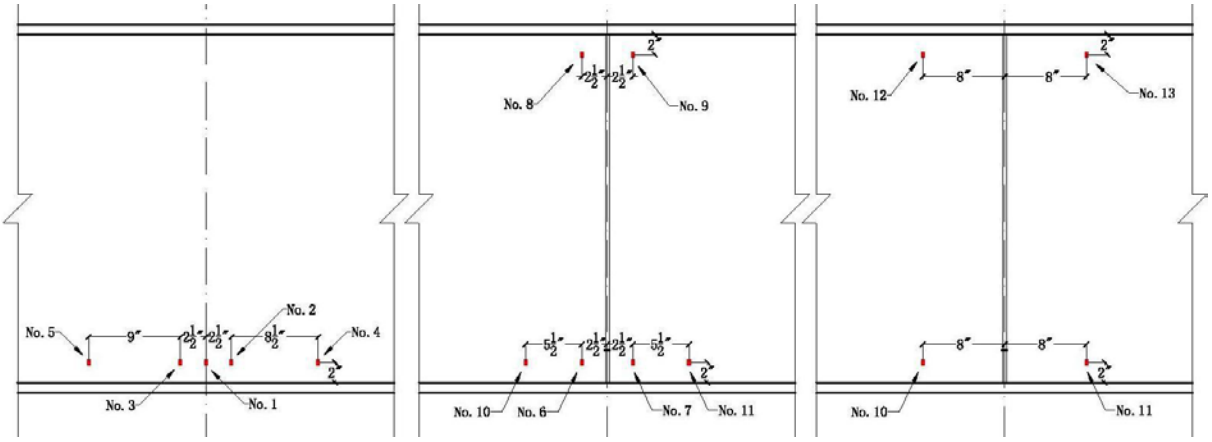

(a) Strain gages on web fascia side (Trial 1) | Before retrofit installed (Trial 1) | After retrofit installed (Trial 2 and Trial 3)

(b) Strain gages on web stiffener side

*Strain gages No.1 – No.9 were abandoned after retrofit installed.

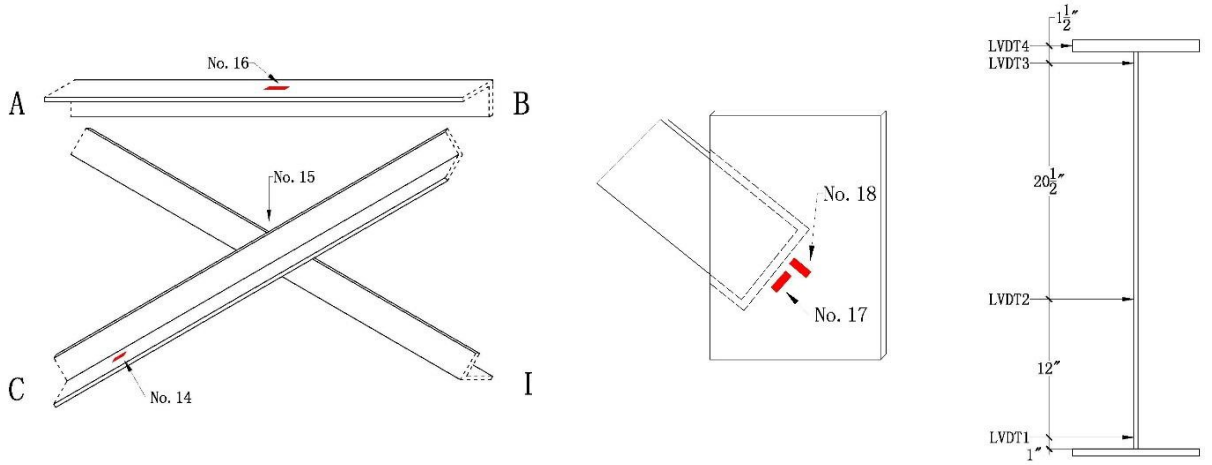

(c) Strain gages on crossframe (d) Strain gages on gusset plate C (e) LVDTs

Figure 4-3: Instrumentation of the 40-deg. skewed specimen

Section 2.2 described the mirror array and procedures used to calculate rotations and approximated stresses in the girder web. The procedures were also performed for the 40-deg.

skewed specimen. Figure 4-4 shows the placement of the mirror array used on the 40-deg. specimen. The layout was slightly different from that used in the 20-deg. skewed test. A column of mirrors was added at the centerline of the girder web in this test, while there was no mirror placed at the girder web centerline on the 20-deg. skewed specimen.

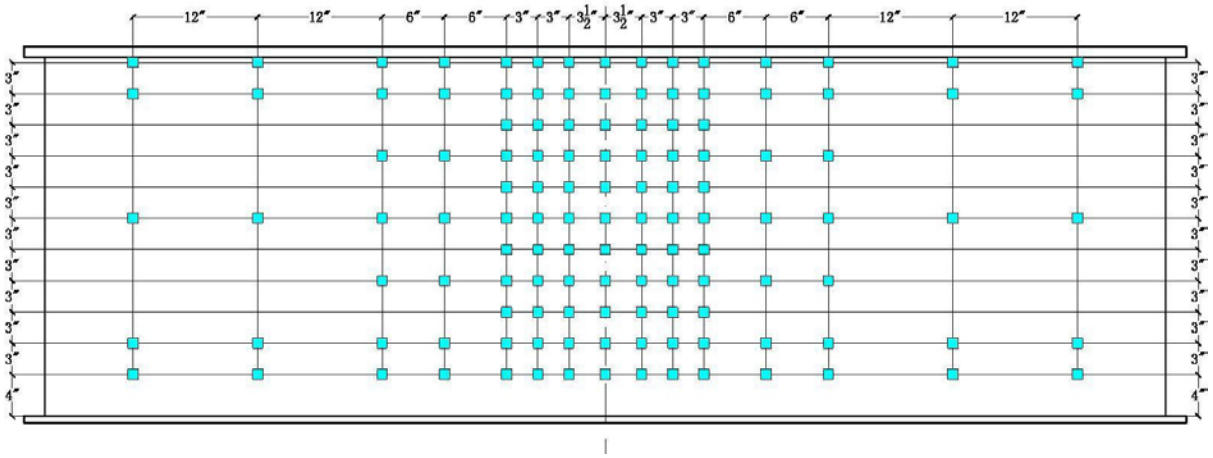

Figure 4-4: Mirror placements for 40-deg. skewed specimen

4.3 Test Procedure

Upward cyclic loading of 0-2.3 kip was provided at a frequency of 2 Hz on the 40-deg. skewed specimen. In the undamaged state, this load range generated an actuator displacement range of 0-0.27 in., which was the same as the displacement range of the undamaged 20-deg. specimen, as shown in Figure 4-5.

The cyclic load applied on the 20-deg. specimen was 0.5-6.2 kip. Load ranges are often selected to be the invariants. However, in this study, the 40-deg. specimen was much more flexible than the 20-deg. specimen. Applying the same load range would have generated an unreasonably large displacement range in the 40-deg. specimen.

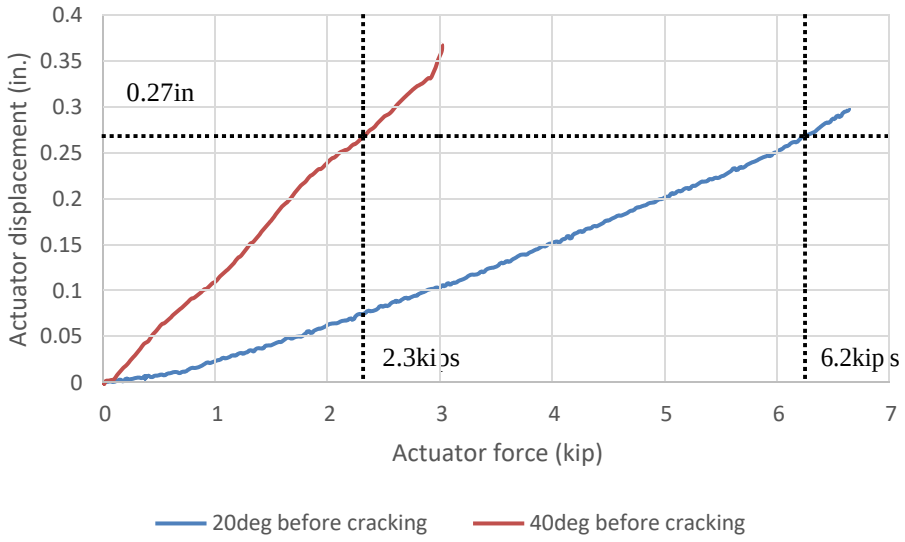

Figure 4-5: Actuator displacement vs. actuator force before specimen cracking for 20-deg. specimen and 40-deg. specimen

The specimen was regularly inspected to detect and measure cracks, using dye penetrant. Three trials were conducted in this test. In Trial 40-1, the specimen was cycled without retrofit to initiate cracks. The angles-with-plate retrofits were installed when the cracks grew to the length shown in Figure 5-1. In Trial 40-2, the specimen was cycled with the angles-with-plate retrofit installed to test the efficacy of the retrofit. Monotonic tests were conducted every 25,000 cycles, during which the actuator load was slowly increased from 0 - 2.5 kip while recording instrumentation data. The retrofit was removed at regular intervals to inspect the cracks. In Trial 40-3, the retrofits were removed to study the fatigue performance of the specimen without retrofit.

A summary of the test is presented in Table 4-1.

Table 4-1: Test summary for the 40-deg. skewed specimen

Trial	Retrofit status	Number of cycles	Total cycles
Trial 40-1	Unretrofitted	313,000	313,000
Trial 40-2	Retrofitted	1,200,000	1,513,000
Trial 40-3	Unretrofitted	1,200,000	2,713,000

Load range: 0-2.3 kip
Load frequency: 2 Hz

Chapter 5 Physical Test of 40-Deg. Skewed Girder-to-Crossframe Connection –Results

5.1 Crack Initiation and Propagation

Since the girder bottom flange was restrained to the laboratory floor while the top flange was allowed to move, the bottom web-gap region was expected to be more sensitive to fatigue than the top web-gap region. However, a 3/8 in. crack (North top 1) was first observed at the north side of the top web-gap region, 17,520 cycles into Trial 40-1 (north was the side for which the crossframe and the girder web formed an obtuse angle, as shown in Figure 4-2). The crack initiated at the top end of the weld connecting the girder web and the stiffener, and grew vertically downward along the weld.

50,000 cycles into Trial 40-1, a 1/4-in. long crack (North bottom 1) was observed on the north side of the bottom web-gap region. It initiated at the bottom end of the girder web to stiffener weld, and grew vertically upward along the weld.

215,000 cycles into Trial 40-1, a 3/16-in. long crack (South top 1) was detected at the top end of the girder web to stiffener weld, on the south side of the top web-gap region. In the south bottom web-gap region, the researchers observed some discontinuous spots shining under the fluctuating load that implied crack initiation (South bottom 1). But, the crack was so small at this point that it was very difficult to measure its length. It is worth mentioning that this crack did not initiate at the bottom end of the weld, which rarely happens in the distortion-induced fatigue tests of web-gap regions.

The angles-with-plate retrofits were installed in both the top and the bottom web-gap regions 313,000 cycles into Trial 40-1. Figure 5-1 presents a schematic drawing showing the crack lengths when the retrofits were installed.

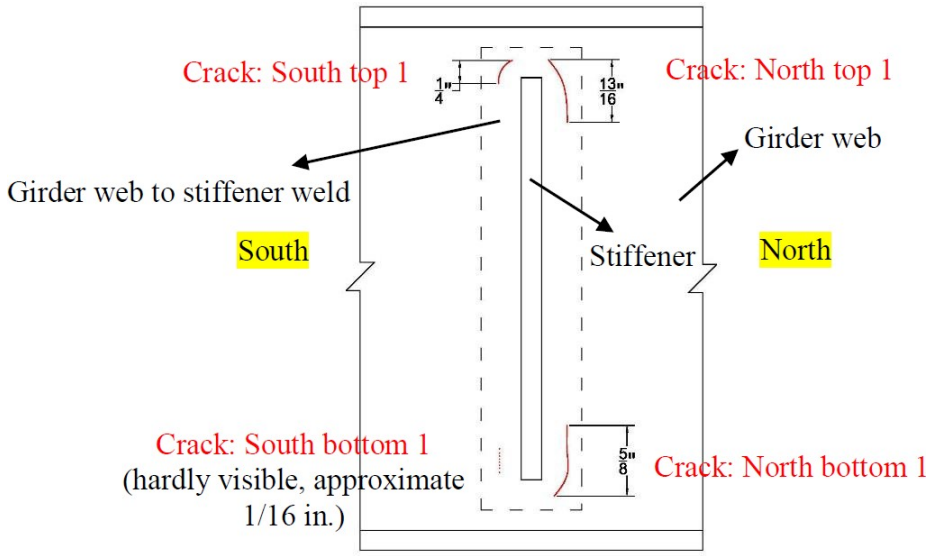

Figure 5-1: Crack pattern in 40-deg. skewed specimen 313,000 cycles into Trial 40-1

In Trial 40-2, the specimen was cycled with the angles-with-pate retrofit installed. 1,200,000 cycles were applied on the specimen in this trial. The retrofit was removed several times to inspect the cracks, and no visible crack propagation was observed.

The retrofit was removed to allow the cracks propagate freely in Trial 40-3, and 1,200,000 cycles were applied. In Trial 40-3, the cracks grew slowly and remained thin for the majority of the cycles. The crack widths did not noticeably increase until 1,050,000 cycles into Trial 40-3.

A 1/4-in. long crack (South top 2) was observed on the south side of the top portion of the stiffener 435,000 cycles into Trial 40-3. Most of the fatigue cracks reported in web-gap regions initiated at the end of the weld connecting the girder web and the stiffener, growing along the weld and then propagating into the girder web and growing horizontally. Cracking of the stiffener was an unexpected occurrence.

786,000 cycles into Trial 40-3, another 1/16-in. long crack (South top 3) was observed on the south side of the top part of the stiffener. After another 145,000 cycles, a new 3/4 in. crack (South top 4) was observed in the same region.

931,000 cycles into Trial 40-3, a 1/2-in. long crack (North bottom 2) was detected at the north bottom end of the girder web to stiffener weld. The cracks propagated into the girder web 1,050,000 cycles into Trial 40-3. A schematic showing the distribution of the cracks 1,150,000 cycles into Trial 40-3 is presented in Figure 5-2.

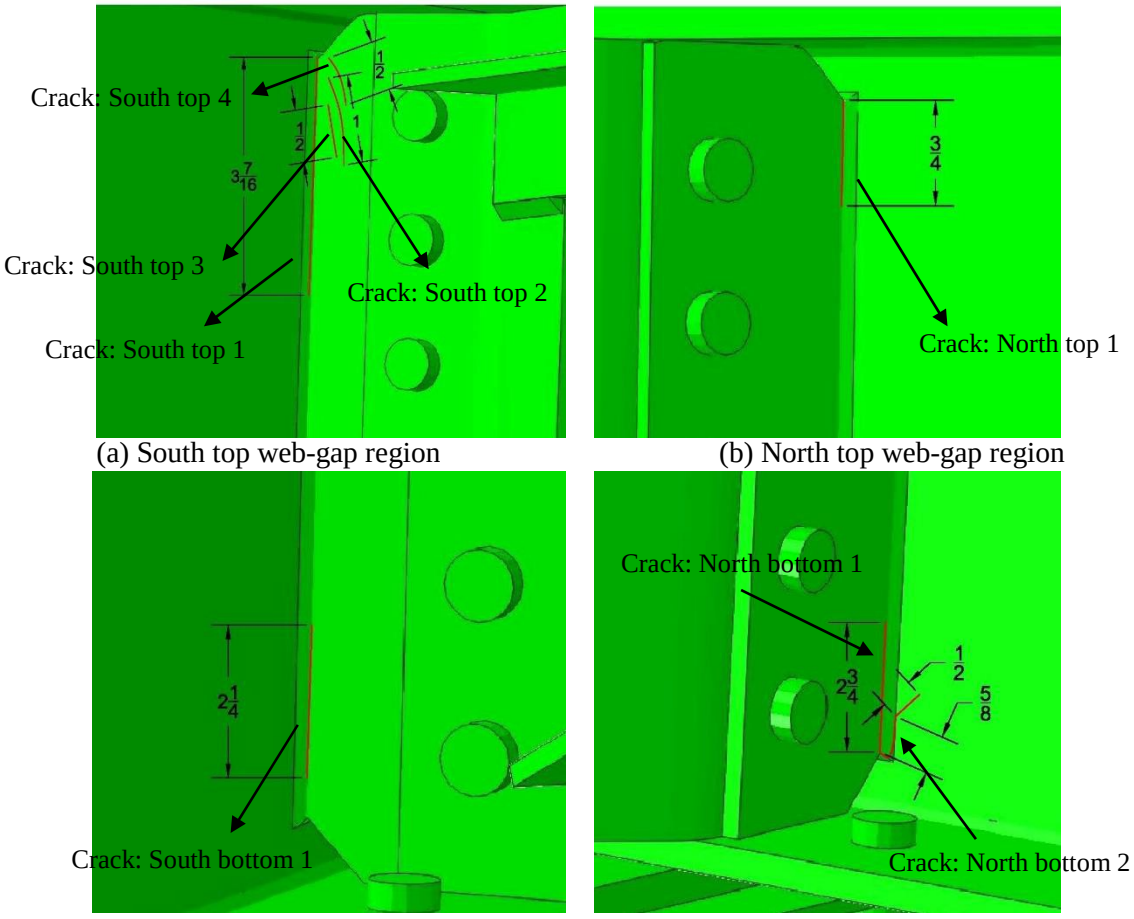

(a) South top web-gap region (b) North top web-gap region

(c) South bottom web-gap region (d) North bottom web-gap region

Figure 5-2: Cracks of 40-deg. skewed specimen 1,150,000 cycles into Trial 40-3

Photographs of the fatigue cracks 1,150,000 cycles into Trial 40-3 are presented in Figure 5-3. Cracks are shown as white lines in the photographs.

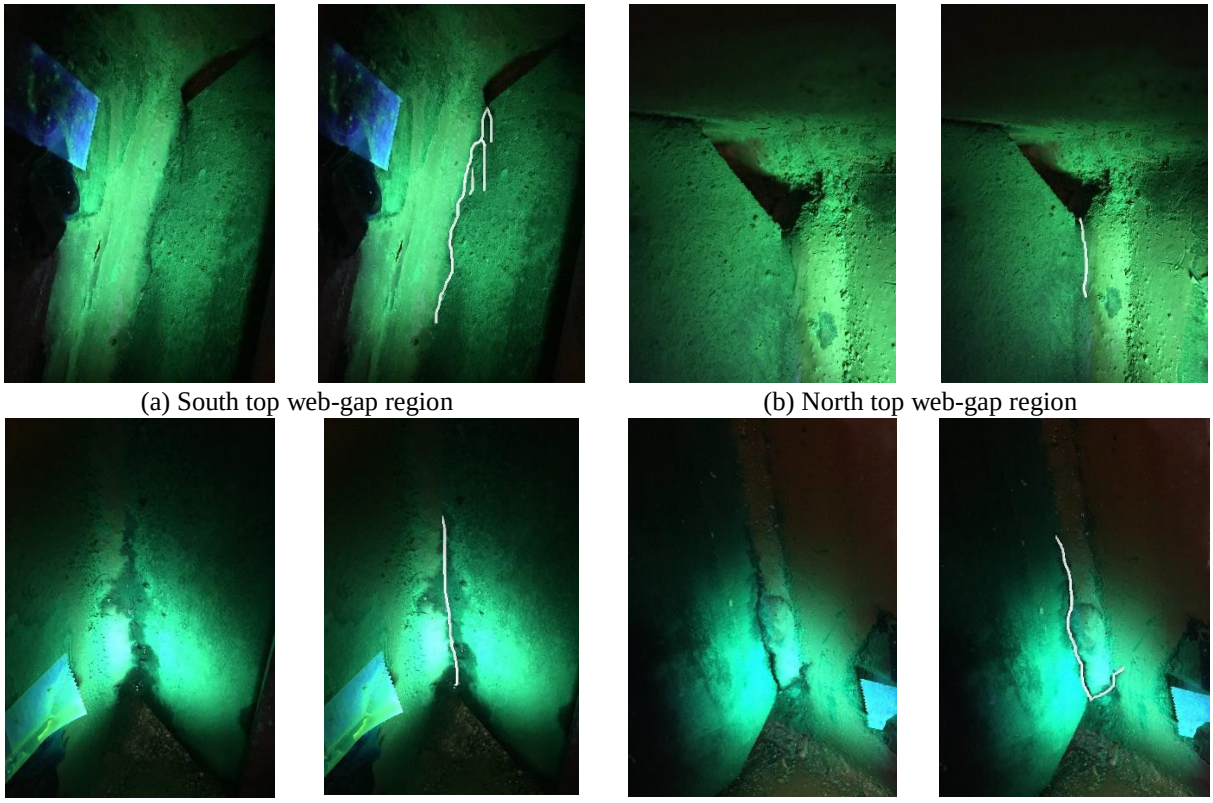

(a) South top web-gap region (b) North top web-gap region

(c) South bottom web-gap region (d) North bottom web-gap region

Figure 5-3: Cracks of 40-deg. skewed specimen 1,150,000 cycles into Trial 40-3

The cracks on the stiffener (Crack: South Top 2, 3, 4, as notated in Figure 5-2) were surface cracks and were very thin. As shown in Figure 5-4, which presents the crack initiation and propagation with respect to the number of applied cycles, propagation of the cracks on the stiffener (Crack: South Top 2, 3, 4, as notated in Figure 5-2) tended to pause after their initiation.

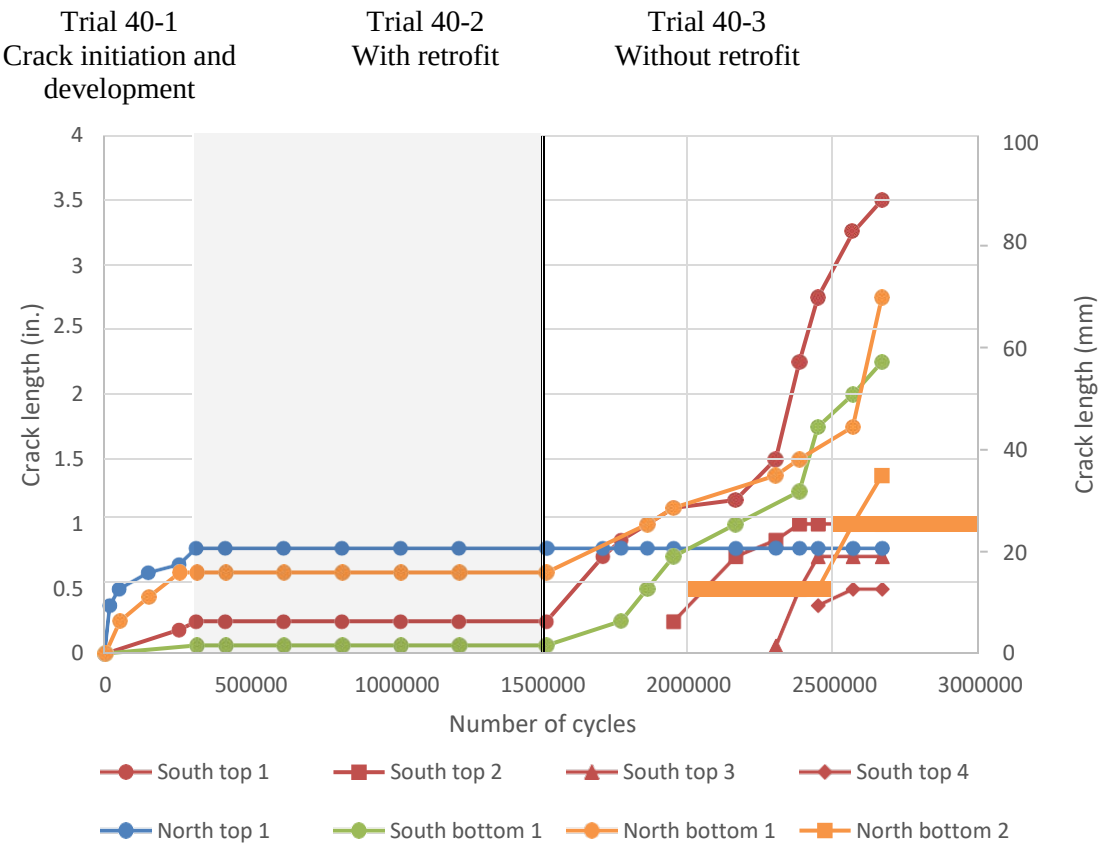

Figure 5-4: Crack propagation vs. number of applied cycles for 40-deg. skewed specimen

5.2 Actuator Displacement

Figure 5-5 presents actuator displacement at 2.5 kip of actuator force with respect to the number of applied cycles. The angles-with-plate retrofits were installed on both the top and the bottom web-gap at the beginning of Trial 40-2. After installing the retrofit, the actuator displacement decreased about 50%. In Trial 40-3, the retrofits were removed, and cracks were allowed to propagate freely. At the end of the test, the connection stiffness had decreased approximately 20% as compared with the beginning of the test.

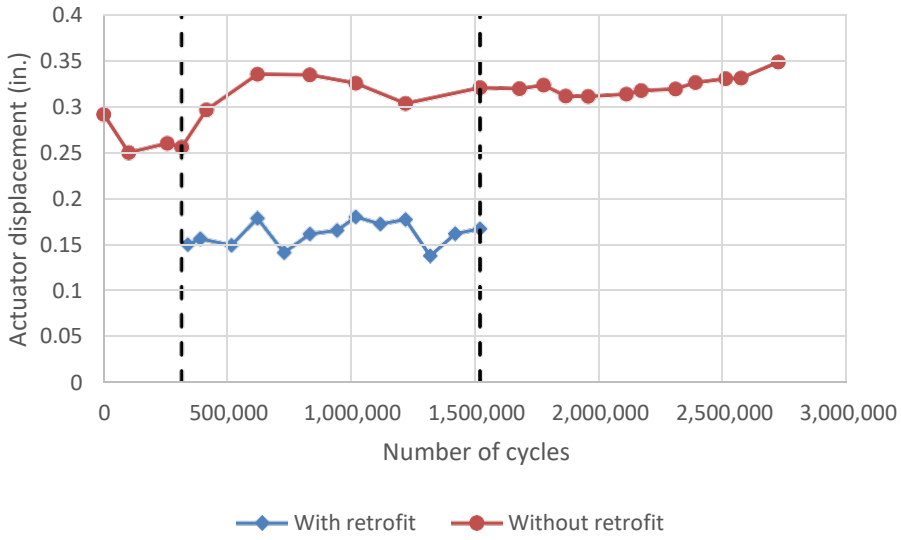

Figure 5-5: Actuator displacement vs. number of applied cycles at 2.5 kip of actuator force for the 40-deg. skewed specimen

5.3 Stress

The strain gage placements are given in Figure 4-3. Figure 5-6 presents the stresses computed from strain gages 1 - 5, which were located in the bottom web-gap region on the fascia side of the girder web. The measurements were taken at the beginning of Trial 40-1. The applied actuator load was 2.5 kip. As expected, large stress gradients existed in the web-gap region, and an unsymmetrical result was observed due to the skewed angle of the connection.

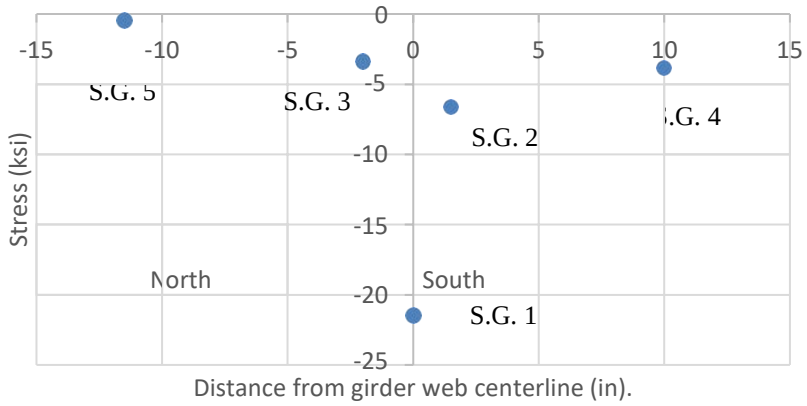

Figure 5-6: Stresses computed from strain gages 1 to 5 at the beginning of Trial 40-1 for the 40-deg. skewed specimen under 2.5 kip of actuator force

As presented in Section 3.1.2, during the test of the 20-deg. skewed specimen, the gusset plate cracked in Trial 20-2, in which the specimen was cycled with the angles-with-plate retrofit installed. Cracking of the gusset plate was unexpected, and there was a concern that it might be the retrofit that caused the gusset plate to crack. Unfortunately, this question was not able to be answered in the physical test since in the 20-deg. skewed specimen no instrumentation was applied on the gusset plate. However, the findings from the 40-deg. skewed specimen can help to address this. As shown in Figure 4-3, in the test of the 40-deg. skewed specimen, strain gages 17 and 18 were attached to the bottom gusset plate to measure the change of the stresses due to installing the angles-with-plate retrofit. Figure 5-7 presents the stresses measured by the two strain gages.

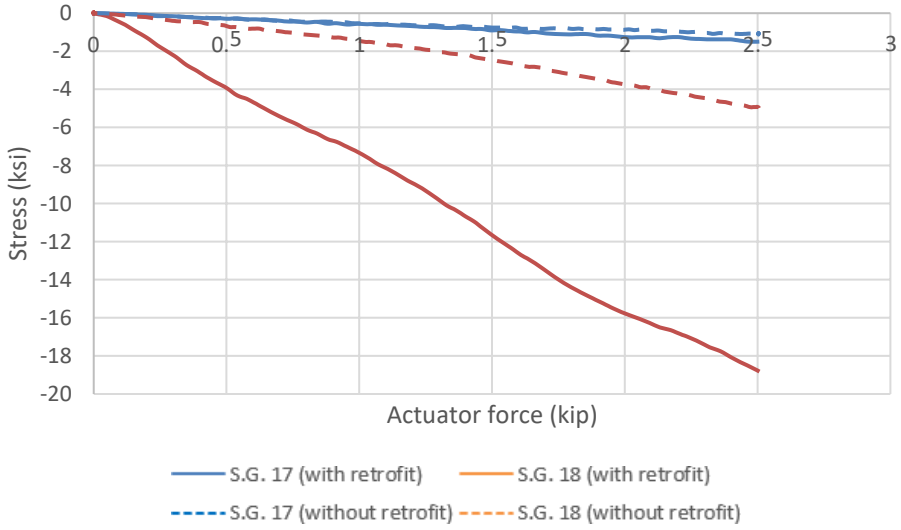

Figure 5-7: Stresses measured by strain gages 17 and 18 placed on the bottom gusset plate for the 40-deg. skewed specimen

Strain gage 17 and 18 were placed parallel and vertical to the weld connecting the crossframe angle and the gusset plate respectively. As shown in Figure 5-7, stresses computed using strain gage 17, which was placed parallel to the weld, were not significantly influenced by the retrofit states. However, the stresses computed from strain gage 18, which was placed

vertically with respect to the weld, did not increase, but significantly decreased after installing the retrofit. Based on this, it is believed that a similar phenomenon also occurred in the 20-deg. skewed specimen, and that the reason for the gusset plate cracking was because the applied load range was very large.

Figure 5-8 presents the stresses computed from strain gages 10, 11, 12, and 13 located on the connection plate side of the girder web, as shown in Figure 4-3. These strain gages were placed outside the retrofit angles. They were not effective in indicating the crack initiation and propagation since the stresses were insensitive to crack growth.

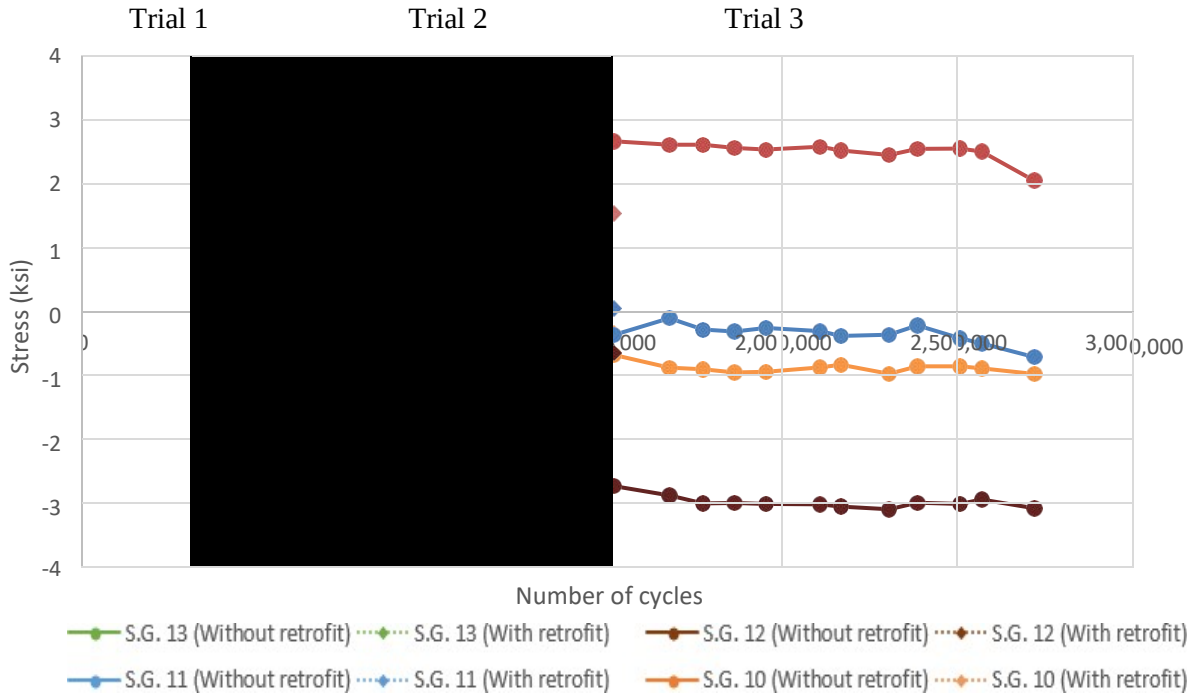

Figure 5-8: Stresses computed from strain gages 10, 11, 12, 13 vs. number of applied cycles for the 40-deg. skewed specimen under 2.5 kip of actuator force

Stresses computed from strain gages located on the crossframe are presented in Figure 5-9. The stress magnitudes deceased after the retrofit was installed. The stresses were insensitive to the initiation and propagation of fatigue cracks in the web-gap region.

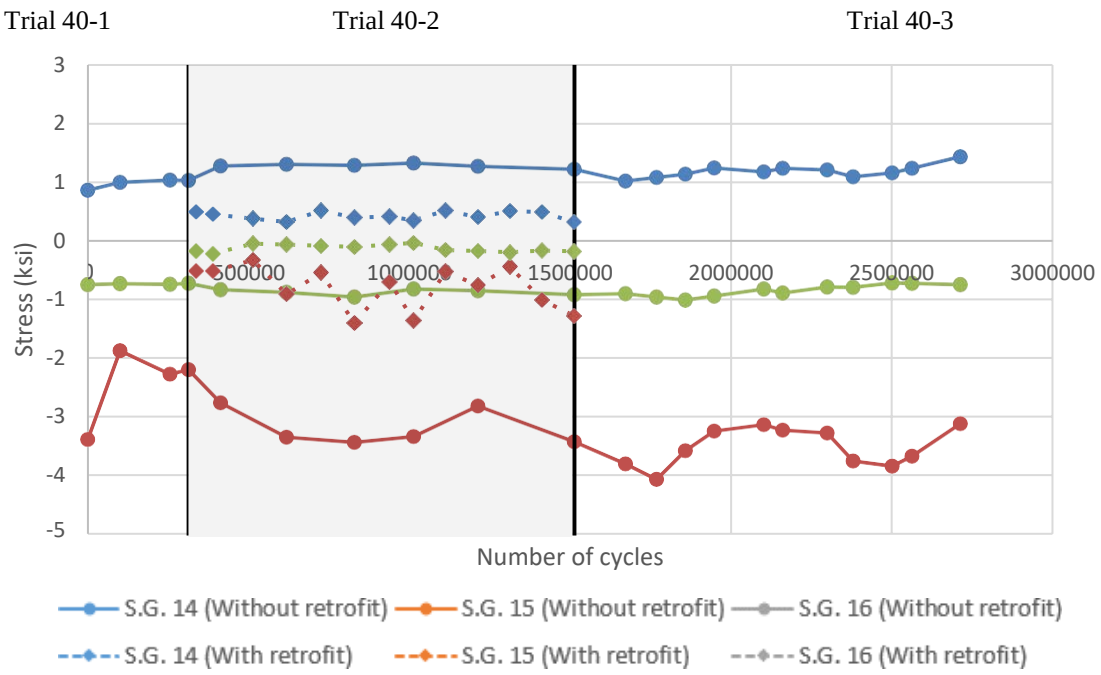

Figure 5-9: Stresses measured by strain gage 9, 10, 11 vs. number of applied cycles for the 40-deg. skewed specimen under 2.5 kip of actuator force

5.4 LVDT

Figure 5-10 presents measurements from the LVDTs for the 40-deg. skewed specimen. The placements of the LVDTs are presented in Figure 4-3. After retrofitting, the relative out-of-plane deformation at the bottom web-gap (the difference between LVDT1 and the bottom flange) was reduced 98.4%; the relative out-of-plane deformation at the top web-gap (the difference between LVDT3 and LVDT4) was reduced 75.9%.

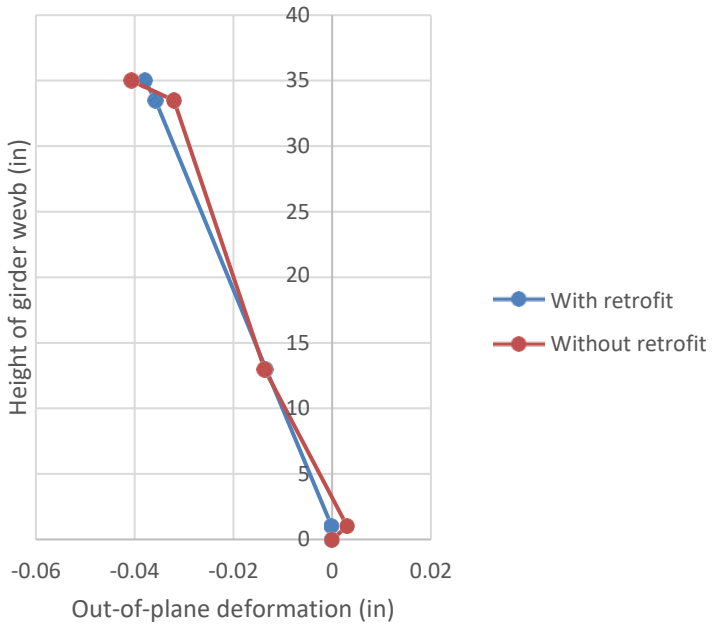

Figure 5-10: LVDT measurements at 2.5 kip of actuator force for the 40-deg. skewed specimen

5.5 Mirror Array Measurements

The results presented in this section were calculated from the data gathered at the end of Trial 40-1 (without retrofit) and the beginning of Trial 40-2 (with retrofit).

5.5.1 Girder Web Rotation

The contour plots for rotations about the girder's Y-axis and X-axis are presented in Figure 5-11 and Figure 5-12, respectively.

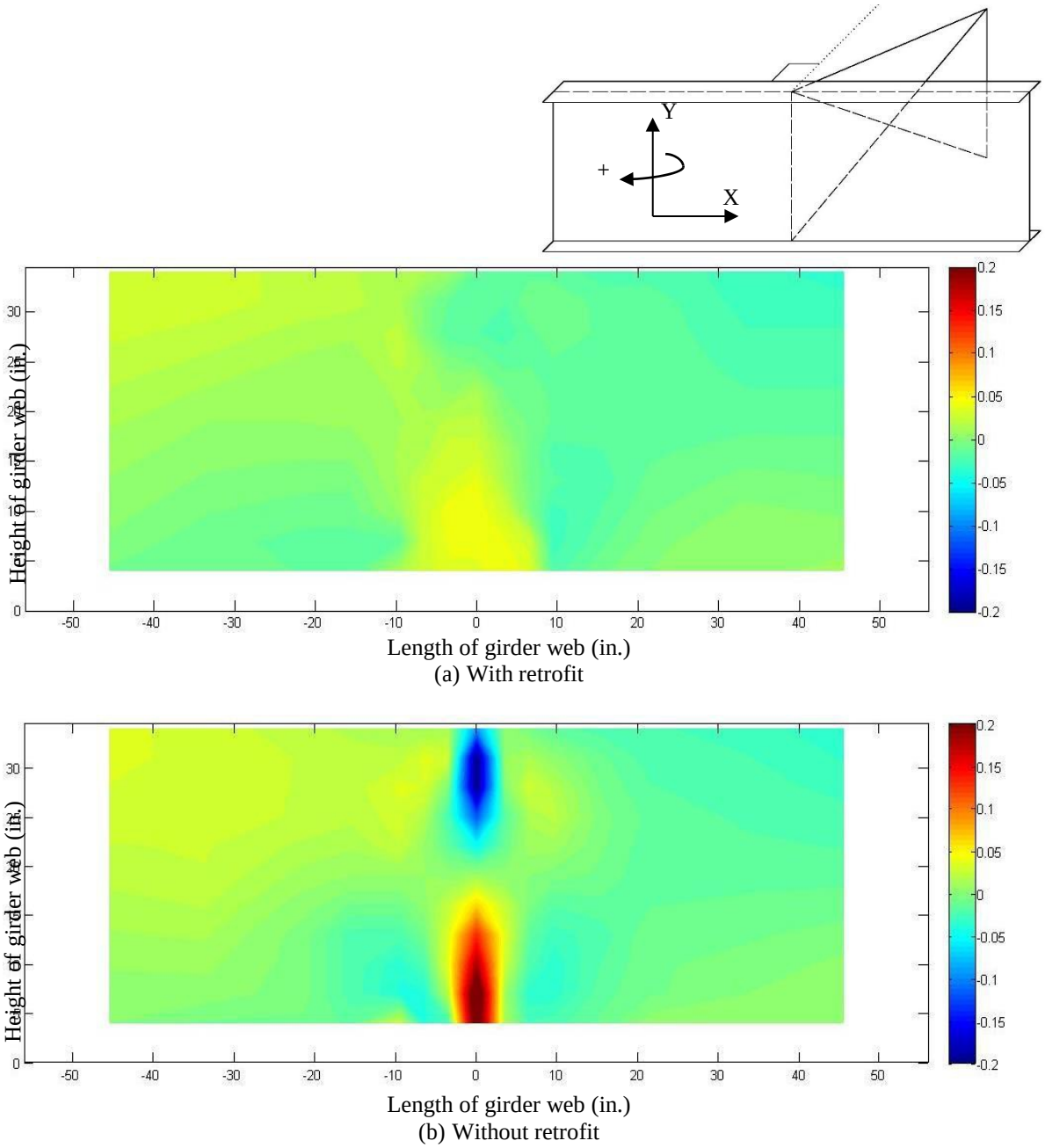

Figure 5-11: Y-axis rotations (deg.) of the girder web computed from mirror array measurements for 40-deg. skewed specimen under 2.5 kip of actuator force

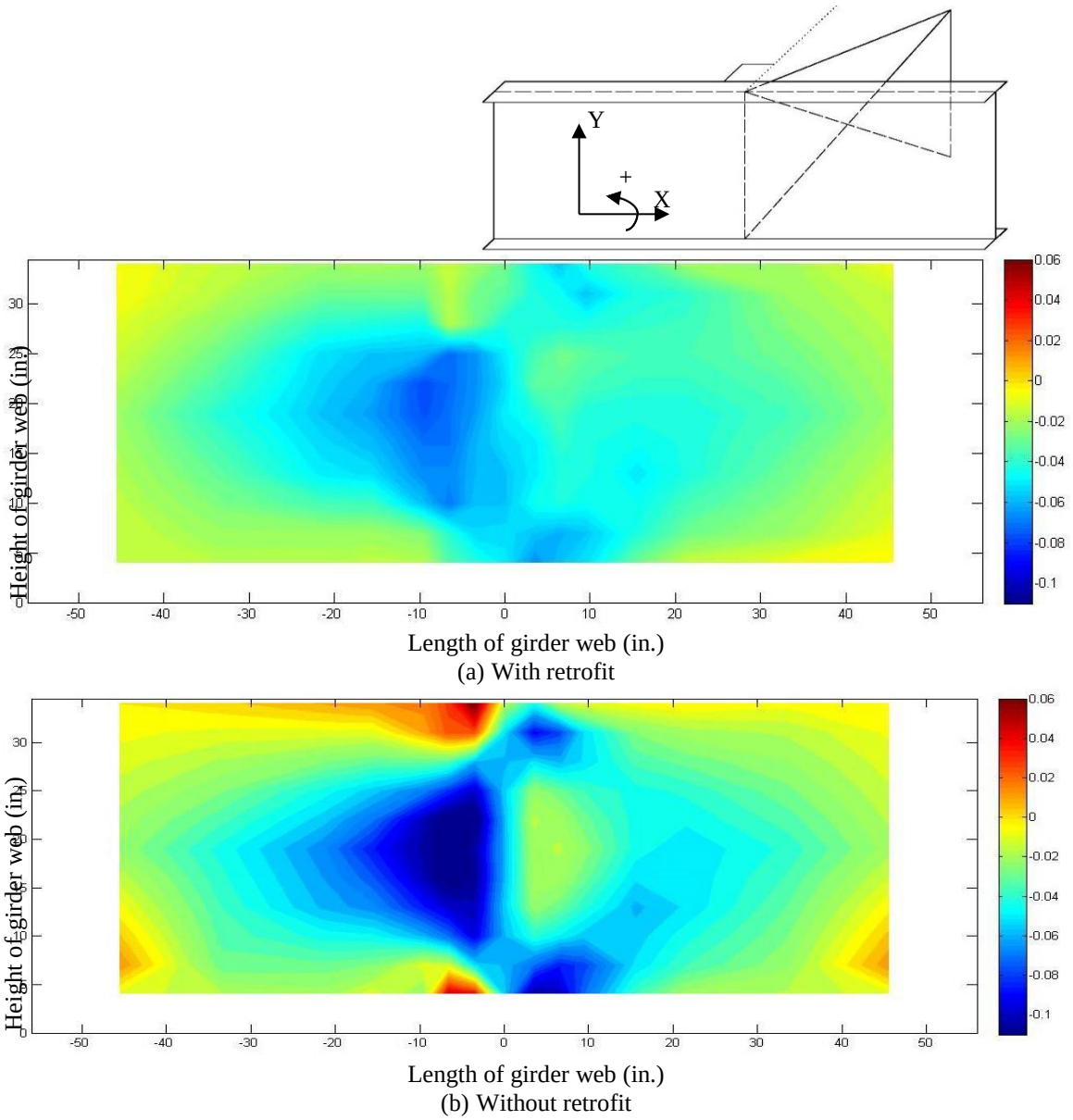

Figure 5-12: X-axis rotations (deg.) of the girder web computed from mirror array measurements for 40-deg. skewed specimen under 2.5 kip actuator force

Deformations in the girder web were significantly reduced after the angles-with-plate retrofit was installed. The effect was especially remarkable in reducing localized Y-axis rotations near the top and bottom web-gap regions. For the Y-axis rotations, the maximum positive and negative values decreased 83% and 83% respectively. For the X-axis rotations, the maximum

positive value reduced 100% (there was no positive X-axis rotation after retrofitting). The maximum negative value reduced 32%.

5.5.2 Approximated Stresses Calculated from Girder Web Rotation

The stress contour plots in X and Y directions derived from the mirror array measurements are presented in Figure 5-13 and Figure 5-14 respectively, using the same procedure described in Section 3.5.2.

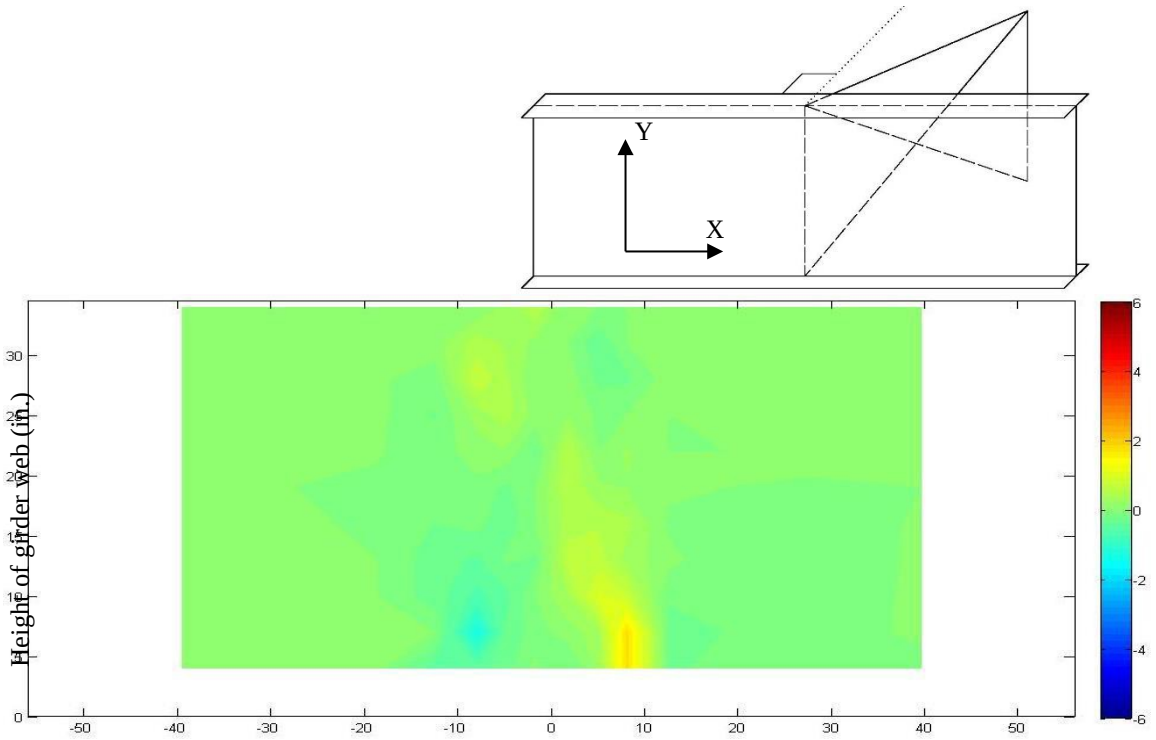

(a) With retrofit

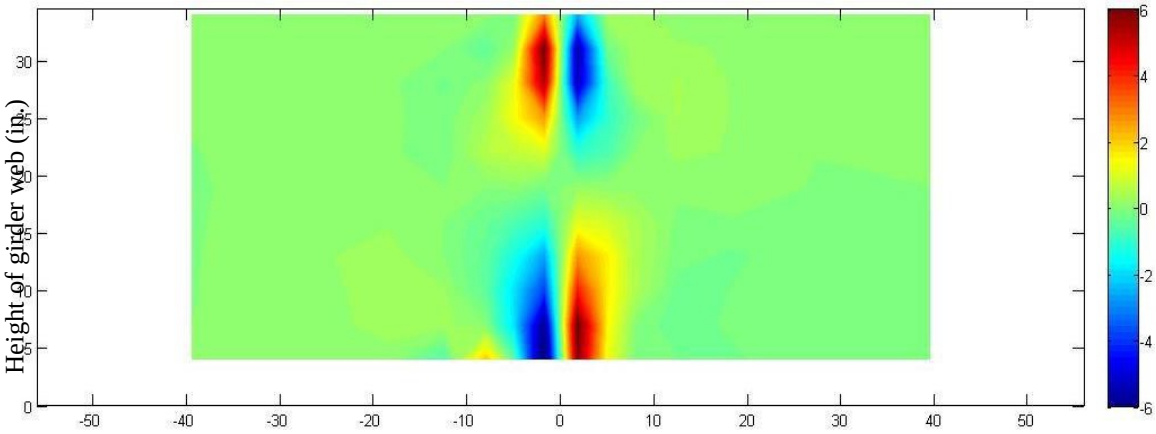

(b) Without retrofit

Figure 5-13: Approximated stress (ksi) in X direction of the girder web for 40-deg. skewed specimen under 2.5 kip of actuator force from mirror array measurements

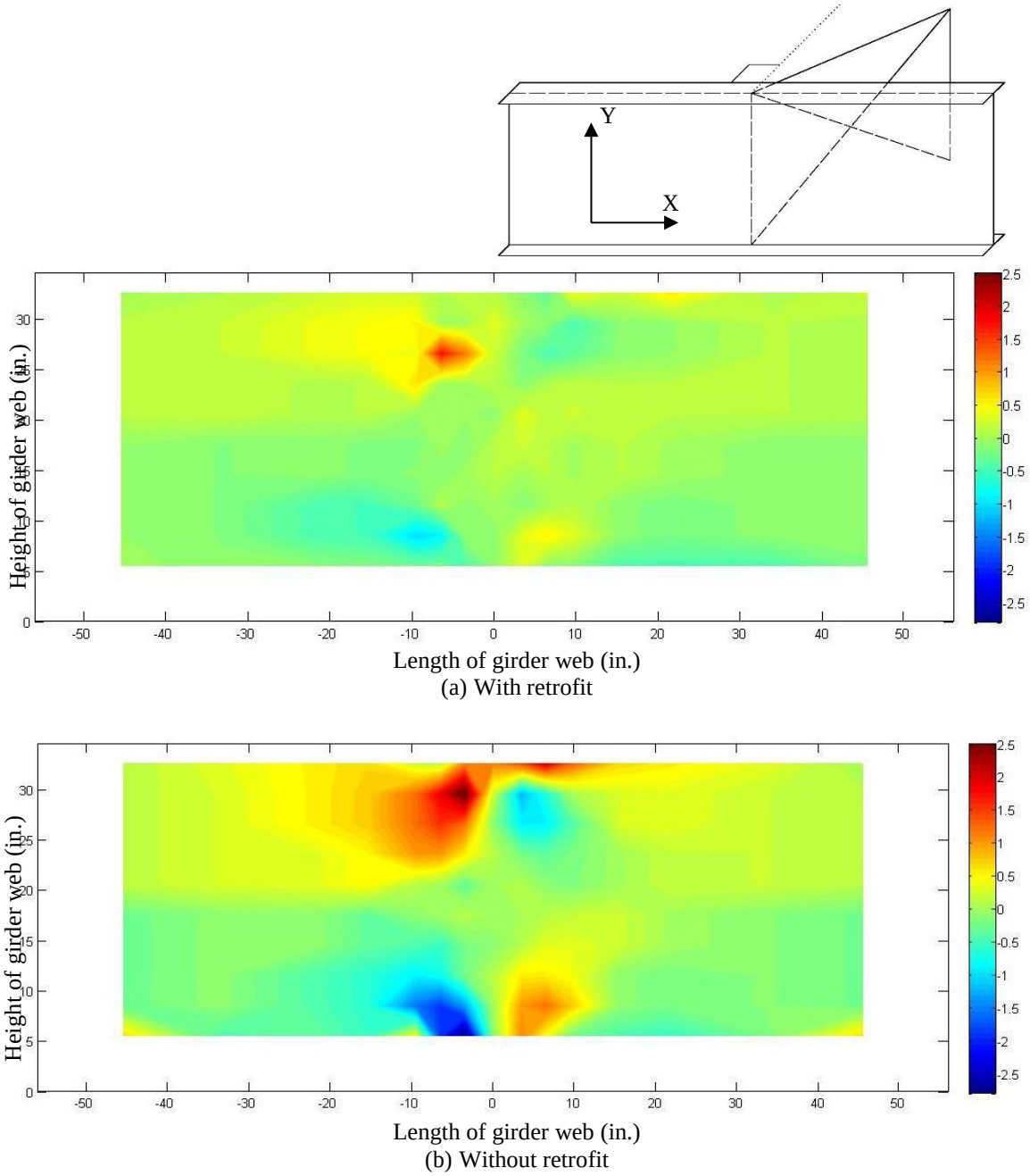

Figure 5-14: Approximated stress (ksi) in Y direction in the girder web for 40-deg. skewed specimen under 2.5 kip of actuator force from mirror array measurements

In reducing localized stresses in the top and bottom web-gap regions, the effect of the angles-with-plate retrofit was very significant. For the approximated stresses in X direction, the maximum tension stress reduced 72% and the maximum compression stress reduced 81%. For

the approximated stresses in Y direction, the maximum tension stress and maximum compression stress reduced 37% and 65%, respectively.

5.5.3 Influence of the Center Mirror Column on the Rotation and Approximated Stress Contour Plots

The center mirror column was added when testing the 40-deg. skewed specimen (there were no mirrors included at the girder web centerline in the test of the 20-deg. skewed specimen). Therefore, the rotation values at the girder web centerline were not recorded in the 20-deg. skewed test. Figure 5-15 presents a comparison of the mirror placements for the two tests. The red ellipse indicates the center mirror column.

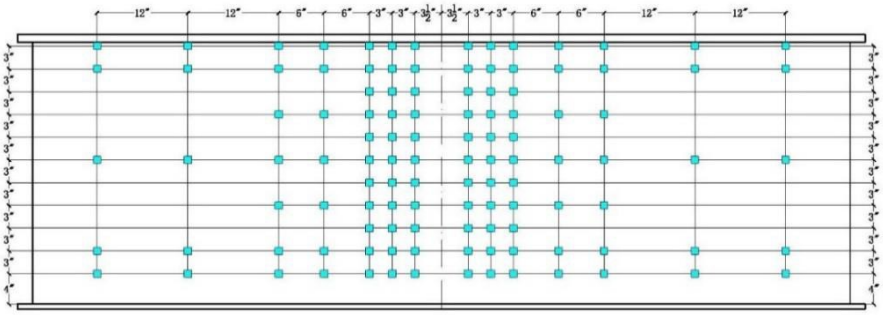

(a) Mirror placements for the 20-deg. skewed specimen

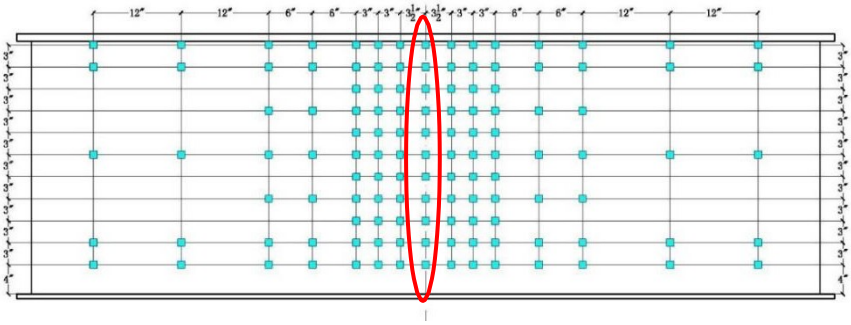

(b) Mirror placements for the 40-deg. skewed specimen

Figure 5-15: Mirror array configurations for 20-deg. and 40-deg. skewed specimens

The influence of the center mirror column on the rotation and approximated stress contour plots are discussed in this section. Figure 5-16 and Figure 5-17 present the results of the 40-deg. specimen when angles-with-plate retrofit was not installed. The title “with center mirror

column", means in the presented figures, rotation values of the girder web centerline were used in calculating and plotting, while the title “without center mirror column” means those values were not used.

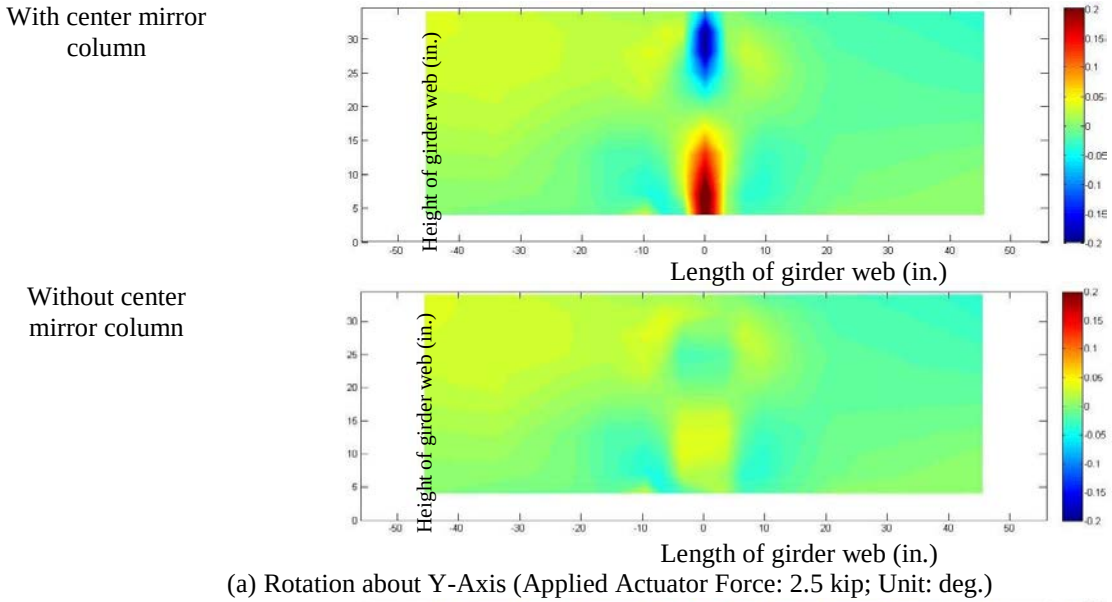

(a) Rotation about Y-Axis (Applied Actuator Force: 2.5 kip; Unit: deg.)

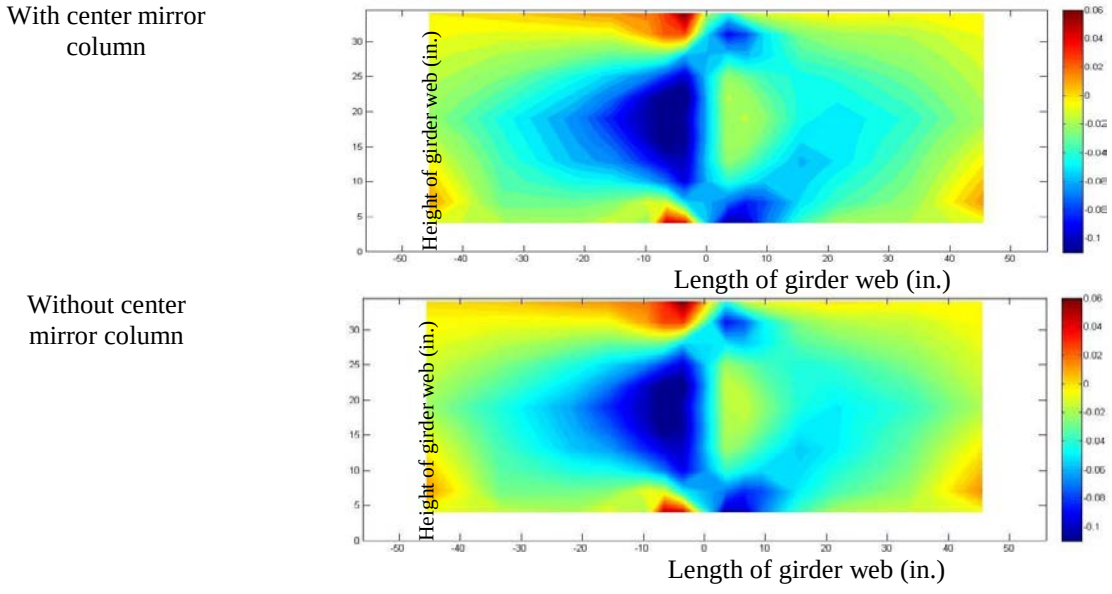

(b) Rotation about X-Axis (Applied Actuator Force: 2.5 kip; Unit: deg.)

Figure 5-16: Influence of center mirror column on rotation plots for 40-deg. skewed specimen

Ignoring the rotation values of the girder web centerline did not significantly affect the X-axis rotation contour plot. However, its influence on the Y-axis rotation contour plot was

significant. The localized deformations near the top and bottom web-gap regions did not appear when the rotation values of the girder centerline were not accounted for. The same phenomenon likely existed for the 20-deg. skewed specimen, in which the rotation values at the girder centerline were not recorded. The X-axis rotation contour plot of the 20-deg. skewed specimen may still be reliable, but the contour plot of the Y-axis rotation likely did not capture some important characteristics.

With center mirror column

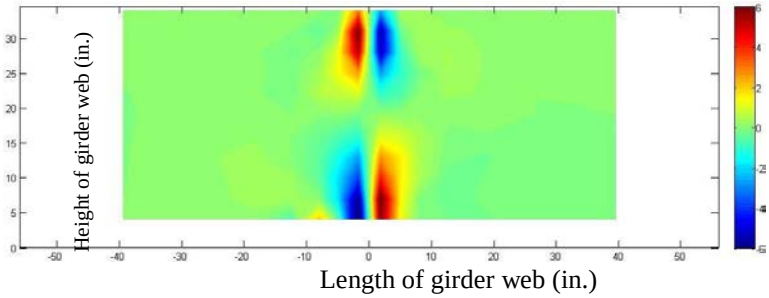

Without center mirror column

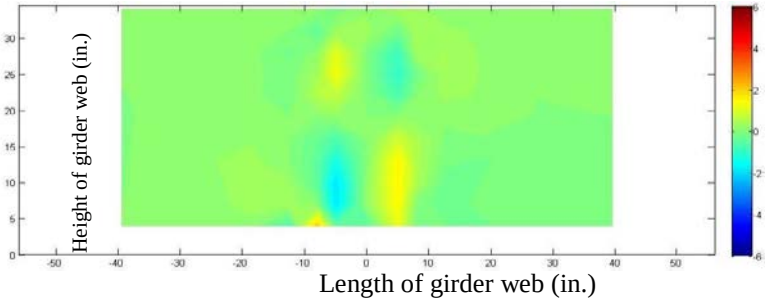

(a) Approximated Stresses in X Direction (Applied Actuator Force: 2.5 kip; Unit: ksi)

With center mirror column

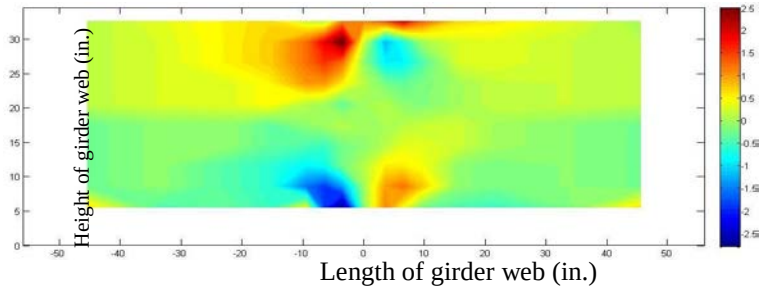

Without center mirror column

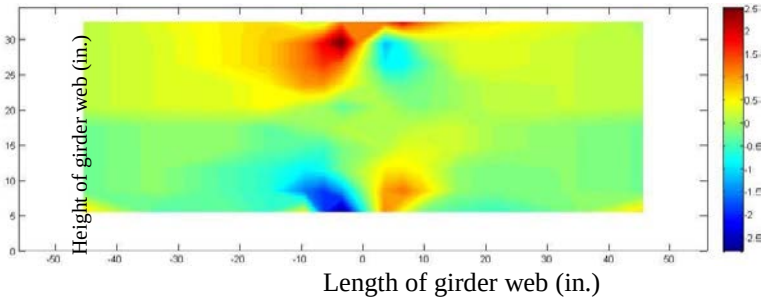

(b) Approximated Stresses in Y Direction (Applied Actuator Force: 2.5 kip; Unit: ksi)

Figure 5-17: Influence of center mirror column on plots of approximated stresses for 40-deg. skewed specimen

In the contour plot showing the X-axis approximated stresses, the calculated stresses near the web-gap region significantly decreased when the rotation values of the girder web centerline were not used in the calculation, while the approximated stresses in Y direction were not significantly affected. This result was predictable since the approximated stresses in X direction

were calculated from the Y-axis rotations. Ignoring the rotation values of the girder web centerline resulted in losing the characteristics of the localized Y-axis rotations. Therefore, the calculated x-axis stresses at the web-gap regions were much smaller. For the test of the 20-deg. specimen, since the rotation values at the girder web centerline were not recorded, the X-axis approximated stresses in the web-gap regions may be much smaller than reality, but the approximated stresses in Y direction are expected to still be reliable.

Chapter 6 Computer Simulations of the Physical Tests

6.1 Configuration of Computer Models

Linear-elastic finite element models were created to carry out the numerical simulations of the subassemblies employed in the experimental study. Three models were created that simulated physical tests with 0, 20 and 40 deg. angles respectively between the transverse connection frame and the girder web, (Fig. 6-1). The physical tests of the 20 and 40 deg. specimens were described in Chapters 2-5 of this report, and physical tests of the non-skewed (0 deg.) specimen were described as part of the literature review. The non-skewed configuration was included in the computational simulations to establish a baseline for the two skewed configurations.

The FE models with 0, 20, and 40 deg. angles between the transverse connection frame and the girder web were designated as 0 deg. model, 20 deg. model and 40 deg. model respectively in this paper. The commercially-available finite element software, Abaqus (2009), was used to create the models and complete the calculations.

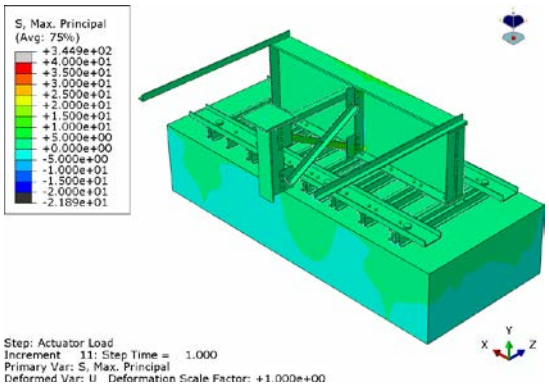

(a) 0° model

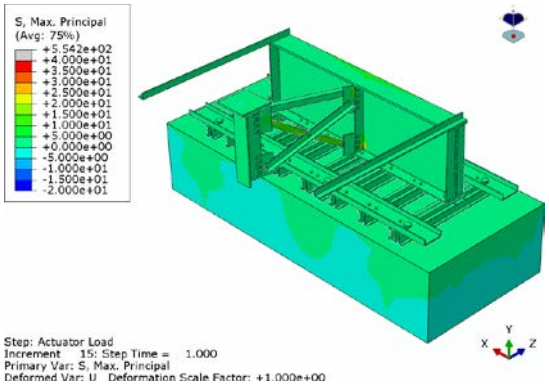

(b) 20° model

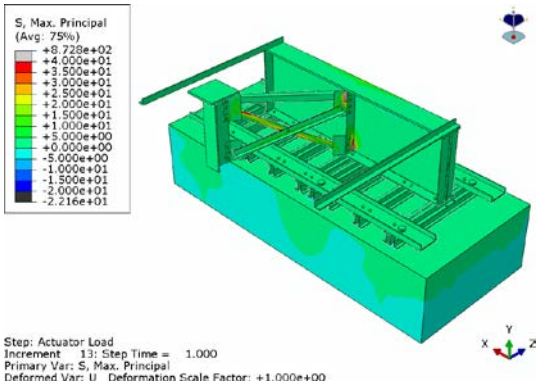

(b) 40° model

Figure 6-1: General configuration of FE models

The general configuration of 0°, 20°and 40°models are shown in Fig 6-1. Numerical computations for each model were carried out based on three cases:

- Uncracked, unretrofitted specimens
- Girders with cracks modeled in the web-gap region, representing the experimentally-observed fatigue damage, and

- Cracked girders, retrofitted with the angles-with-plate retrofit.

Each model shown in Fig 6-1 was comprised of approximately 660,000 elements, using C3D8R reduced integration brick elements with 24 deg. of freedom. Various analyses were performed with different element sizes to determine the appropriate mesh density. The adopted element sizes were determined to be insensitive to the computational results. To obtain more accurate computational results, it was necessary to employ a more dense mesh at critical locations, especially at the web-gap region. The girder web was partitioned to have three mesh zones of different mesh density, including a normal mesh size zone, a reduced mesh size zone, and a transition zone. Hexahedral elements were used in all three zones (Fig. 6-2).

The element size was set to 1/2 in. in the normal mesh size zone and 0.05 in. in the reduced mesh size zone. The transition zone was used to transfer from the coarse element size to the fine element size in the reduced mesh size zone.

The reduced mesh size zone was defined to be a rectangular area centered on the transverse connection plate with a width of 2 in., and height of 2.3 in., stemming from the bottom of the girder web (Fig. 6-2). The transition zone was a rectangular area surrounding the reduced mesh size zone with a width of 10.9 in. and height of 6.3 in. (Fig. 6-2). Element thickness was 0.19 in. in the normal mesh size zone and transitioned to 0.06 in. in the reduced mesh size zone.

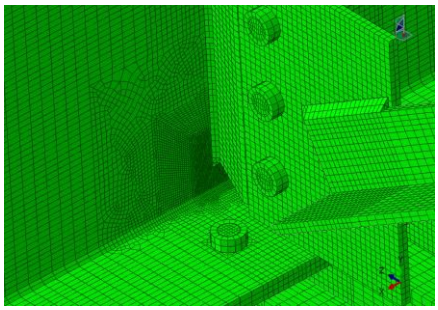

(a) Elevation view with transverse connection plate

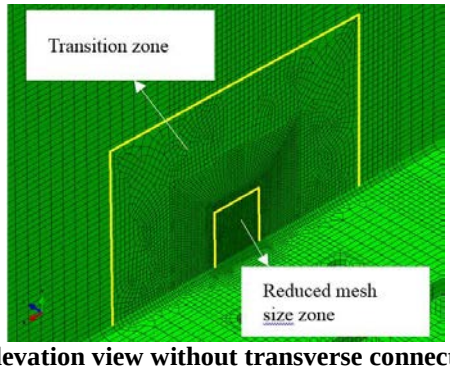

(b) Elevation view without transverse connection plate

Figure 6-2: Partitioned mesh zones at the web gap region

Each of the four fillet welds in the web-to-flange region was assigned a triangular cross-section with a size of 3/16 inch. Swept tetrahedral elements were used to simulate these four fillet welds, and the sizes of the elements were set to be in accordance with the adjacent elements in the girder web.

Hexahedral elements were used in the end stiffeners, and the element size was set as 0.23 in. The end stiffeners were connected to the flange and the web using tie constraints.

Various element types and mesh sizes were used in the transverse connection plate (Fig. 6-3). The 0.23 in. hexahedral element was used at the clipped ends. At the bolt holes, the circumference of each bolt hole was divided into 16 equal segments and each segment was taken as a hexahedral element in order to maintain the circular shape of the bolt hole in the numerical calculations (Fig. 6-3). 1/4 in. hexahedral elements were used over the rest of the transverse connection plate (Fig. 6-3).

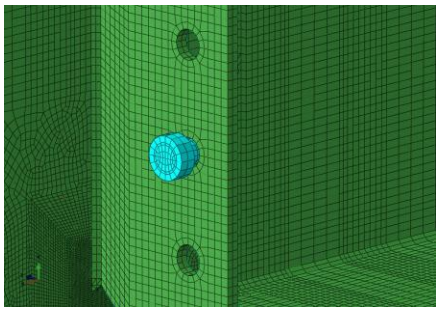

Figure 6-3: Mesh configuration at the transverse connection plate

The bolts on the transverse connection plate were explicitly simulated and a single 29-kip force was applied to each tensioned bolt. To match the elements of the bolts with the elements of bolt holes to reduce the computation amount and time, the circumference of each bolt was divided into 16 equal segments and each segment was taken as a hexahedral element.

The welds between the transverse connection plate and the web were simulated using swept tetrahedral elements with sizes in accordance with adjacent elements in the girder web.

The floor tie-down system was explicitly modeled, and 1/2-in. hexahedral elements were used to simulate the channels. In simulating the bolts and bolt holes on the channels, the same mesh technique used for the bolts and bolt holes in the transverse connection plate was employed. A force of 50 kip was applied to each bolt in the channels.

Tie constraints were used to model the connections between the channels and the bottom flange of the girder. A contact interaction was employed to simulate the interaction between the concrete floor and the steel elements with the coefficient of friction of 0.3.

The effect of the concrete deck limiting the deflection of the girder was modeled by using the concrete floor with the bottom fully fixed. The structural hexahedral element was used for the concrete floor, with an element size of 2 in. The bolt holes in the concrete floor were simulated using the same meshing technique used for the holes in the transverse connection plate (Fig. 6-4).

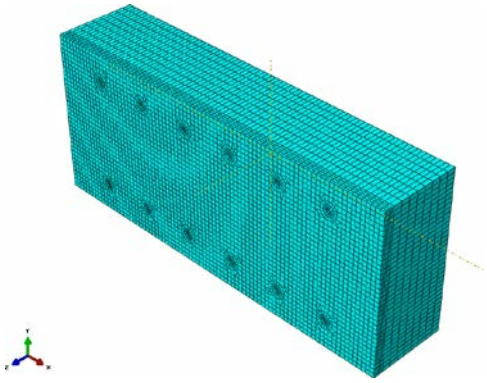

(a) Overall view

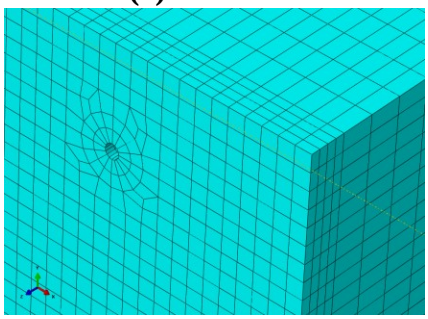

(b) Mesh at bolt holes

Figure 6-4: Mesh technique for concrete floor

Steel members in the specimens were simulated with a Poisson's ratio of 0.3 and elastic modulus of 29,000ksi. The concrete material was modeled as a block of elastic material with the Poisson's ratio of 0.2 and elastic modulus of 4,000ksi.

A single 6 kip upward force was applied to the WT section that was connected to the crossframe member, which was in turn connected to the actuator in the subassembly (Fig. 6-1).

Computational results and analysis

To compare computational results between different models and cases, the hot spot stress (HSS) technique was employed. Each HSS path was defined at a distance of 0.2 in. away from the weld toe to extract stresses near locations where cracks were observed in the specimens, in such a way that the computed stresses were less affected by large stress gradients in the web gap regions (Fig. 6-5). This distance was selected to be equivalent to half the thickness of the web (t_w=3/8 in.). A one-point HSS procedure from Maddox (2002) was used in this study.

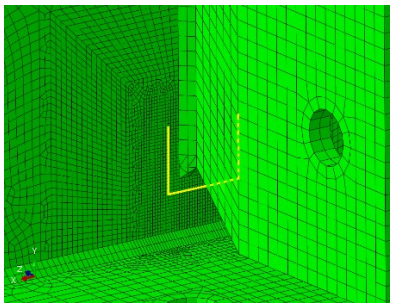

Figure 6-5: HSS path

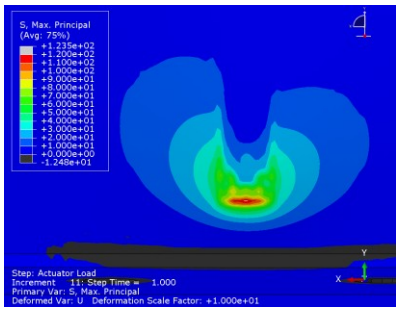

(a) 0° model

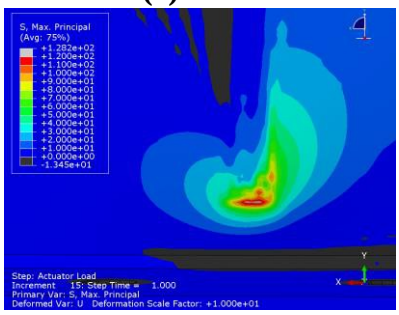

(b) 20° model

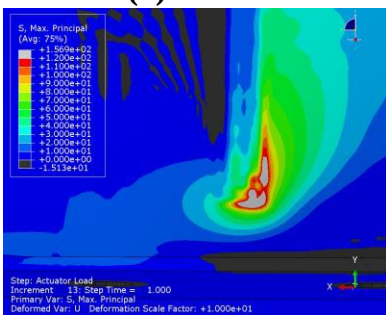

(c) 40° model

Figure 6-6: Computed maximum principal stresses in the web-gap region without cracks

From direct comparisons between computer simulations and experimental results, it was observed that the largest maximum principal stress demands in the numerical models correlated very well with locations where cracks formed in the specimens. Therefore, it was deemed appropriate to use maximum principal stress as a measure of vulnerability to fatigue damage.

The computational results for the case without cracks is shown in Fig. 6-6, and results for the cracked, unretrofitted specimen are shown in Fig. 6-7. In models where cracks were included, the cracks observed in the experimental specimens were explicitly simulated using the extended finite element method (XFEM). In the 0-deg. model, the crack pattern included a 3/4-in. tall horseshoe shaped crack around the transverse connection plate-to-web weld (Fig. 6-7-a). In the 20-deg. model, the crack pattern consisted of a horseshoe-shaped crack around the transverse connection plate-to-web weld with a 1/4-in. tall left leg and a 1-1/4-in. tall right leg (Fig. 6-7-b). In the 40-deg. model, the crack pattern was horseshoe-shaped crack around the transverse connection plate-to-web weld, with a 1/4-in. tall left leg and a 2-in. tall right leg (Fig. 6-7-c).

As previously described, the angles-with-plate repair was used in this study as the retrofit measure, and it included a backing plate and two angles, as shown in Fig 6-8. Results for the models of cracked, retrofitted specimens are shown in Fig 6-9.

Computed HSS demands in the bottom web-gap region in the different models and cases are summarized in Table 1. According to the HSS values, it can be seen that after the cracks occurred in the girders, maximum principal stresses in the bottom web-gap region decreased 23% in the 0-deg. specimen, 13% in the 20-deg. specimen, and increased 2% in the 40-deg. specimen, with respect to the uncracked girders.

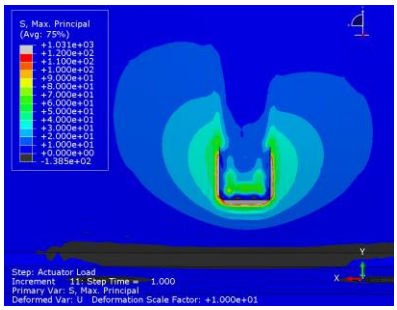

(a) 0°model

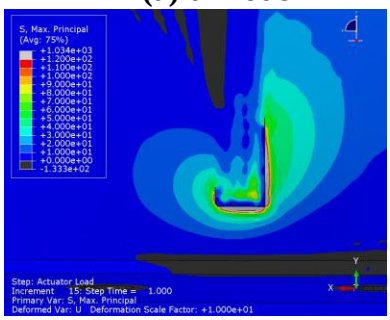

(b) 20°model

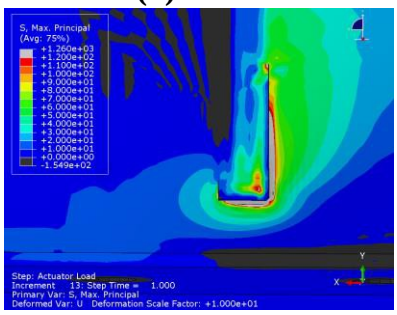

(c) 40°model

Figure 6-7: Computed maximum principal stresses in the cracked web-gap region

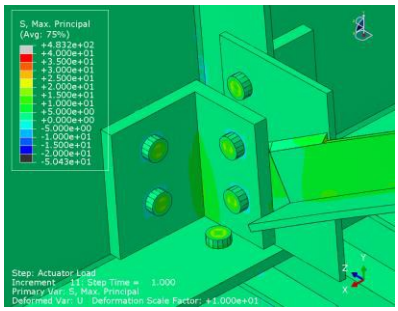

(a) 0°model

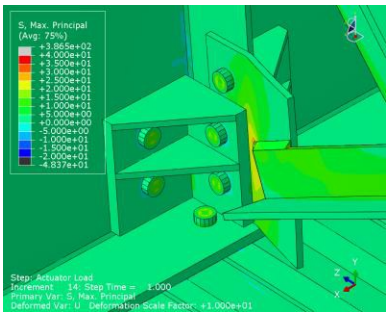

(b) 20°model

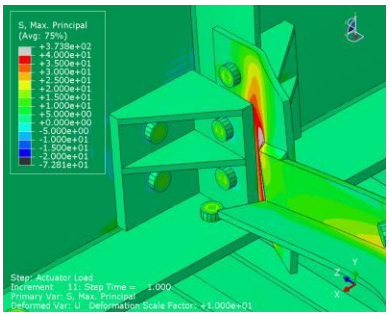

(c) 40°model

Figure 6-8: Configuration of the angles-with-plate retrofit

The HSS values shown in Table 6-1 also exhibit the high efficiency of the retrofit measure. After installing the retrofits, maximum principal stresses decreased significantly in the web-gap regions, about 41% in the 0-deg. specimen, 56% in the 20-deg. specimen and 66% in the 40-deg. specimen.

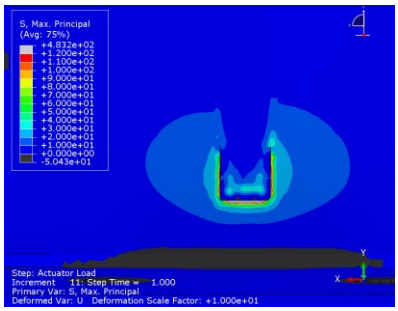

(a) 0°model

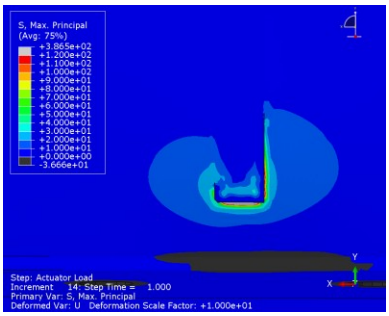

(b) 20°model

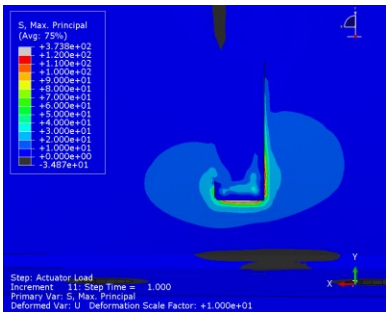

(c) 40°model

Figure 6-9: Computed maximum principal stresses in the web-gap region for cracked, retrofitted models

Table 6-1: Maximum HSS in the bottom web-gap region

Model	0-deg.	20-deg.	40-deg.
Uncracked	40.7 ksi	44.5 ksi	51.4 ksi
Cracked	31.5 ksi	38.8 ksi	52.6 ksi
Cracked and retrofitted	18.5 ksi	16.9 ksi	17.6 ksi

Chapter 7 Comparison of Physical Tests and Computer Simulations

A comparison of the physical test results and the computer simulation results are provided in this section. It is worth mentioning that in the computational simulations described in Chapter 6, an actuator load of 6 kip was simulated for all of the models. Since the applied actuator load used in the monotonic loading of the physical test for the 40-deg. skewed specimen was 2.5 kip, in this section, a 2.5 kip actuator load was applied in the computer models for the 40-deg. skewed specimen, making the physical test results and the computer simulation results comparable.

7.1 Stresses Computed from Strain Gages

A comparison between the stresses computed from strain gages and stresses extracted from the computer simulations is made in this section. Some measured stresses exhibited a relatively large difference compared with their corresponding computer simulation results, especially for those in the regions where large stress gradients existed, for example, strain gages 5 and 6 in Figure 7-1, and strain gage 1 in Figure 7-3. In those regions, a small offset in the strain gage position could result in a very different measurement. However, in general, the physical test results and the computer simulation results matched well.

7.1.1 20-Deg. Skewed Girder-to-Crossframe Specimen

A comparison of stresses between the physical tests and the computer models is presented in the following figures (Figure 7-1 and Figure 7-2). Stresses computed from strain gages are shown in blue, while stresses extracted from computer models are shown in orange.

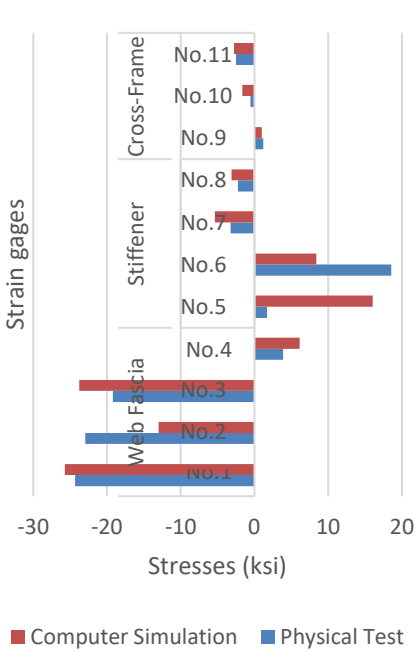

(a) Comparison between FE results and physical test results

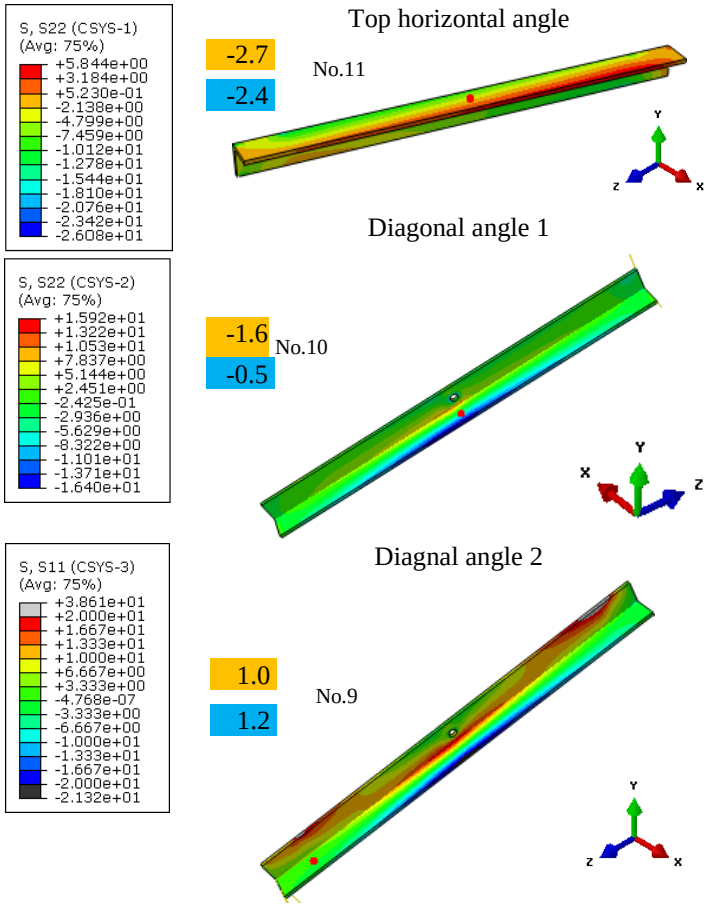

(b) Stress on Crossframe (ksi)

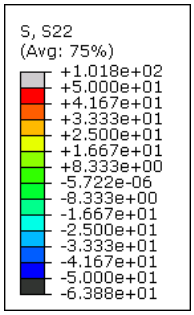

(ksi)

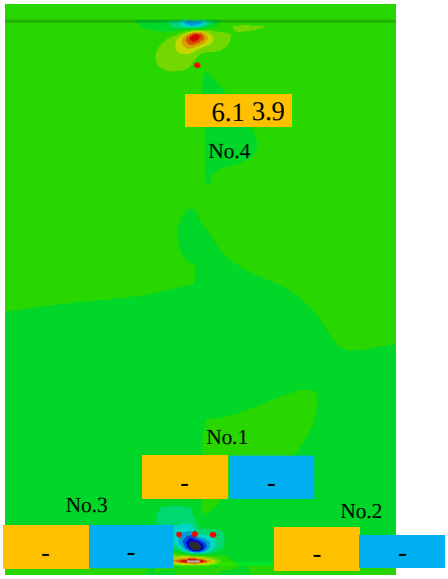

(c) Stress on girder web fascia side (ksi)

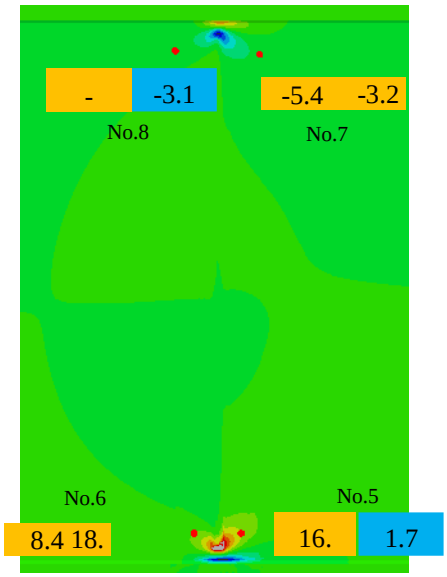

(d) Stress on girder web stiffener side (ksi)

*Stresses are shown in the same direction as their corresponding strain gages

Figure 7-1: Comparison between FE results and physical test results for 20-deg. skewed specimen without retrofit installed, under 6 kip of actuator force

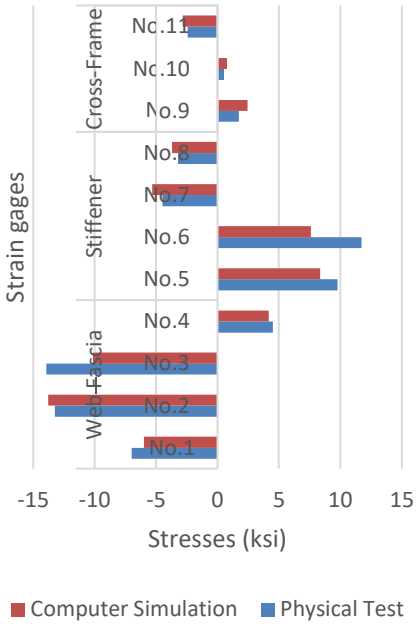

(a) Comparison between FE results and physical test results

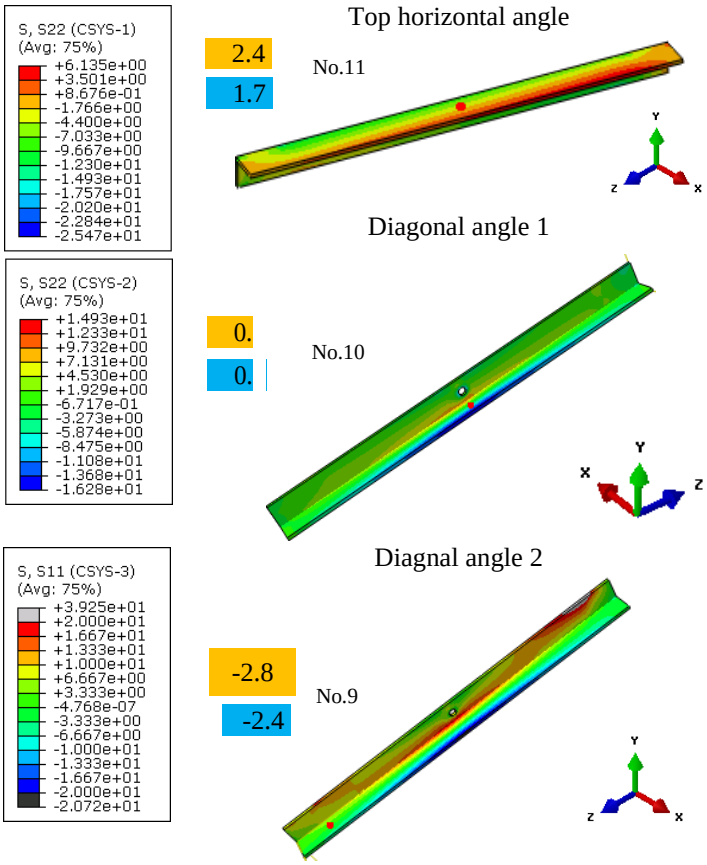

(b) Stress on Crossframe (ksi)

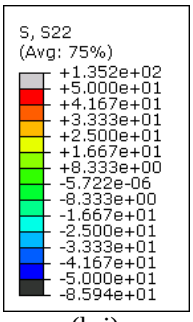

(ksi)

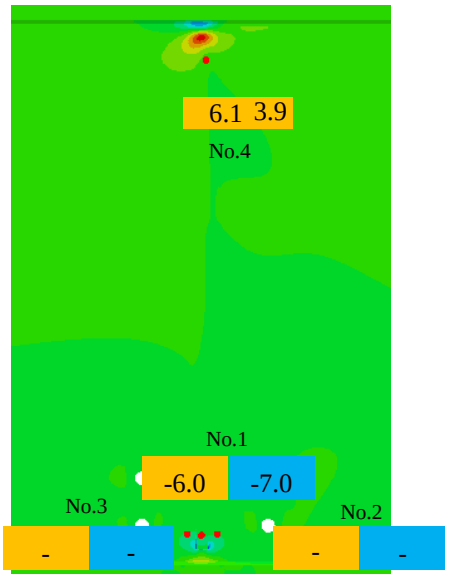

(c) Stress on girder web fascia side (ksi)

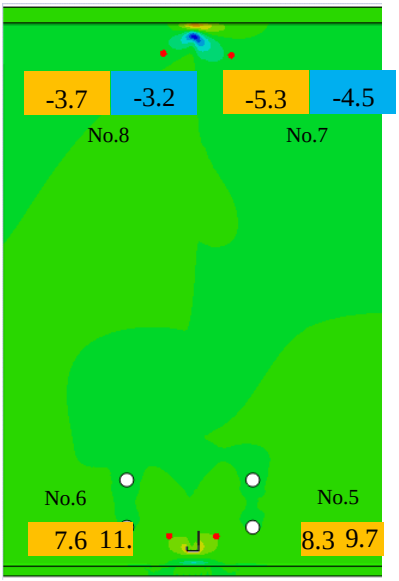

(d) Stress on girder web stiffener side (ksi)

*Stresses are shown in the same direction as their corresponding strain gages

Figure 7-2: Comparison between FE results and physical test results for 20-deg. skewed specimen with retrofit installed, under 6 kip of actuator force

7.1.2 40-Deg. Skewed Girder-to-Crossframe Specimen

The strain gage placements used in the 40-deg. skewed specimen are presented in Figure 4-3. Figure 7-3 presents a comparison in stresses between the physical test and the computer simulation.

Only the results for the unretrofitted case are presented in this section, because there was no corresponding computer model for the case with the retrofit installed in the top web gap. Retrofits were installed in both the top and the bottom web-gap regions in the physical test of the 40-deg. skewed specimen because cracks were observed in both of the two regions. However, only the bottom web-gap regions were retrofitted in the computer models since the cracking of the top web-gap region was unexpected.

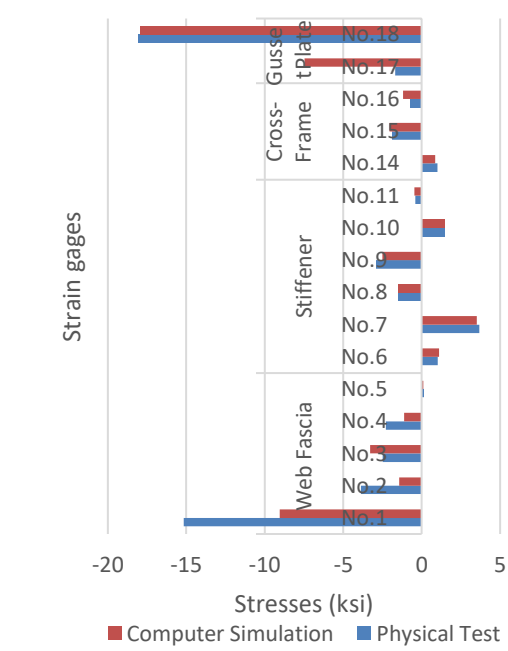

(a) Comparison between FE results and physical test results

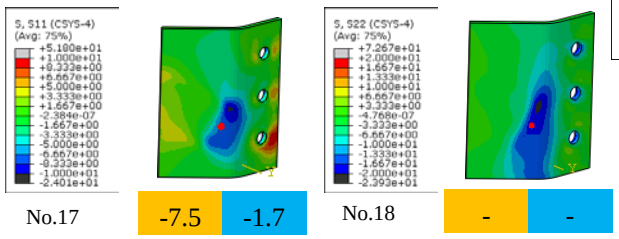

(b) Stresses on bottom gusset plate (ksi)

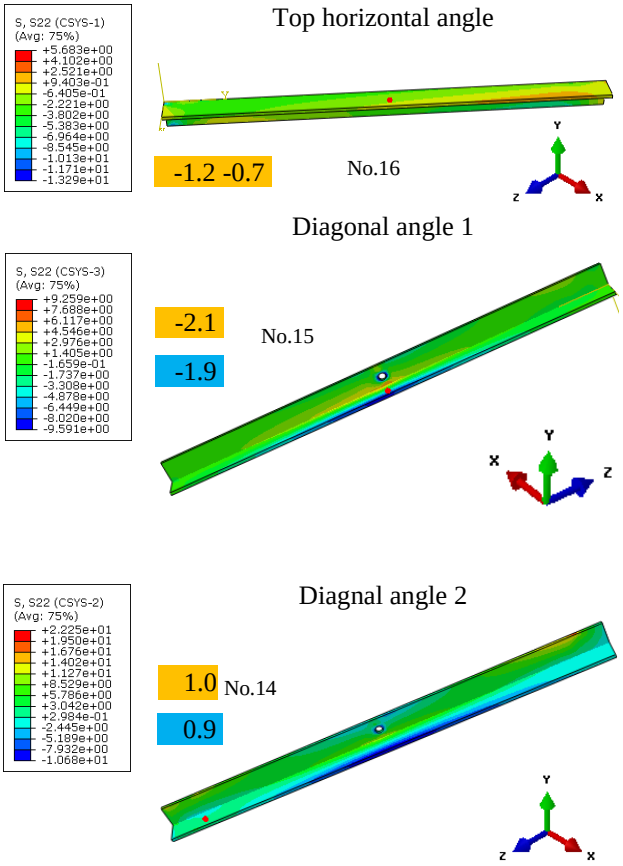

(c) Stress on crossframe (ksi)

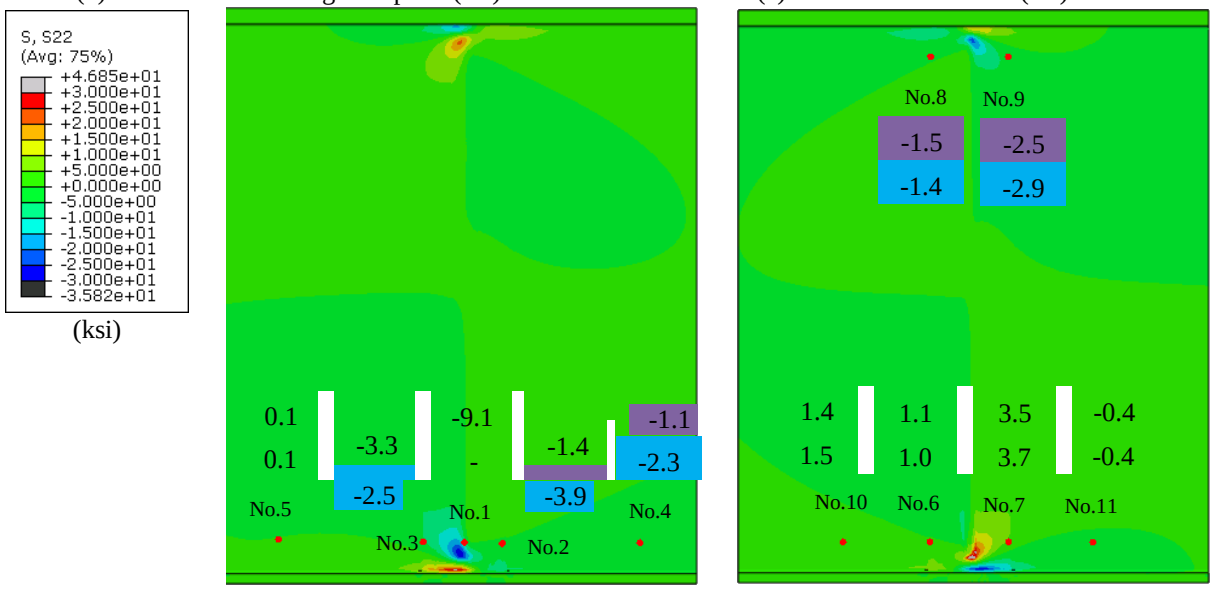

(d) Stresses on girder web fascia side (ksi) (e) Stresses on girder web stiffener side (ksi)

*Stresses are shown in the same direction as their corresponding strain gages

Figure 7-3: Comparison between FE results and physical test results for the 40-deg. skewed specimen without retrofit installed under 2.5 kip of actuator force

7.2 Stresses Approximated from Girder Web Rotations

The approximated stresses were calculated from the girder web rotations obtained from the mirror array measurements, and were presented as contour plots in Section 3.5.2 and Section 5.5.2. A comparison between the stresses approximated from the girder web rotations and the stresses obtained in the computer simulations is given in this section. The edges of the girder web have been presented as the rectangular border in the following figures. In the approximated stresses contour plots, data in some regions were not available and are shown as blank. Therefore, blank areas were intentionally left in the computer simulation results to make the two results comparable.

7.2.1 20-Deg. Skewed Girder-to-Crossframe Specimen

Figure 7-4 and Figure 7-5 provide a comparison between the stresses approximated from the girder web rotations and the stresses obtained in the computer simulations for the 20-deg. skewed specimen. The two results matched well on the distribution of the stresses in Y direction. However, the stress distributions in X direction did not compare well.

The mismatch for stresses in X direction can be explained by the missing center mirror column in the 20-deg. test. Mirrors were not placed at the centerline of the 20-deg. skewed specimen. As discussed, for the results of the 40-deg. skewed specimen, neglecting the rotation values of the center mirror column resulted in losing characteristics of the stress distribution in the X direction, while the approximated stresses in Y direction were not significantly affected. The center mirror column may influence the approximated stresses of the 20-deg. skewed specimen in the same way as it affected the 40-deg. skewed specimen.

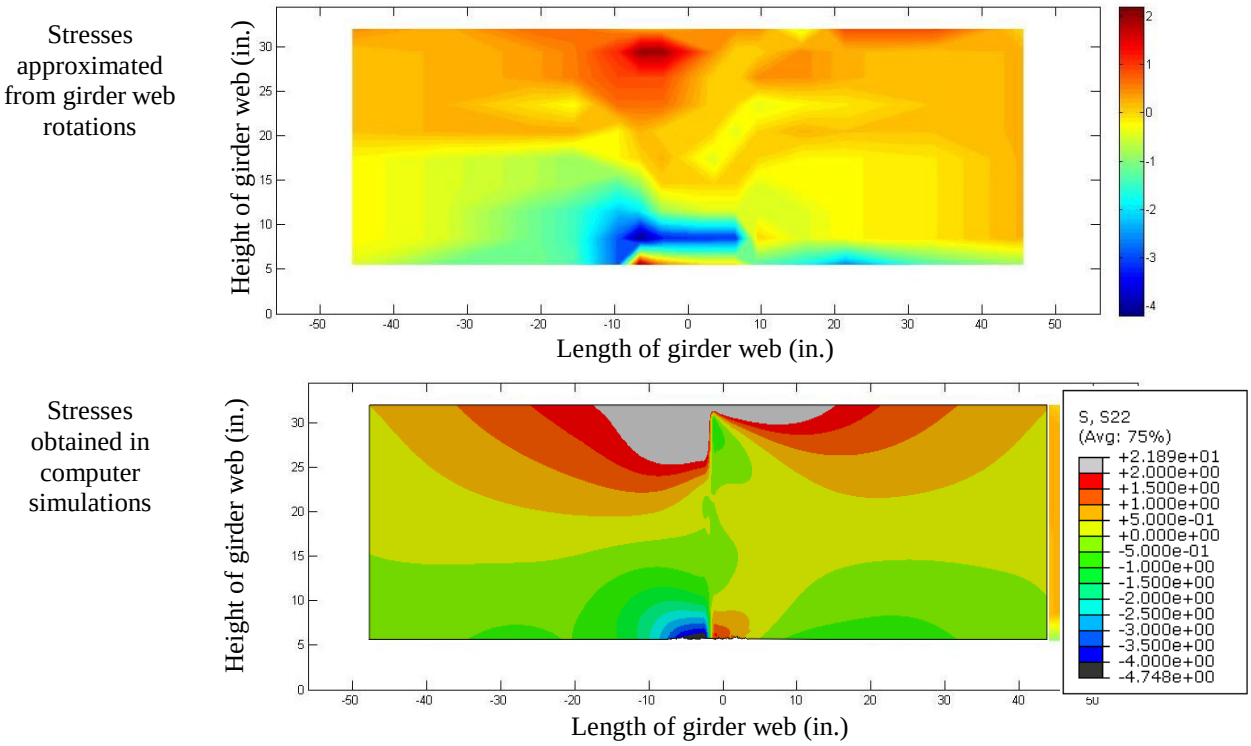

(a) Stresses in Y direction - without retrofit installed (applied actuator force: 6 kip; unit: ksi)

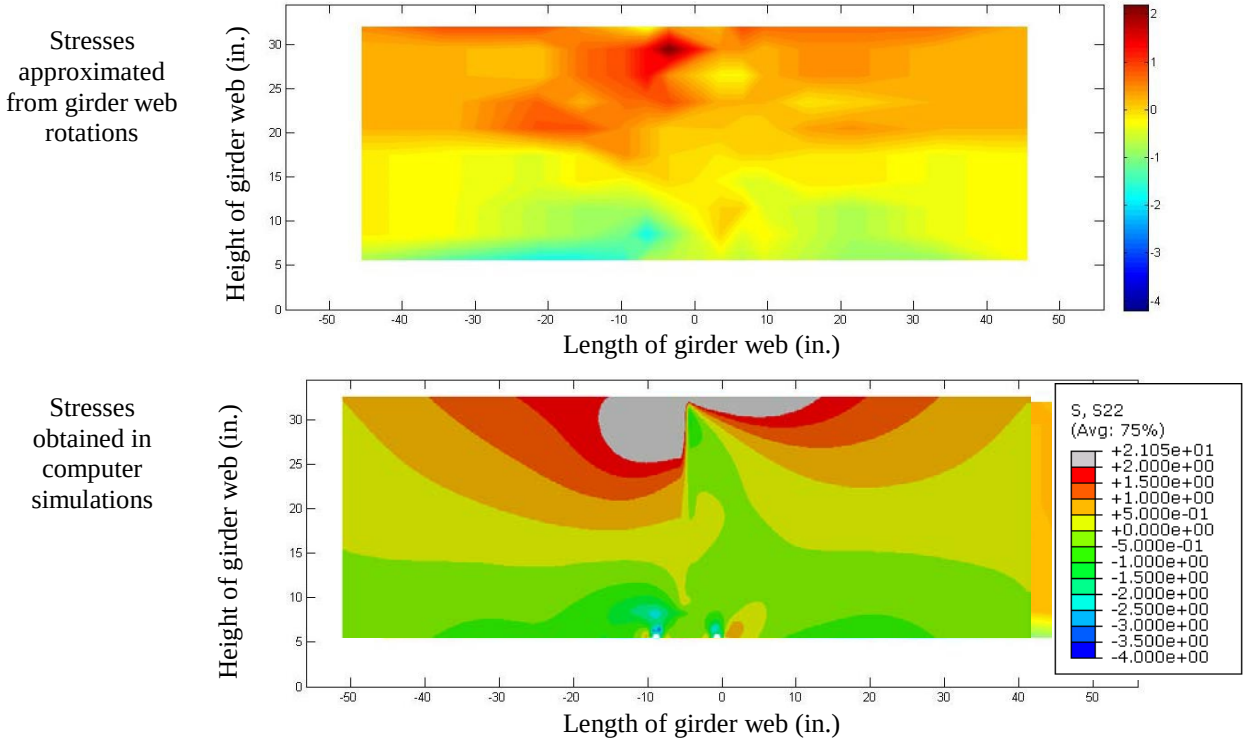

(b) Stresses in Y direction - with retrofit installed (applied actuator force: 6 kip; unit: ksi)

Figure 7-4: Comparison between stresses in Y direction calculated from girder web rotations and obtained from computer simulations for 20-deg. skewed specimen

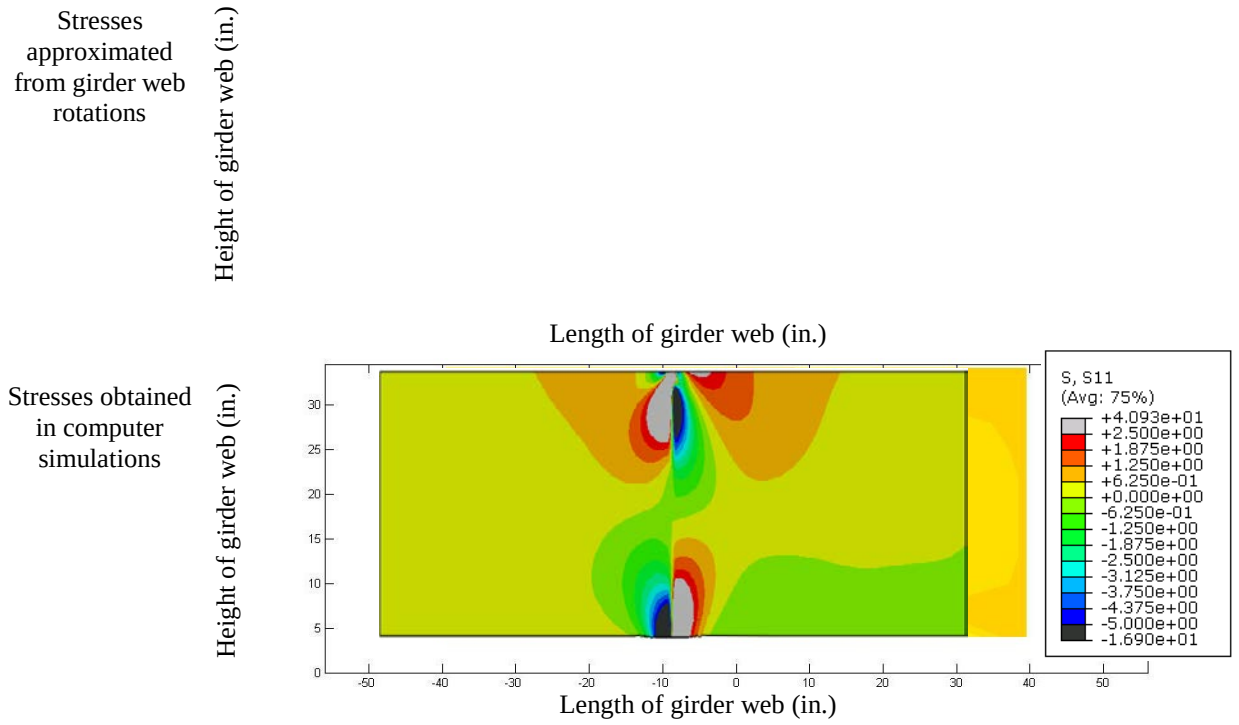

(a) Stresses in X direction - without retrofit installed (applied actuator force: 6 kip; unit: ksi)

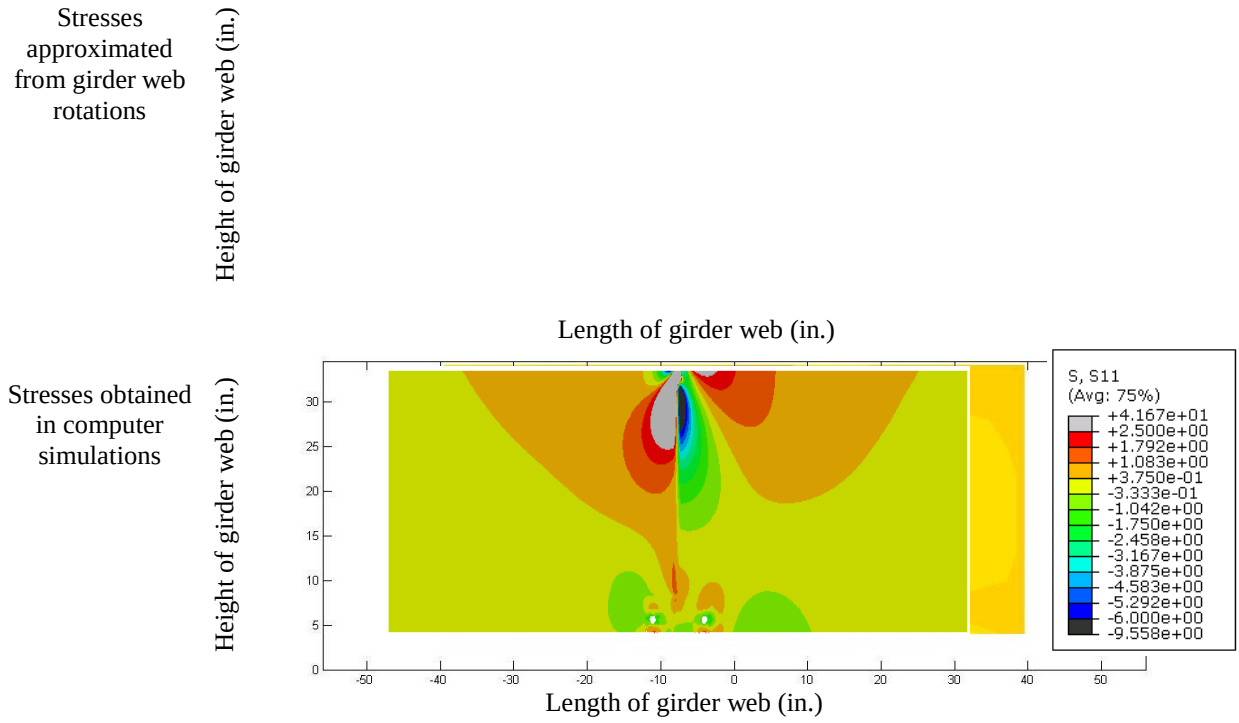

(b) Stresses in X direction - with retrofit installed (applied actuator force: 6 kip; unit: ksi)

Figure 7-5: Comparison between stresses in X direction calculated from girder web rotations and obtained from computer simulations for 20-deg. skewed specimen

7.2.2 40-Deg. Skewed Girder-to-Crossframe Specimen

A comparison between stresses approximated from girder web rotations and stresses derived from the computer simulations for the 40-deg. skewed specimen is given in Figure 7-6.

The case without the retrofit installed is presented. As shown in the following figure, the physical test results and the computer simulation results matched each other well. The stress distributions were almost identical.

Stresses approximated from girder web rotations

Height of girder web (in.)

Length of girder web (in.)

Stresses obtained in computer simulations

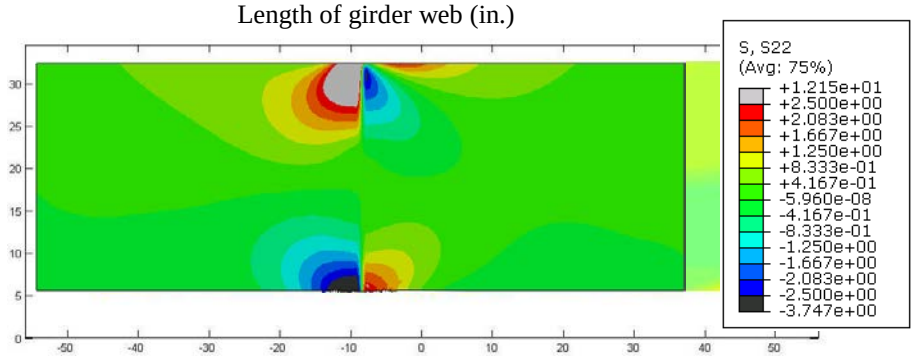

(a) Stresses in Y Direction - Without Retrofit Installed (Applied Actuator Force: 2.5 kip; Unit: ksi)

Stresses approximated from girder web rotations

Height of girder web (in.)

Length of girder web (in.)

Stresses obtained in computer simulations

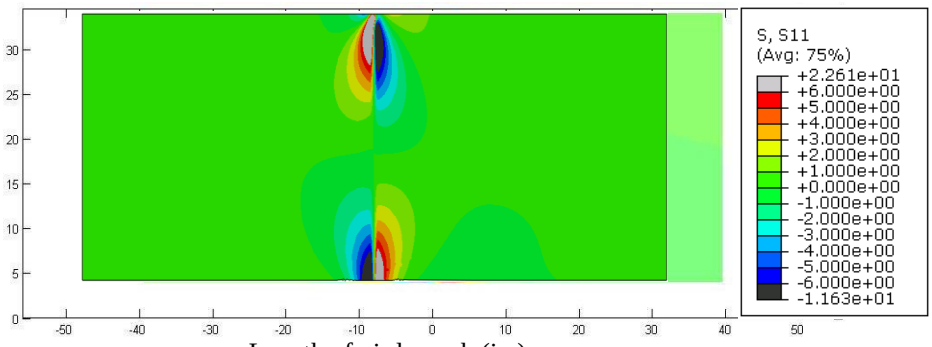

(b) Stresses in X Direction – Without Retrofit Installed (Applied Actuator Force: 2.5 kip; Unit: ksi)

Figure 7-6: Comparison between stresses calculated from girder web rotations and stresses obtained from computer simulations for 40-deg. skewed specimen without retrofit installed

Chapter 8 Influence of Angles-with-Plate Retrofit on Crossframe Gusset Plate Stresses

As described in section 3.1.2, in the test of the 20-deg. skewed specimen, the crossframe gusset plate cracked while the angles-with-plate retrofit was in place. This section explores the influence of the angles-with-plate retrofit on stresses at the gusset plate.

In the test of the 40-deg. skewed specimen, two strain gages were attached to the gusset plate as described in Section 5.3. Results indicated that after installing the angles-with-plate retrofit, stresses on the gusset plate did not increase, but significantly decreased.

Figure 8-1 presents a comparison from the computer simulations, of the gusset plate stresses for cases with and without the angles-with-plate retrofit installed. Under the same actuator loads, maximum principal stresses on the gusset plate in the unretrofitted condition increased as the connection became more skewed. However, after retrofitting, only the straight connection saw stresses increase in the gusset plate, and it was a very small amount (less than 5%). In the 20-deg. skewed and the 40-deg. skewed connections, the maximum principal stresses on the gusset plate decreased 43% and 58%.

Figure 8-1 presents the deformation of the gusset plates, with respect to the undeformed configuration. Without the retrofit installed, the distortion of the gusset plate became more severe as the skew angle increased. After retrofitting, the gusset plate deformation decreased due to the stiffness of the attached angles, thus resulting in the stress reduction. Both the computer simulations and the strain gages used in the physical test indicated that the angles-with-plate retrofit was unlikely to be the reason the gusset plate cracked in the 20-deg. skewed specimen. Instead, this failure is attributed to the very large load range applied to the specimen.

With retrofit installed

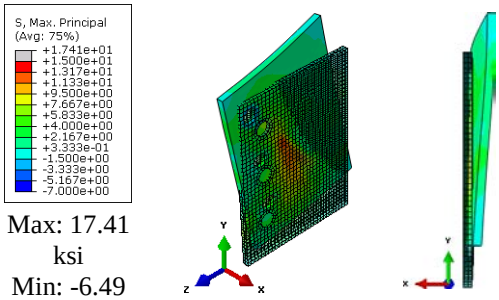

Max: 17.41 ksi
Min: -6.49 ksi

Without retrofit installed

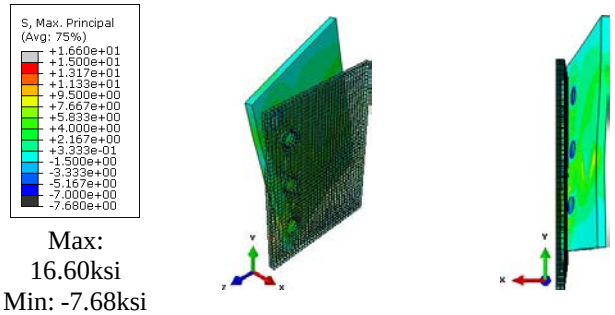

Max: 16.60ksi
Min: -7.68ksi

(a) Models of straight girder-to-crossframe connection
(Applied actuator force: 6 kip)

With retrofit installed

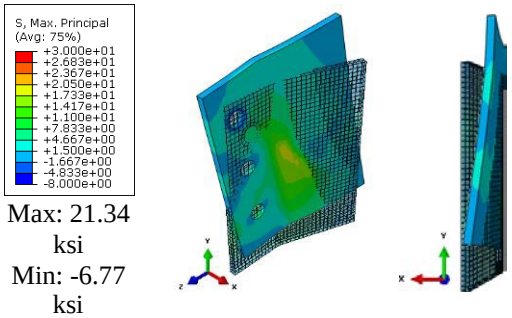

Max: 21.34 ksi
Min: -6.77 ksi

Without retrofit installed

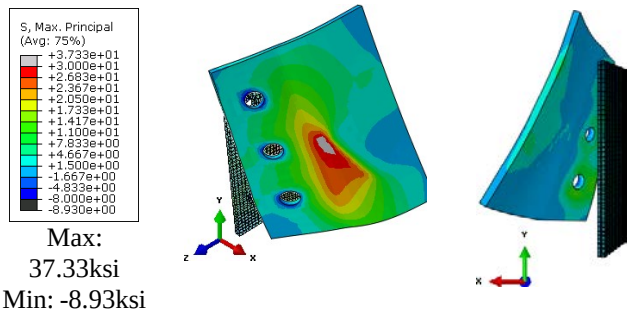

Max: 37.33ksi
Min: -8.93ksi

(b) Models of 20-deg. skewed girder-to-crossframe connection
(Applied actuator force: 6 kip)

With retrofit installed

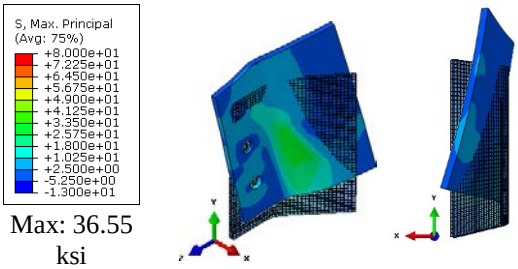

Max: 36.55 ksi
Min: -7.08 ksi

Without retrofit installed

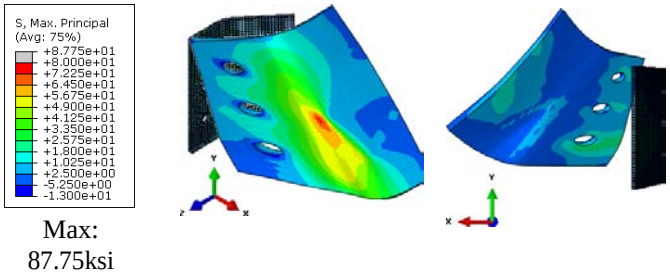

Max: 87.75ksi
Min: -12.99ksi

(c) Models of 40-deg. skewed girder-to-crossframe connection
(Applied actuator force: 6 kip)

*[1] The colored shapes present the deformed shapes. The shadows present the undeformed shapes. The deformation scale factors are 50× for all of the models.

*[2] Only the bottom web-gap regions were retrofitted in the computer simulations. (However, in the physical test of the 40-deg. skewed specimen, retrofits were attached on both the bottom and the top web-gap regions.)

*[3] 6 kip actuator loads were simulated in the computer simulations. (However, in the physical test of the 40-deg. skewed specimen, the applied actuator loads were 2.5 kip.)

Figure 8-1: Comparison of gusset plate stresses with and without angles-with-plate retrofit installed

Chapter 9 Conclusions

In this study, fatigue tests were performed on 20-deg. and 40-deg. skewed girder-to-crossframe subassemblies to evaluate the effectiveness of a newly-developed retrofit technique, called the angles-with-plate retrofit, in mitigating distortion-induced fatigue damages in web-gap regions. A series of companion finite element analyses were also performed and presented. A comparison of the physical test results and the finite element analysis results are provided. The following conclusions can be drawn from this study,

1. **For the skewed girder-to-crossframe connections tested in this study, the angles-with-plate retrofits were very effective in stopping crack initiation and propagation, reducing localized deformations in the web gap regions, and reducing stresses in the web-gap regions.**

   Crack initiation and propagation in the test of the 40-deg. skewed specimen was halted after installing the angles-with-plate retrofits. For the 20-deg. skewed specimen, although crack propagation not fully stop with the retrofit installed, crack growth slowed significantly in the retrofitted trial. In the unretrofitted trials, the crack growth rates in the south bottom and north bottom web-gap regions were 58 and 106 inches per one million cycles respectively, while in the retrofitted trials, the crack growth rates were only 0.6 and 0.3 inches per one million cycles. Based on this comparison, the efficacy of the retrofit was quite good.

   For the 20-deg. skewed specimen, deformations in the bottom web-gap region were reduced 94% after installing the retrofit. For the 40-deg. skewed specimen, after installing the retrofits, deformations in the bottom and the top web-gap regions decreased 98.4% and 75.9%, respectively.

The approximated stresses in the web-gap regions calculated from the measured rotation values decreased significantly after installing the angles-with-plate retrofit. For the 20-deg. skewed specimen, after installing the retrofit, the maximum tension and compression stresses in the bottom web-gap region decreased 68% and 89% in the X-direction. In the Y-direction, the maximum tension and compression stresses decreased 99% and 58%, respectively. For the 40-deg. skewed specimen, after installing the retrofits, the maximum tension and compression stresses were reduced 72% and 81% in the X-direction, and were reduced 37% and 65% in the Y-direction.

2. **Fatigue cracks were found in the bottom web-gap region in the 20-deg. skewed specimen, and both the bottom and the top web-gap regions in the 40-deg. skewed specimen.**

Since the bottom flange was restrained, the bottom web-gap region was expected to be more sensitive to fatigue than the top. Fatigue cracks were found in the bottom web-gap regions in both of the tests as expected, but the top web-gap region also cracked in the test of the 40-deg. skewed specimen.

3. **During cyclic loading, fatigue cracks on the 40-deg. skewed specimen remained very thin but grew in length for most of the cycles in the unretrofitted condition.**

The cracks on the 40-deg. skewed specimen grew to more than 3 in. long, but remained very thin until 1,050,000 cycles into Trial 3. After that, the cracks at the bottom web-gap region suddenly became wider and deeper over just 100,000 cycles. In a real bridge structure, these types of cracks would be very difficult to detect until the crack widths increased sufficiently.

4. **The gusset plate cracking that occurred in the test of the 20-deg. skewed specimen indicated that the angles-with-plate repaired the web gap detail sufficiently such that a "lesser" fatigue detail suffered cracking.**

   The bottom gusset plate of the 20-deg. skewed specimen cracked with the angles-with-plate retrofit in place. The stresses measured from the strain gages attached on the 40-deg. specimen and the computer simulation results all indicated that for the skewed connections, the stresses on the gusset plates did not increase, but decreased after installing the retrofits.

5. **The strain gages attached close to the cracked web-gap could be effective tools to indicate crack propagation.**

   Attached close to the cracked web-gap, the strain gages applied in the test of the 20-deg. skewed specimen were sensitive to the growth of cracks. However, the strain gages placed on the 40-deg. skewed specimen were insensitive to crack propagation. It may be because the strain gages were placed too far away from the web-gap in that test.

6. **The physical test results and the computer simulation results agreed well**

   The stresses measured by the strain gages attached on the physical specimen agreed well with the stresses extracted from the computer simulations. The stress contour plots obtained from the mirror array measurements and the computer simulations were almost identical.

The angles-with-plate retrofit successfully halted crack propagation in both the 20-deg. and the 40-deg. skewed crossframe to girder connection subassemblies. The localized deformations and stresses in the web-gap regions were also significantly reduced after retrofitting. A comparison of the physical test results and the finite element analysis resultsindicated that the

two agree well with each other. Therefore, the finite element analysis, which showed that after retrofitting the peak maximum principle stresses reduced 56% and 66% in the 20 deg and 40 deg models respectively, should be reliable.

References

AASHTO (2013). “LRFD Bridge Design Specifications, 6th Ed.” American Association of State Highway and Transportation Officials, Washington, D.C.

Alemdar, F., Nagati, D., Matamoros, A., Bennett, C., and Rolfe, S. (2014). "Repairing Distortion-Induced Fatigue Cracks in Steel Bridge Girders Using Angles-with-Plate Retrofit Technique. I: Physical Simulations." J. Struct. Eng., 10.1061/(ASCE)ST.1943-541X.0000876, 04014003.

Alemdar, F., Overman, T., Matamoros, A., Bennett, C., and Rolfe, S. (2014). "Repairing Distortion-Induced Fatigue Cracks in Steel Bridge Girders Using Angles-with-Plate Retrofit Technique. II: Computer Simulations." J. Struct. Eng., 10.1061/(ASCE)ST.1943-541X.0000874, 04014004.

Bennett, C., Matamoros, A., Barrett-Gonalez, R., Rolfe, S. (2014). “TPF-5(189): Enhancement of Welded Steel Bridge Girders Susceptible to Distortion-Induced Fatigue.” Structural Engineering and Engineering Materials SM Report No. 106, University of Kansas, Lawrence, KS.

Bonet, E. (2014). “Utilizing Fiber-Reinforced Polymers to Retrofit Steel Bridge Girders Damaged by Fatigue Loading.” Master’s Thesis, University of Kansas, Lawrence, KS.

Connor, R. and Fisher, J. (2005) Identifying Effective and Ineffective Retrofits for Fatigue Cracking in Steel Bridges using Field Instrumentation. Structures Congress 2005: pp. 1-9.

Dexter, R. J., Ocel, J. M. (2013). “Manual for Repair and Retrofit of Fatigue Cracks in Steel Bridges.” Draft Report to Federal Highway Administration No. FHWA-IF-13-020, University of Minnesota, Minneapolis, MN.

Fisher, J. W. and Mertz, D. R. (1984). “Fatigue and Fracture in Steel Bridges.” The Conference on Bridges, Pittsburgh, PA, 10-21.

Hartman, A. S. (2013). “Analytical and Experimental Investigation for Distortion-Induced Fatigue in Steel Bridges.” Ph.D. Dissertation, University of Kansas, Lawrence, KS.

Hassel, H., Bennett, C., Matamoros, A., and Rolfe, S. (2013). "Parametric Analysis of Crossframe Layout on Distortion-Induced Fatigue in Skewed Steel Bridges." J. Bridge Eng., 10.1061/(ASCE)BE.1943-5592.0000388, 601-611.